FEASIBILITY OF RADIATION DOSE PLANNING GUIDED

SURGICAL RESECTION IN SPINAL TUMOURS

by

Raphael Y. Jakubovic

Master of Science, Ryerson University, 2014

Bachelor of Science, Ryerson University, 2011

Bachelor of Talmudic Letters, Yeshivas Bais Yisroel, 2006

A dissertation presented to Ryerson University

in partial fulfillment of the requirements for

the degree of Doctor of Philosophy

in the program of Biomedical Physics

Toronto, Ontario, Canada, 2017

© Raphael Y. Jakubovic, 2017

AUTHOR'S DECLARATION FOR ELECTRONIC SUBMISSION OF A DISSERTATION

I hereby declare that I am the sole author of this dissertation. This is a true copy of the thesis, including any required final revisions, as accepted by my examiners.

I authorize Ryerson University to lend this dissertation to other institutions or individuals for the purpose of scholarly research.

I further authorize Ryerson University to reproduce this dissertation by photocopying or by other means, in total or in part, at the request of other institutions or individuals for the purpose of scholarly research.

I understand that my dissertation may be made electronically available to the public.

Feasibility of radiation dose planning guided surgical resection in

spinal tumours

Doctor of Philosophy 2017

Raphael Y. Jakubovic

Biomedical Physics

Ryerson University

Abstract

The objective of high dose stereotactic radiotherapy regardless of application is to treat the malignancy while minimizing the radiation dose to the surrounding healthy tissue. In the context of spinal tumours this paradigm is difficult since the rigid dose tolerance of the spinal cord precludes optimal dose coverage of the epidural disease. To achieve adequate coverage spine separation surgery is performed, increasing the distance from the spinal cord to the malignancy and facilitating adequate radiation treatment planning. This approach has been validated with delivery

of maximum tolerable dose and local control rates over 90%.

The objective of this dissertation is to establish the feasibility of intra-operative, dose guided, spine separation surgery. In the current clinical context, spine separation surgery is performed prior to radiation treatment planning and contours are placed based on postoperative resected tumour volumes. The extent of surgical resection is not dictated by the dosimetric constraints of the spinal cord and relies solely on the clinical expertise of the operating neurosurgeon. Further, though a skilled surgeon can perform precise tumour debulking with or without the aid of millimetre resolution neuronavigation devices, determination of surgical debulking progress with accuracy comparable to treatment delivery cannot be recognized without intraoperative imaging. To achieve this goal, we introduced pre-surgical dosimetric planning with tracked high frequency micro-ultrasound imaging into the operating theatre to inform the surgeon of the surgical progress while considering the dosimetric objectives.

In this dissertation, we assessed the dosimetric advantage of spine separation surgery on a millimetre by millimetre basis in a retrospective simulation study. Feasibility of intraoperative navigation with submillimetre resolution was established by quantifying the application accuracy of surgical navigation in the context of cranial and spinal surgery. Accuracy quantification was performed, assessing our revolutionary optical topographical imaging system and benchmarked versus existing commercially available neuronavigation systems. Finally, to establish feasibility of radiation dose planning guided surgical resection we integrated a high frequency micro-ultrasound system into the operating theater during spine separation surgery. Thus, by implementing sub-millimetre high frequency micro-ultrasound imaging and neuronavigation, incremental gains towards establishing the feasibility of intraoperative dose planning by iteratively updating the extent of tumour resection were recognized.

Acknowledgements

I would like to thank my supervisors, Dr. Victor Yang & Dr. Ana Pejović-Milić, for their support and guidance over the course of my academic career. I consider myself privileged to be mentored by these individuals and look forward to working with them in the future.

Dr. Yang has overseen my progression from graduate student to independent researcher, providing valuable insight into my Doctoral research, contributing to the development of fundamental critical thinking skills which will only assist me in furthering my career objectives. Dr. Yang runs a truly unique research laboratory, where with sufficient motivation, a student can carry out novel, cutting edge bench to bedside research, utilize state-of-the-art technologies, and apply their knowledge to directly impact patient care. Further, Dr. Yang's support in the advancement of my career as a clinical Medical Physicist and appreciation for family values, especially after the birth of our twin sons, is a testament to a certain quality of character not always evident in typical supervisor/student relationships. It has been an honour working with Dr. Yang and I look forward to collaborating in the future.

Dr. Pejović-Milić has served as my mentor over the last decade, serving as teacher, mentor, and finally colleague. Dr. Pejović-Milić has always shown confidence in my abilities as I evolved from a Medical Physics undergraduate student with no physics background, through the successful completion of my both my MSc and PhD. Dr. Pejović-Milić also provided my first exposure to a research environment as a summer research assistant, which only served as motivation for further research pursuits. I have always admired Dr. Pejović-Milić's passion for physics and consider myself privileged to have had the opportunity to interact with her.

I would like to thank Dr. Richard Aviv, who although did not actively supervise my PhD, served as a guide and advisor throughout. Dr. Aviv played a major role in the development of my research abilities early in my career and has served as a mentor and advisor over the last several years.

I would like to thank Dr. Mark Ruschin and Dr. Carl Kumaradas for serving as members

Dedication

This dissertation is dedicated in loving memory of my grandfather, David Richler OB"M and my mother-in-law, Gloria Anne Cohen OB"M to whom of which I both shared special relationships. May their memories be for a blessing.

To my parents who continue to support me and believed in my abilities before I had the confidence to fulfill as only parents could.

To my siblings, Marcel, Eli, and Abi, who have each achieved in their own right, for your words of encouragement.

To my children, Tamar, Ezra, & Noam who have graciously accompanied me on this sojourn. I hope that you will have the opportunity I've had to follow your dreams and accomplish great things.

And finally.

To my wife, Pnina

"Learn from yesterday, live for today, hope for tomorrow.
The important thing is not to stop questioning" (Albert Einstein)

I could not have achieved this milestone without you and for that I will forever be indebted. You have stood by me with support over the last number of years, and I stand with you today, reflecting on all we have accomplished, anticipating a future of love, health, and happiness. It is my hope that we continue to share in even greater successes as we embark on our "tomorrow", and bring much joy into the world throughout our lives.

Contents

3 Benchmark Analysis 53

4 Validation of OTI System 75

List of Tables

List of Figures

Chapter 1

Introduction and Background

1.1 Introduction

The incidence and diagnosis of spinal tumours has been steadily increasing due to earlier detection and visualization of disease, improved treatment outcomes of primary disease, and a growing elderly population.[1,2] Most commonly, spinal tumours proliferate metastatically, occurring 20 times more frequently than primary spine pathologies.[3] The propensity for metastatic proliferation to the spine has been suggested to arise from unregulated hematological flow through the venous plexus, resulting in the deposit of metastatic disease via the epidural space, as proposed by Oscar Batson in 1940.[4] Spinal metastases have been estimated to occur in 50 – 70% of all cancer patients with approximately 10 – 20% or 5% of all cancer patients (25,000 annually) presenting as clinically symptomatic.[2,5 – 7]

The prognosis for patients diagnosed with spinal metastases is poor, with median (range) survival of 7 months (3 – 16 months) overall and 3 – 6 months for patients with epidural disease extension.[8,9] Tumours can directly infiltrate the epidural space through the extension of the tumour into the spinal canal, or more commonly, metastasize into bone and extend into the epidural space (Figure 1.1).[9] Irrespective of mechanism, the

extension of the tumour compresses the spinal cord, resulting in demyelination, axonal disruption and vascular damage.[9] Patients initially present with localized back pain, progressively increasing in intensity over time, developing into mechanical back pain related to spinal instability. Furthermore, patients may present with varying degrees of neurological symptoms including, weakness, sensory loss, sphincter dysfunction and paralysis, significantly impacting the patient's quality of life.[3]
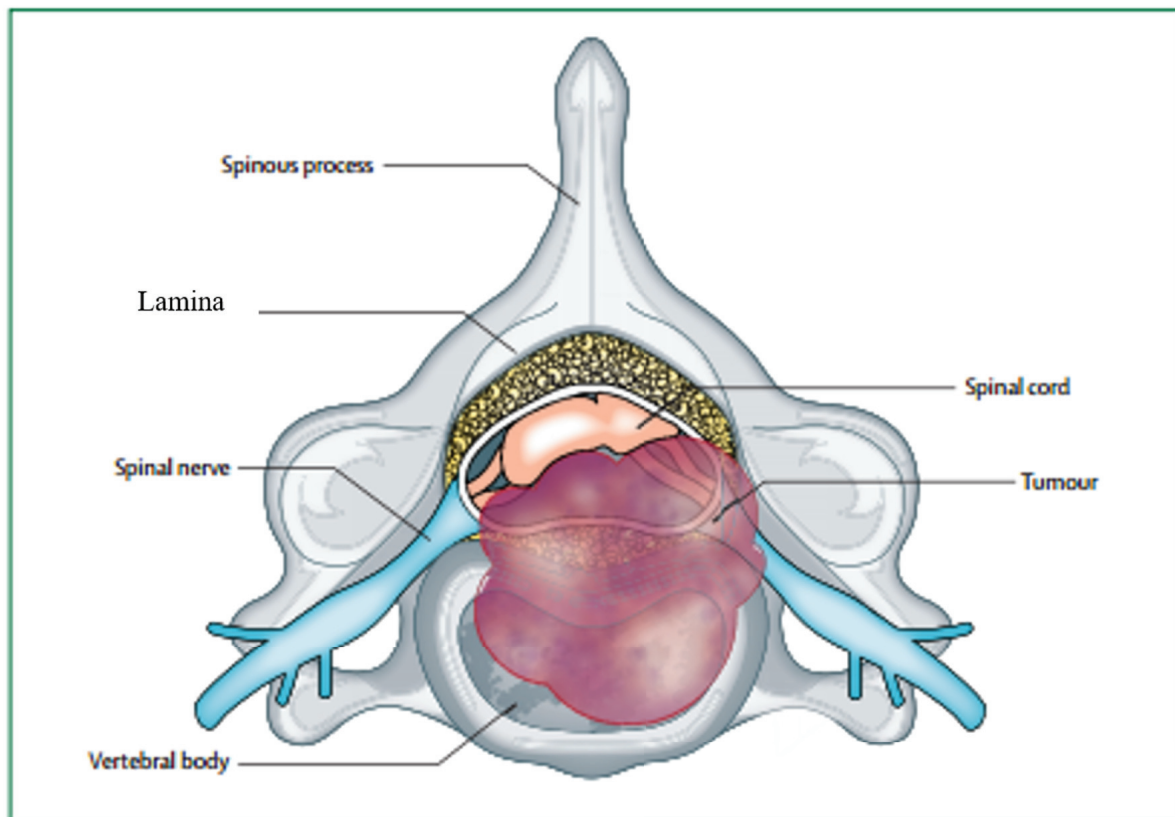
Figure 1.1: Schematic of epidural disease causing cord compression: Tumour is in close proximity to the spinal cord causing compression. Reprinted from The Lancet Neurology with permission from Elsevier. [9]

1.2 Treatment of Spine Tumours

The treatment of spinal tumours has advanced over the last several decades and there are currently various treatment options, including open and minimally invasive surgical decompression, stabilization, and tumour resection, conventional and stereotactic external beam radiation therapy, vertebral augmentation, and various systemic therapies involving bisphosphonates, radioisotopes and chemotherapy.[1] This advancement has been quite impressive as previous treatment for metastatic cord compression was limited to invasive surgical intervention via laminectomy or external beam radiotherapy.[9]

The evolution of the treatment has been tortuous and the surplus of treatment options has made the clinical decision making increasingly complex. Clinical decision making depends on a variety of neurological and imaging characteristics following the neurologic, oncologic, mechanical instability, and systemic disease (NOMS) framework.[10] Neurologic assessment is primarily based on the degree of epidural spinal cord compression as assessed by the grading systems proposed by Bilsky et al.[11] or Ryu et al.[12], but does consider whether there is associated myelopathy or radiculopathy. Oncologic assessment considers primary tumour histology and the expected responsiveness to currently available treatments. Mechanical instability is based on lesion location, presence and frequency of pain, type of pain (i.e. mechanical or non-mechanical), lesion characteristics (i.e. lytic, blastic, or mixed), radiographic spinal alignment, presence and degree of vertebral body collapse and involvement of posterolateral spinal elements as assessed by the Spinal Instability Neoplastic Score (SINS).[13] Finally, treatment decision is based on the ability of the patient to tolerate the procedure. An outline of the NOMS framework is shown in Figure 1.2.[10]

Prior to these advancements the primary outcome measure of treatment was pain control as limited survival times were associated metastatic spine disease diagnosis.[14] Improvements in outcomes were recognized by expanding the surgical approach to include circumferential decompression via an anterior approach rather than laminectomy alone, but little evidence existed to support surgery as a sole treatment option.[5] As the precision of radiation treatment delivery improved and precise targeting of the epidural disease component was feasible, conventional radiotherapy (CRT) quickly became the
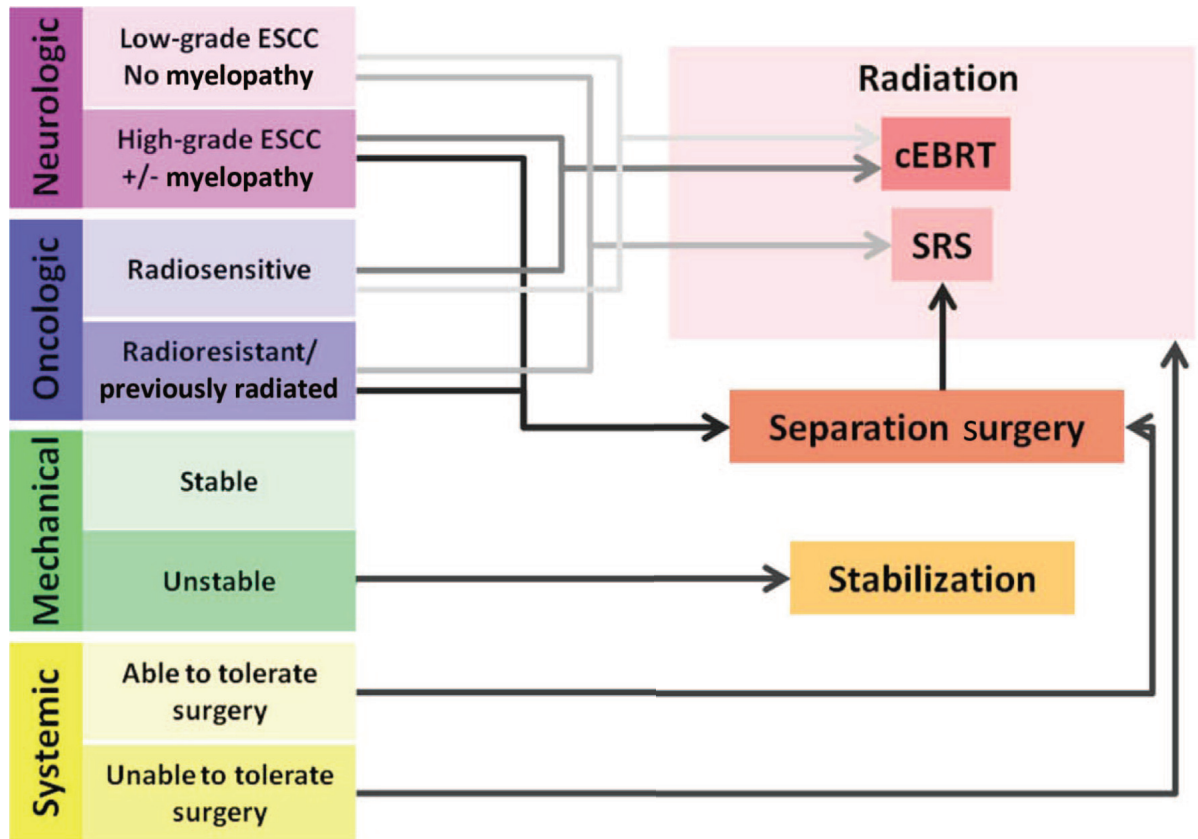
Figure 1.2: NOMS treatment decision framework. Reprinted from The Oncologist with permission from John Wiley & Sons.[10]

preferred treatment for practitioners, due its non-invasiveness and little clinical evidence showing the benefit of decompression. SBRT or spine radiosurgery has since become preferred over CRT, facilitated by technological advancements including but not limited to image guidance, intensity modulation, multi-leaf collimation, and dynamic arc radiotherapy. This has shifted the treatment paradigm from palliative to curative, and pain control to local control, as cytotoxic doses can be delivered to the tumour while sparing the spinal cord. As such, the majority of radiation oncologists have integrated SBRT into their standard clinical practice.[15,16]

Adoption of SBRT for spinal tumours has been rapid due to local control rates of 80 – 90% seen one year post treatment and reported efficacy in traditionally radio-resistant pathologies.[17] This is a major improvement in the treatment paradigm since much of the literature has been limited to reporting pain control as a primary endpoint, and no randomized studies exploring the efficacy of SBRT have been reported. The scant literature based on imaging response shows estimated local control rates ranging form 50 – 80% using CRT.[18] SBRT has also been shown to be effective for palliation, providing pain relief in over 80% of patients nearly 1 year following treatment versus 60% in patients treated with CRT.[19,20] Despite reports of increased efficacy and low rates of SBRT induced toxicity, concerns over vertebral compression fracture, radiation myelopathy, pain flare, and esophageal toxicities have been expressed.[21] These complications can be avoided with careful treatment planning and risks are reduced by increasing fractionation or, in the case of pain flair, treatment with steriods (i.e. dexamethasone).[21]

The current treatment paradigm has become increasingly intricate with the introduction of SBRT since the delivered radiation dose is limited by the proximity of the disease to the spinal cord and surgical resection is limited by the need to maintain spinal integrity. This challenge is solved by combining decompression and surgical resection of the tumour with SBRT, in a procedure coined "spine separation surgery", which has shown demonstrable survival benefit and pain reduction.[5] Tumour debulking facilitates SBRT, allowing delivery of the maximum tolerable dose to the spinal cord with increased dose delivery to the epidural disease. This open surgery approach has been established as superior to radiotherapy alone, resulting in improved functional outcomes (i.e. ambulation, pain, infections, blood clots, and survival time) and local control rates > 90%.[5,15]

1.3 Stereotactic Body Radiation Therapy (SBRT)

Stereotactic radiosurgery (SRS) is defined as the precise and complete destruction of a chosen target containing healthy and/or pathological cells, without significant concomitant or late radiation damage to adjacent tissues.[22] Fundamentally, this means that the radiation dose delivered is high enough to control the lesion and concentrated enough to minimize damage to the normal surrounding tissue. SRS achieves this result by using multiple beam geometries to create a conformal beam capable of delivering a high dose of radiation and ultimately destroying the tumour. SBRT is analogous to SRS delivering a high dose of radiation to an extracranial tumour, while limiting dose to the surrounding tissue. SBRT fuses the principles of intracranial SRS with conventional radiotherapy, whereby large doses are delivered to the patient in fewer fractions, resulting in a high biological effective dose (BED).[23] SBRT has been employed in a number of solid tumours, including, lung, liver, pancreas, kidney, prostate, and spinal tumours and has been shown to at least compare favorably to surgery in regards to outcomes in primary and metastatic disease with minimal adverse effects.[24,25] However, the utility of SBRT is limited and has not been typically used for treatment of large, infiltrative or poorly defined pathologies.[24]

From a radiobiological perspective, the goal of SBRT is to achieve maximum biological effect by delivering few fractions of high dose radiation. As such, SBRT is utilized to induce both direct and indirect mechanisms of cell damage, while allowing for moderated dose delivery to the surrounding tissues and facilitating normal tissue recovery.[25,26] Due to the high doses typically employed by SBRT, the accuracy of the treatment delivery is paramount. Therefore, based on the recommendations of the AAPM Task Group 101, SBRT involves integration of modern imaging, simulation, treatment planning and delivery technologies into all phases of the treatment process to ensure accurate delivery of radiation.[24] While submillimetre accuracy in treatment delivery can be achieved in the modern radiotherapy suite, actual human studies have shown uncertainties in tar-

geting accuracy and reproducibility of ≈1.5 millimetres.[27,28] Since multiple sources of error are inherently involved in the treatment process, including during patient setup and immobilization, image fusion, and contouring of the target and organs at risk, specialized SBRT training is imperative to ensure millimetre accuracy.[24]

Traditionally, the use of SBRT has been limited by dose constraints to surrounding tissue and uncertainty introduced by organ motion.[23] Spine SBRT is particularly challenging as intrafraction motion on the order of millimetres can have profound clinical impact increasing the risk of radiation myelopathy.[29] Specifically, a hypothetical 3 mm positioning error has been shown to double the delivered radiation dose.[30] Considering the large dose fractions delivered in SBRT (i.e. 24 Gy/2 fraction or 30 – 45 Gy/5 fractions) relative to conventional radiation therapy (8 Gy/1 fraction, 20 Gy/5 fractions or 30 Gy/10 fractions) and the dose constraints of the spinal cord, millimetre treatment planning accuracy is essential.[19,23,31,32]

Advances in treatment delivery by using multiple overlapping focused radiation beams, coupled with the aforementioned millimetre resolution required for treatment planning, has facilitated widespread adoption of SBRT as a viable curative treatment in spine tumours. However, the proximity of the epidural disease to the spinal cord precludes SBRT as a stand-alone treatment modality. Two primary patterns of treatment failure have been identified originating from the vertebral body adjacent to the treatment site and from within the epidural space.[19,33,34] In particular the epidural space has received additional attention as increased failure has been associated with the proximity of the disease to the spinal cord which presumably limits delivery of dose to the epidural disease component.[19] Therefore, surgical resection is essential, creating an effective buffer between the spinal cord and epidural disease, such that subsequent SBRT can be delivered.

1.4 Spine Separation Surgery

In the current clinical model, where the goal of treatment for spinal tumours is curative rather than palliative, spine separation surgery acts as a facilitator for SBRT whereby the surgeon removes the bone and incrementally resects the offensive tissues circumferentially away from the spinal cord. The surgical approach is to first remove the bone adjacent to the diseased tissue via laminectomy, and subsequently resect the tumour (Figure 1.3). In the case of spinal instability, the surgeon will insert hardware as necessary. This systematic methodology ensures that the surgeon will perform a minimal surgery in order to create an adequate buffer zone between the epidural disease and the spinal cord. This buffer zone ensures that a cytotoxic dose can be delivered to the diseased tissue and not the spinal cord, thus sparing the patient from any potential cord toxicity. Representative axial and sagittal CT images, pre- and post- spine separation surgery are shown in Figure 1.4. Once the patient has recovered from the surgery (5 – 21 days) radiotherapy is administered.[35]

In the context of spinal metastases, SBRT is particularly challenging considering the rigid dose constraints of the spinal cord. While the objective dose to the tumour at our institution is generally 24 Gy in two fractions for patients not treated previously, the maximum dose allowed to the spinal cord is 17 Gy.[36,37] To achieve the required doses a combined surgical resection/SBRT approach is employed, increasing the margin between the spinal cord and the epidural disease, maximizing dose to the tumour and reducing the dose to the spinal cord. While the amount of tissue requiring resection can be estimated based on the extent of epidural disease, the precise balance between surgical resection and SBRT has not been determined. Treatment planning is further compounded by the use of high density surgical hardware (steel or titanium) which attenuate the photon beams distal to the hardware, necessitating correction during treatment planning.[38,39] The dosimetric effect can be impactful, resulting in approximately 6% underestimation of dose in front of the hardware due to electron backscatter, or approximately 7% overestimation behind due to photon attenuation.[40] Moreover, treatment planning occurs after surgical resection thus requiring the surgeon to determine the extent of tissue to resect based on the extent of epidural disease with little regard to the actual radiation dose distribution.
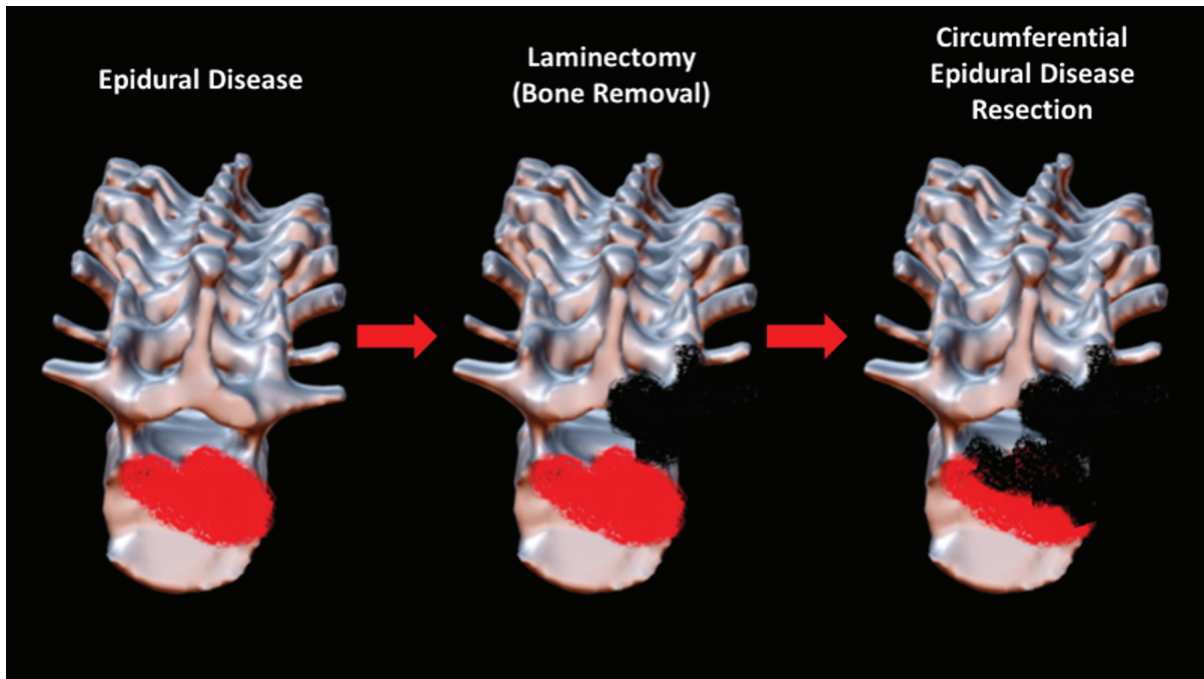
Figure 1.3: Surgical approach for spine separation surgery: Epidural disease component (red) causing spinal cord compression (left). Surgeon exposes the vertebral body and removes bone via laminectomy (centre). Surgeon incrementally resects epidural disease to create a buffer zone between the epidural disease and spinal cord (right).
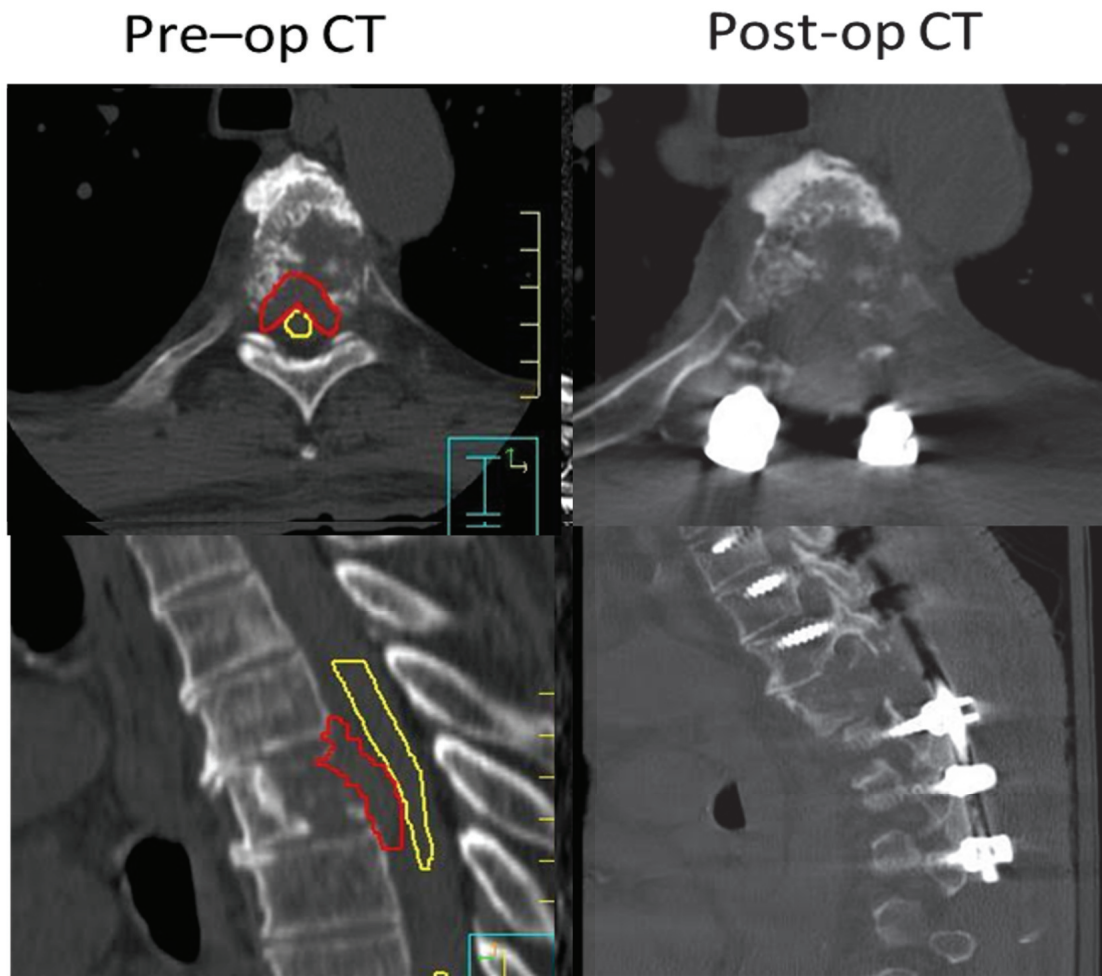
Figure 1.4: Pre- and post- operative spine separation surgery: Axial and sagittal CT images demonstrating pre-surgical spinal cord (yellow) and epidural disease (red) contours. Epidural disease contours identify tissue targeted for resection (left panel). Postoperative axial and sagittal CT demonstrates instrumentation above and below the diseased vertebral body with bone removed.

Spine separation surgery provides a distinctive barrier between the radiosensitive spinal cord and the gross tumour volume (GTV), thus improving the coverage of the planning treatment volume (PTV) while respecting the rigid dose tolerances of the spinal cord. At our institution, the PTV comprises a 2 mm expansion over the clinical target volume (CTV), which represents the spinal segment at risk of microscopic disease extension.[36] The planning risk volume (PRV) is a 1.5 mm margin applied to the organ at risk (i.e. the spinal cord).[36] Typically, the goal of the surgery is to create a $2 - 3$ mm barrier between the disease and the spinal cord allowing for the delivery of high dose of radiation to the target. Generally, this is achieved via laminectomy with instrumented fusion to maintain spinal stability and the epidural disease is resected circumferentially. The expected dose fall-off is approximately 10% per millimetre of resected tissue at the epidural disease/spinal cord interface.[31] This approach facilitates improved SBRT by downgrading the extent of epidural disease and thus improving local control when compared to SBRT alone or conventional external beam radiotherapy.[24,41]

Surgical resection of the epidural disease prior to radiation therapy is a reasonable tactic considering a primary mode of treatment failure originates within the epidural space.[33,34,42] The presence of epidural disease is limiting as the spinal cord constraint is rigid, and the spinal cord dose exposure although safe is not able to control disease. Therefore, surgical advances are in need to decompress and stabilize the spine while minimizing morbidity.[1,15] Applying minimally invasive spine surgery is one strategy. However, the ability determine the exact balance between resection and decompression is just as important, especially within the context of optimized radiation delivery. Currently, the surgeon does not have this information available during surgery and if real-time image guided epidural resection is achieved, specific tissues can be surgically targeted, thus minimizing morbidity. Simulated incremental epidural disease contours representing surgical resection margins are shown in Figure 1.5.

While there are well defined parameters for contouring metastatic tumours prior to surgery, postoperative treatment strategies vary.[43] Specifically, in question is whether to: 1) treat only residual postoperative epidural disease, 2) to include epidural disease visualized on the preoperative MRI, 3) to extend cranio-caudally as is typical of epidural
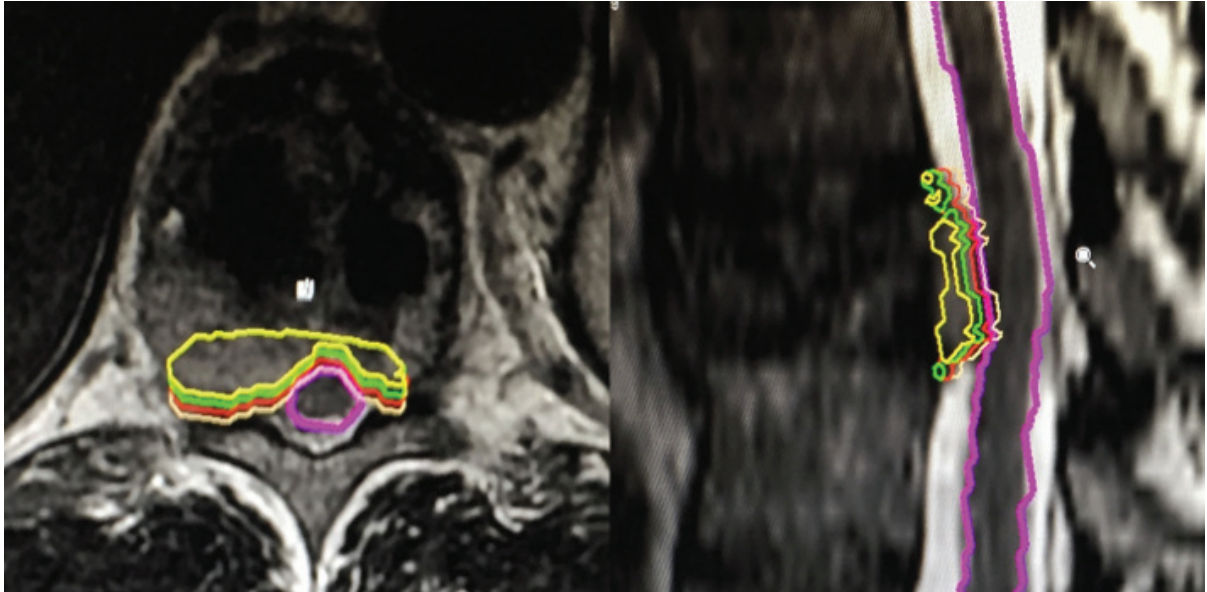
Figure 1.5: Incremental tumour resection: Simulated millimetre tumour resection contours.

disease, 4) to include the pedicles and posterior elements, and 5) to treat entire epidural space using donut configuration to ensure complete coverage of the epidural space.[33,34]

1.5 Surgical Navigation for Pedicle Screw Insertion

Surgical navigation in the context of spinal surgery has undergone significant evolution over the last several years. This technological advancement has been driven by need as the number of individuals with back pain in the United States has been estimated at over 100 million. Further, the direct and indirect costs associated with back pain has been assessed at $50 – $200 billion annually.[44,45] Considering the prevalence of spine conditions in the elderly (i.e. 43.2 million people aged 65 and above in the United States in 2012), and an aging demographic, the number of spinal surgical procedures is expected to rise, creating a significant market for surgical guidance systems in spinal surgery.[46]

Spinal surgery often includes spinal decompression and fusion, stabilizing the spine and alleviating pain, resulting in improved quality of life. This common surgical procedure is used to treat a variety of conditions including trauma, spinal deformity, degenerative or neoplastic diseases and infection.[47] Surgery is challenging for surgeons as insertion of implants (e.g. pedicle screws, lateral mass screws, rods, etc.) deep into the vertebral body requires a high degree of precision without proper visualization beyond the surface of the bone. Instrumentation is further complicated by the proximity of the screw trajectory to the spinal cord and adjacent vasculature (i.e. arteries or veins). Considering that perforation of pedicle and lateral mass screws can cause nerve root injury, vertebral artery injury, or spinal cord injury it is imperative that the surgery be thoroughly planned to account for these differences in patient anatomy while ensuring spinal stability without proper visualization beyond the bone surface.[48]

Misplaced pedicle screws are common with breach rates of 3% to 55% previously reported often resulting in neurological deficits, vascular injury, chronic pain, or failed back syndrome.[49 – 51] Pedicle screws are inserted using a blunt-tipped pedicle finder or drill that is advanced through the spongy trabecular bone providing excellent hold with resistance to screw pullout forces. Since the spine is comprised of trabecular bone surrounded by a shell of compact cortical bone the surgeon generally relies on tactile feel to discern trabecular from cortical bone (Figure 1.6). Screws are implanted into the bone, and guided through the narrow vertebral pedicle. Traversing the pedicle without breaching bone is challenging as there is considerable variability in pedicle width between populations, and bone resistance varies depending on patient age and bone density.[47,52,53]

Precise surgical insertion of these implants can be achieved using surgical navigation, reducing the risk of complications. To minimize the risk associated with spinal fusion procedures, various navigation systems have been designed to aid the surgeon with lateral and pedicle screw fixation. These navigation systems allow surgeons to visualize complex subsurface anatomic structures and have been shown to increase the accuracy of screw placement compared to freehand and fluoroscopy guided techniques.[55,56] Current technologies rely on infrared (IR) tracking and preoperative imaging (CT or MRI). Localization of the target area is a time-consuming exercise, achieved using preoperative imaging and/or fiducial markers. Localization techniques require extensive set-up and
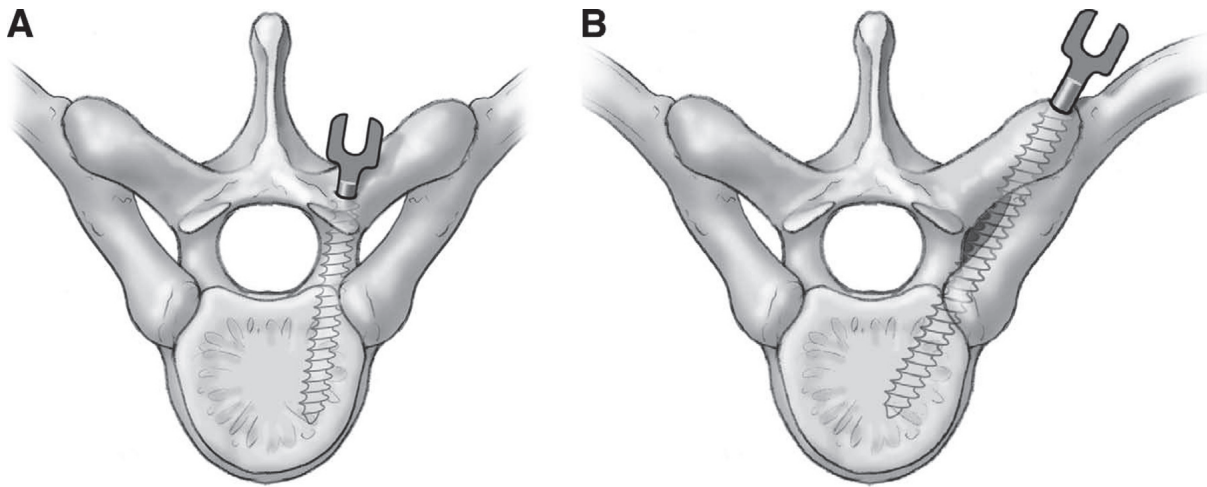
Figure 1.6: Pedicle screw fixation: (A) Ideally, the pedicle screw is placed through the thoracic pedicle directly into the vertebral body without breaching the pedicle cortex. (B) The "in-out-in" technique takes advantage of the greater diameter of the pedicle-rib unit compared with that of the thoracic pedicle alone. The size of the unit allows it to accommodate much larger screw diameters or to be used for a salvage procedure when placement into the thoracic pedicle fails. Reprinted from Operative Techniques in Neurosurgery with permission from Elsevier.[55]

introduce spatial variations as the patient position is determined by preoperative imaging and do not account for movement of the reference frame or the spine during patient positioning and/or during surgery. Intraoperative verification using fluoroscopy, mobile x-ray or computed tomography may minimize these variations but frequency of temporal update is limited due to the risks associated with ionizing radiation. Current commercially available systems include: ARCADIS Orbit 3D (Siemens, Munich, Germany), Ziehm Imaging mobile C-arm technology (Ziehm Imaging, Nuremberg, Germany), StealthStation O-Arm (Medtronic, Minneapolis, MN, USA), eNLight and NavSuite (Stryker Corporation, Freiburg, Germany), and VectorVision (Brainlab, Feldkirchen, Germany).

The existing navigation systems are limited by the requirement that a registration procedure is performed to relate the image space anatomy shown by the navigation system and the exposed anatomy of the patient.[49] The anatomical position of a reference frame in a fixed location (i.e. spinous process) is used to relate the imaging space to the intraoperative patient position. Registration is achieved using a point-pairing algorithm based on a landmark based paired point matching algorithm requiring the surgeon to manually select landmarks.[57] The system then provides a numeric registration error, generally in terms of millimetres, to indicate discrepancy between the chosen landmark points and the probed anatomical positions.[58] To improve the registration error, additional information may be acquired for surface-matching registration, where additional points are selected randomly with the probe on the exposed surface.[57] The registration process is often time consuming and disruptive to the surgical workflow.

Another important consideration for using preoperative images for image-guided navigation is that there may be significant variations between the imaging data and the surgically exposed anatomy.[57] While preoperative imaging is performed with the patient supine surgical approaches are performed in the prone position. This necessitates registration at each vertebral level further disrupting the surgical workflow and resulting in even longer surgical times. According to a recent survey, only $\approx 10-15\%$ of surgeons use navigation with surgeons citing a lack of training or equipment and increased operating room time.[59,60]

1.6 Optical Topographical Imaging (OTI)

Optical Topographical Imaging (OTI) is a low cost imaging modality using structured light which allows for visualization of the surgically exposed area and the underlying structure without exposure to ionizing radiation. OTI allows for visualization of the surgically exposed area and provides continuous visualization of the vertebrae without exposure to ionizing radiation. Fusion of the optical data to three-dimensional 3D rendering of preoperative CT data has the ability to dynamically guide the insertion of screws with the high degree of precision necessary for surgical navigation. Optical data can also be fused with CT, MR and ultrasound data to provide dynamic imaging feedback during surgery.

The current OTI system is a stand-alone system and cart carrying a camera pod on an articulating arm that can be rolled into the operating room for use in spinal surgery (Figure 1.7). The camera pod is composed of 2 cameras, and a projector. Each camera pod has two flash units for static imaging and the projector is used for dynamic imaging. The projector illuminates a patterned light of known structure and periodicity (i.e. grids, repeating bars, etc.) that is recorded by the cameras and used to reconstruct the 3D topography of the patient. Analysis of depth distortions of the projected patterns allows for 3D point cloud mapping of the topography correlating to the various height disparities. The OTI system registers the acquired 3D point cloud to pre-acquired imaging data (i.e. CT, MRI, OTI) using an iterative closest point (ICP) algorithm. The algorithm evaluates a cost function that minimizes the disparity between the two data sets (OTI obtained during surgery and reference CT or MRI obtained preoperatively) based on a pre-registration point picking protocol. The OTI system also utilizes an infrared (IR) tracking system containing two IR cameras surrounded by IR LEDs to illuminate the tracking volume. The IR system is currently used to track surgical tools using passive-reflective markers. A schematic of the OTI experimental navigation system and clinical workflow is shown in Figure 1.8.
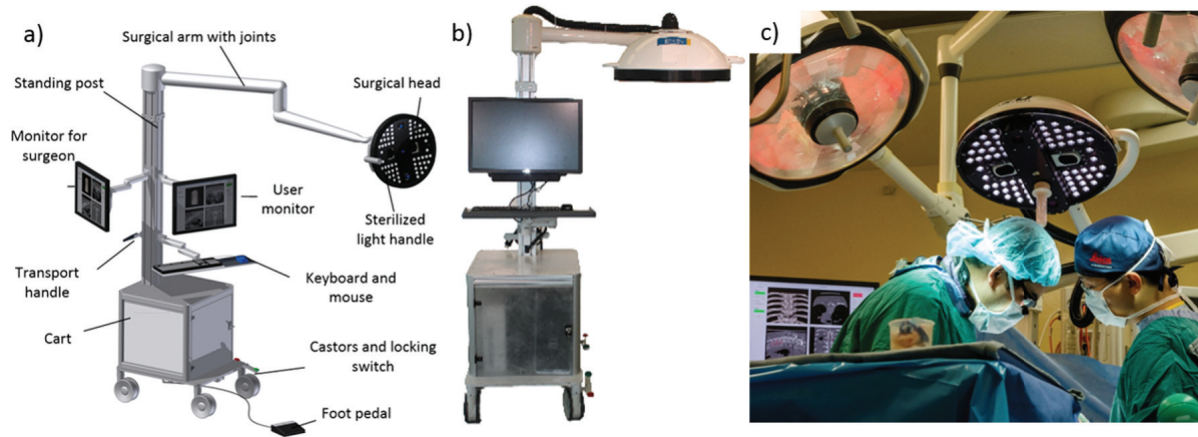
Figure 1.7: Integrated topographical imaging system: (A) Mock-up schematic of the integrated OTI system. Includes articulating surgical light head for positioning, stereoscopic cameras and projector for surface acquisition, near infrared tracking for surgical tools, and dual monitors for surgeon visualization and system operator (B) Fabricated integrated OTI system. (C) Low profile OTI system in operation during surgery.

1.7 Accuracy of Surgical Navigation for Craniospinal Surgery

Various navigation systems designed to guide pedicle screw fixation lack a quantitative measure to assess the accuracy of the procedure. Generally, reported registration errors represent deviations relative to fiducial landmarks calculated by the root mean square distance between the corresponding fiducials in the image and patient space after rigid-body registration.[61] While registration error can be quantified and reflects registration accuracy, it does not represent the accuracy of the procedure. In contrast measurement of the true screw accuracy by comparing the reported position of a tracked probe in the image space and a known surgical anatomy in the patient space is both quantifiable and clinically relevant. Further, while visual verification of the location is performed following registration, quantitative measures are not provided by the system. Several alternative parameters have been suggested including fiducial localization and registration error, target registration error, and angular deviation.[62,63] However, many of these techniques quantify error using the preoperative CT and an intraoperative screenshot without mea-
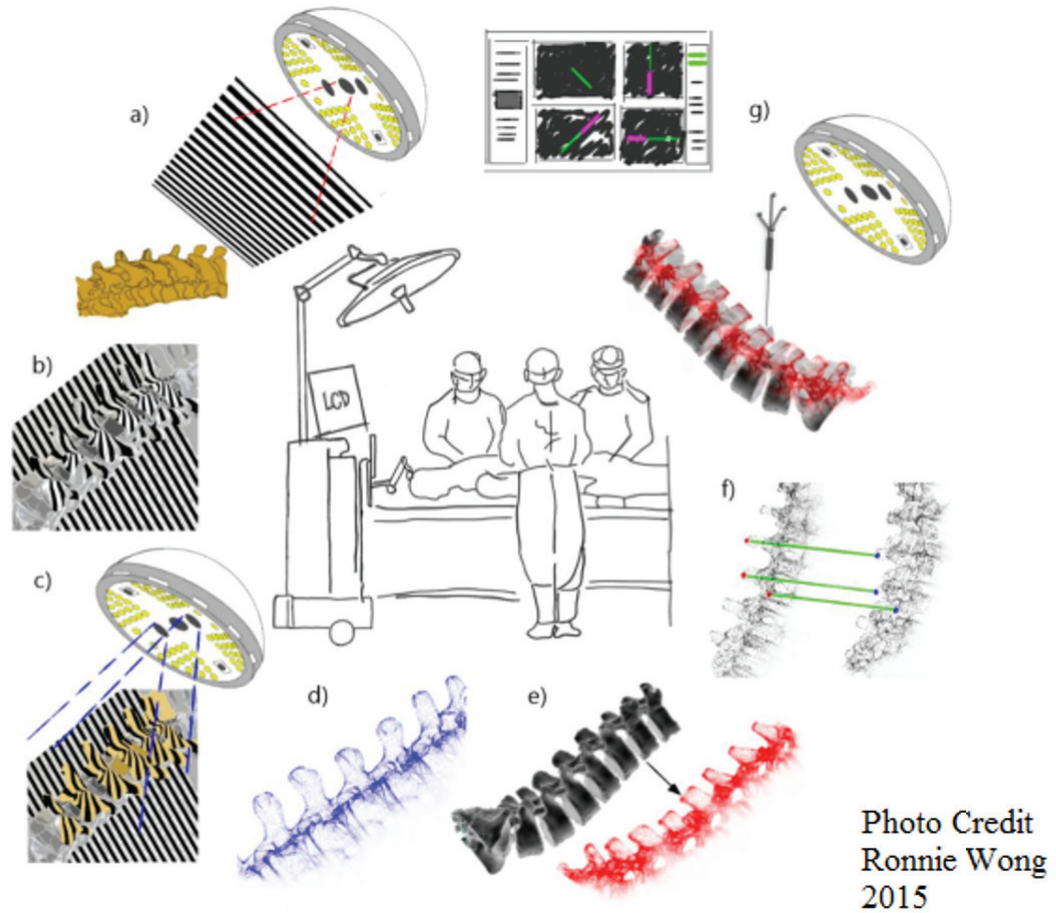
Figure 1.8: Schematic of the OTI experimental navigation system: (A) Bar code pattern projected onto spinal surface, (B) Pattern distorts around the spine, (C) Stereo cameras capture pattern distortion around spine and depth information, (D) The distortion and camera disparity helps create an accurate surface of the spine, (E,F) Modified ICP algorithm bridges CT spine scans and actual spine surface data, (G) Surgical tool position and orientation are mapped in real-time to the bridged spine surface data

suring the true postoperative screw trajectory.

Regarding the true application accuracy of navigated cranial surgery, the literature is scant. Few studies quantify application accuracy the generally accepted reported accuracies are primarily based on benchtop or phantom experiments. For example, the anecdotally assumed submillimetre accuracy of stereotactic frames, is actually $2.5 - 3.5$ mm when analyzed in-vivo,[64,65] and although application accuracies of $1 - 2$ mm are achievable using implanted fiducials, the true application accuracy is approximately 4 mm.[66] Therefore, it is crucial to take the accuracy requirements into account since accuracy requirements may vary depending on the surgical indication (i.e. a 4 mm margin is sufficient for craniotomy but not spinal decompression/instrumentation or deep brain stimulation).

1.8 Stereoscopic Binocular Tracking and Camera Drift

The OTI navigation system makes use of stereoscopic binocular cameras and a projector to acquire a surface image in addition to an infrared tracking system (NDI – Polaris Spectra) to track surgical tools during the procedure. Both make use of stereoscopic images to reconstruct the three-dimensional scene using the image information from both cameras. This is achieved by localizing features in the images from each camera and assuming epipolar geometry, where the epipolar plane is defined by the centres of the cameras and the point of interest. Once the features are located the three-dimensional co-ordinates can be calculated based on the focal distance and distance between the cameras (Figure 1.9).[67]

$$x_1 = (X + b/2)f/Z \qquad (1.1)$$

$$x_2 = (X - b/2)f/Z \qquad (1.2)$$

$$Disparity = \Delta \quad x = bf/Z \, or \quad Z = bf/\Delta x \tag{1.3}$$

Where x_1 & x_2 are the x coordinates of the two images (from two cameras), X is the actual coordinate, b is the distance between the centres of the camera, f is the focal distance, and Z is depth.

However, during surgery, the introduction of camera drift may significantly impact the accuracy of the experimental navigation system. The exact source of the drift is unknown but several possibilities must be acknowledged. Specifically, thermal expansion of the aluminum and acrylonitrile butadiene styrene (ABS) camera housing within the navigation head as well as a shift in optics within the cameras would have significant impact. Further, there are several points of torsion due to the structural design of the OTI system and various screw connections comprising the surgical light head. While linear expansion of the aluminum and other materials can be modelled (Equation 1.4), the exact source of the drift is likely multidimensional and not easily reconciled.

$$\Delta L = \alpha L_0 \Delta T \tag{1.4}$$

where, α is the linear expansion co-efficient for commercial aluminum, Δ L is change in length, L_0 is baseline length, and Δ T is change in temperature.[63]

A representation of the camera drift experienced during a temperature controlled thermal drift experiment with stereoscopic images acquired at 30°C (Figure 1.10a) and 46°C (Figure 1.10b) is shown.

To account for camera drift and allow accurate navigation an active calibration algorithm was implemented. The protocol obtains a structured light image of a cranial reference frame with a known geometry and computes warping in order to determine calibration factors and adjust for optical drift (Figure 1.11). Use of predefined geometry facilitates fast, accurate re-calibration during the course of surgery without undergoing a rigorous calibration procedure.
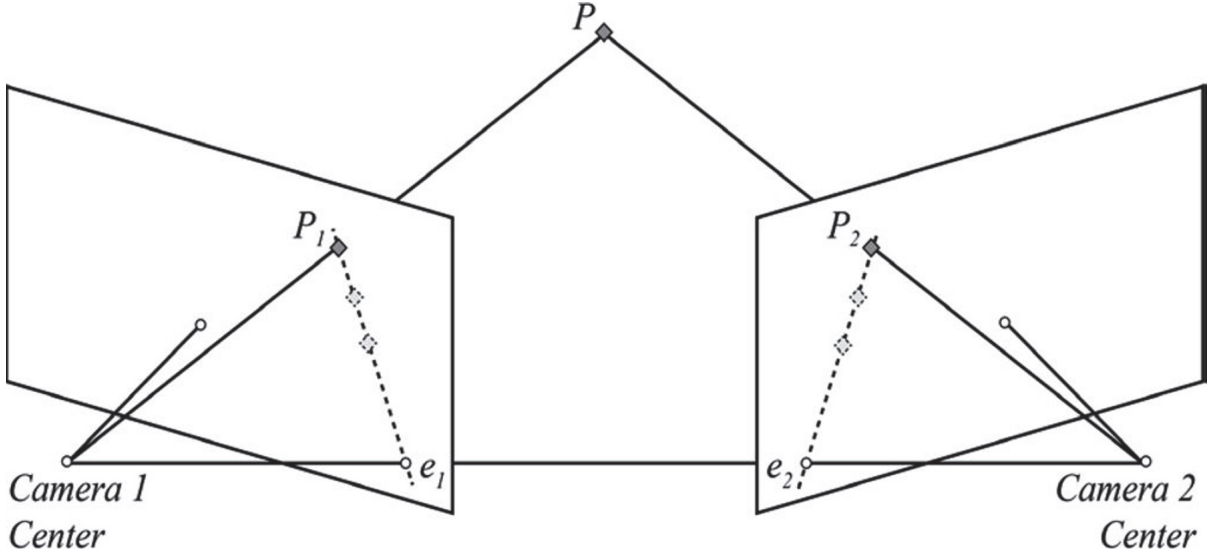
Figure 1.9: Illustration of the principle of epipolar geometry in stereo correspondence. To calculate the 3D location of a point P three steps are needed: (1) Identify the pixel coordinates of P in Camera 1 (P1), (2) search the image of Camera 2 to find the corresponding pixel coordinate of P image 2 (P2) and (3) project and compute the 3D location of P from the coordinates of P1, P2, and the known camera geometry. Epipoles (e1 and e2) are defined at the intersection of each image plane and the vector between the camera centres. The epipolar plane is the plane containing the camera centres and point P. The search for the correspondence pixel P2 can be limited to the line created by the intersection of the epipolar plane and the image plane of Camera 2. Sensor systems that restrict correspondence search to the epipolar lines can exhibit ghosting of features along the reduced search vector due to correspondence uncertainty. Reprinted from Medical Physics with permission from John Wiley & Sons.[68]
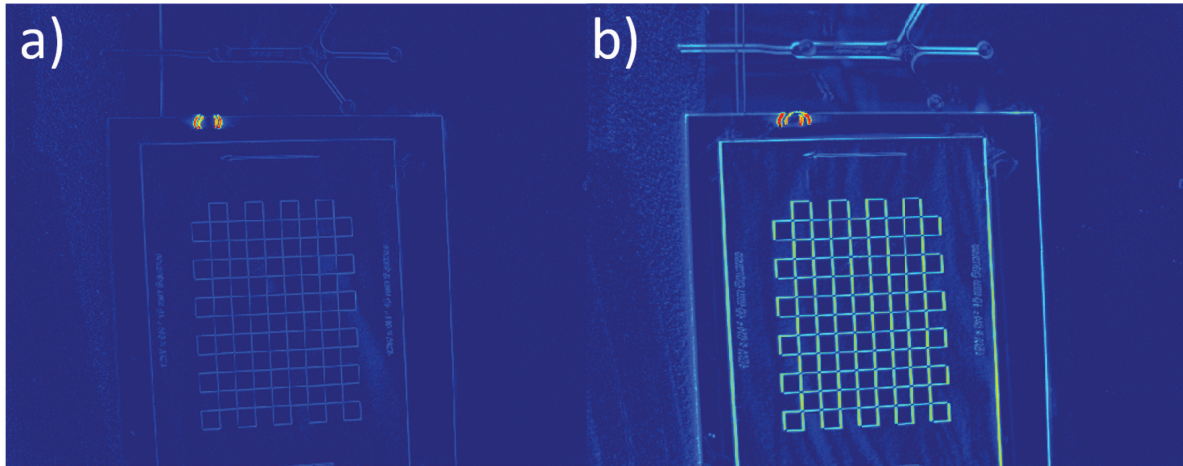
Figure 1.10: Thermal drift phenomenon: Significant camera drift seen during temperature controlled thermal drift experiment. Stereoscopic acquisition of a checkerboard configuration image at (A)30° C and (B) 46° C shows noticeable drift.
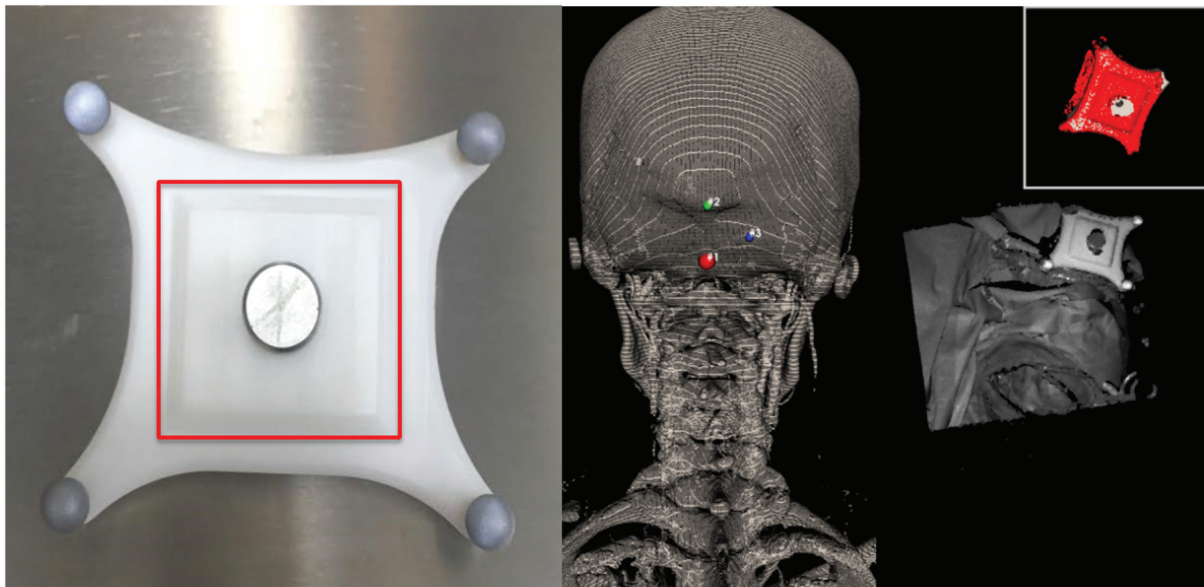
Figure 1.11: Cranial reference frame for active calibration:Cranial Reference Frame for Active Calibration: Left Panel: Measurements are normalized to known geometry of reference from highlighted in red; Right Panel: Intraoperative calibration optical surface image is matched to predefined geometry of reference frame highlighted in red.

1.9 Intraoperative High Frequency Micro-Ultrasound μUS

The use of intraoperative imaging for neurosurgical applications has gained traction in recent years enabled by technological advances in neuronavigation. This is a major step forward towards improving surgical outcomes, as surgical neuronavigation bridges the gap between the assumed anatomical landscape based on preoperative imaging or surface anatomy, providing a real-time update of the surgical field. However, most available imaging modalities currently available (i.e. fluoroscopy, CT, MRI) are not designed for intraoperative use particularly with regards to size, sterility, and usability (i.e. exposure to radiation, magnetic field etc.). Further, most available modalities either provide merely a snapshot in time or expose the patient to additional radiation precluding true real-time dynamic imaging. Conversely, uptake of ultrasound in the operating theater is prevalent considering it provides real-time visualization beyond the surface anatomy without disrupting the surgical workflow or exposing the patient to additional radiation.

μUS differs from conventional ultrasound as it utilizes high energy, high frequency waves allowing for increased imaging resolution. Progress in the field of micro-ultrasound and the introduction of high frequency transducers have enabled the visualization of tissue at microscopic resolutions. The trade-off to improved spatial resolution is a resulting decrease in penetration depth. Whereas conventional probes deliver spatial resolution of 0.5 – 1 mm versus penetration depths greater than 100 mm, μUS delivers spatial resolution on the order of 15 – 100 μm with limited depth penetration up to 15 mm.[69] This advantage is obtained by using higher frequency ultrasound probes beyond the 3.5 – 12 MHz (central frequency) used in conventional ultrasound. The VevoMD Imaging platform, by Fujifilm Visualsonics, recently licensed by Health Canada and the FDA is a high-frequency clinical ultrasound system featuring B-mode, M-mode, Doppler mode and Power Doppler mode imaging. The VevoMD system improves on traditional ultrasound transducers which typically have central frequencies of below 10 MHz, conferring spatial resolutions ranging from 10 – 300 μm and focal depths of 17 mm, 9 mm and 5 mm respectively. Three ultrasound probes capable of imaging up to 1000 frames per

second have been designed with varying central frequencies (MD201;15MHz, MD400;30 MHz and MD700; 50 MHz).

The utility of μUS has been shown in a several studies encompassing arteriovenous fistula monitoring[70], pediatric vascular development[71], hand transplantation[72], and intima and medial thickening as predictive of a number of clinical conditions.[73 – 77] In the context of spine, where the bone is generally removed via laminectomy and the probe can be placed directly into the surgical exposure, utilization of these μUS probes will allow significant improvement in imaging resolution, facilitating visualization of structures below 100 μm. This will allow dynamic visualization of microscopic imaging features currently not seen using conventional ultrasound including white and gray matter tractography, neural networks, vascular networks, and tumour characteristics with micrometre resolution; a distinct advantage during neurosurgical procedures.

1.10 Navigated Intraoperative High Frequency Micro − Ultrasound

Navigated intraoperative ultrasound is well established in brain using optical tracking technologies to register ultrasound data to pre-surgical CT or MRI and track surgical tools during surgery (Figure 1.12).[78,79] This facilitates dynamic intraoperative imaging unattainable with traditional preoperative CT/MRI without exposing the patient to additional radiation. With regards to spine, intraoperative three-dimensional ultrasound has been used intraoperatively, establishing the feasibility of continuous, real-time tracking of spinal tumours during surgery and determining the location and size of the tumour.[78,80] Generally, the ultrasound probe is guided by an optical tracking device eliminating the need for registration to the pre-acquired CT or MRI during surgery.[78] However, clinical adoption of tracked intraoperative ultrasound for spinal tumour resection has been limited.[78,80] A number of possible reasons have been suggested including suboptimal contrast within the surgical field, limited spatial resolution, geometric con-

straints, and lack of clinical training.[81,82] Therefore, substantial opportunity exists for the integration of μUS into the operating theatre, capable of conferring micrometre spatial resolution and facilitating excellent discrimination between distinct types of tissues (i.e. gray matter, white matter, edema, etc.) in real-time.

1.11 Pre-clinical High Frequency Micro-Ultrasound

Feasibility of high frequency ultrasound imaging in porcine spinal cord was established using the VisualSonics pre-clinical ultrasound system Vevo 3100 and the precursor to the clinical VevoMD system. Ultrasound probes at 21 MHz and 40 MHz central frequencies were fixed to a linear stage to scan an excised porcine spinal cord. 3-Dimensional ultrasound images were reconstructed on the ultrasound system. Following image acquisition axial and longitudinal histological staining was performed on the spinal cord and representative images are shown (Figure 1.13).

1.12 Clinical Experience: Intraoperative Ultrasound

Case Studies

To date, we have performed seven surgeries with the goal of achieving spinal cord decompression. Three patients underwent navigated tumour debulking procedures and ultrasound images of the spinal cord were obtained for all patients. Four of the studies are included in the case report under submission comprising Chapter 6. The remaining three patient experiences are described below.
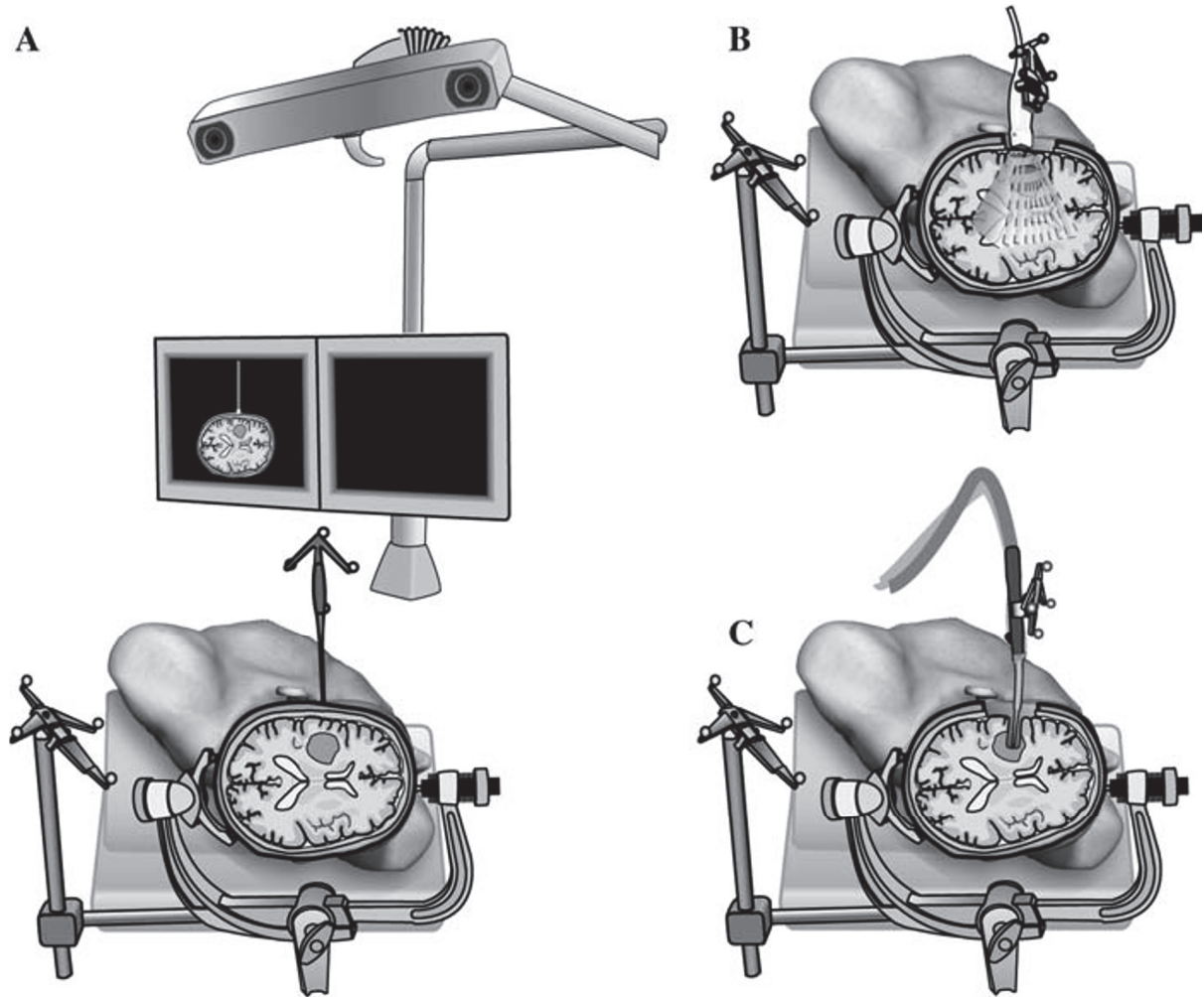
Figure 1.12: Intraoperative ultrasound: Ultrasound-based neuronavigation. (A) Navigated preoperative planning in the operating theatre using a tracked pointer. All surgical instruments are tracked by an optical camera system and the surgeon steers the instruments by looking at the navigation monitor to the left. (B) Freehand 3D ultrasound acquisition using a tracked ultrasound probe (real-time 2D ultrasound can be viewed on the right monitor). (C) Navigated resection using a tracked Cavitron Ultrasound Surgical Aspirator. Reprinted from the European Journal of Neurosurgery of with permission from Springer[80]
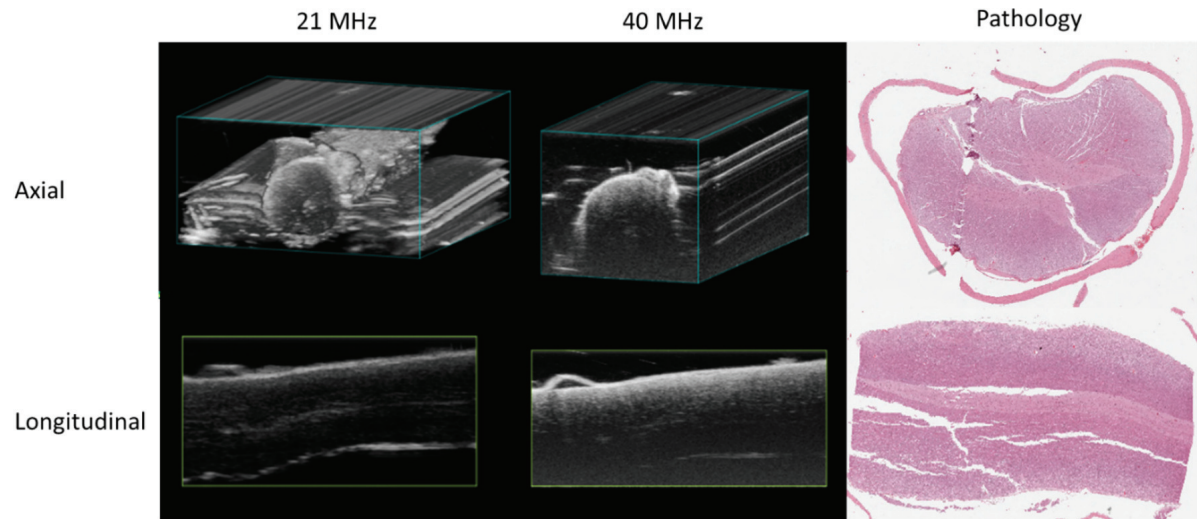
Figure 1.13: Axial and longitudinal high frequency micro-ultrasound images with central frequencies of 21 MHz and 40 MHz accompanied by representative pathological slides.

Patient 1

49 year old male experiencing T7 – T9 compression and fracture caused by a cystic expansile syrinx extending from T5 – T11. The patient was not diagnosed with malignant disease and was therefore not a candidate for radiation therapy. To achieve decompression the patient underwent surgical insertion of a cystoplueral shunt (Figure 1.14). Preoperative MRI was fused CT for navigation prior to surgery. The VevoMD system was brought to the operating theater under the Health Canada special access program. Axial and longitudinal ultrasound high frequency micro-ultrasound images were obtained intraoperatively at a central frequency of 30 MHz (Figure 1.15). Postoperatively patient symptoms improved due to the insertion of the shunt and drainage of the cyst. Postoperative changes are shown in Figure 1.14.

Patient 2

69 year old male with a diagnosis of metastatic thyroid cancer in the lumbar spine and hip having previously undergone fractionated radiotherapy (30 Gy/10 fractions to
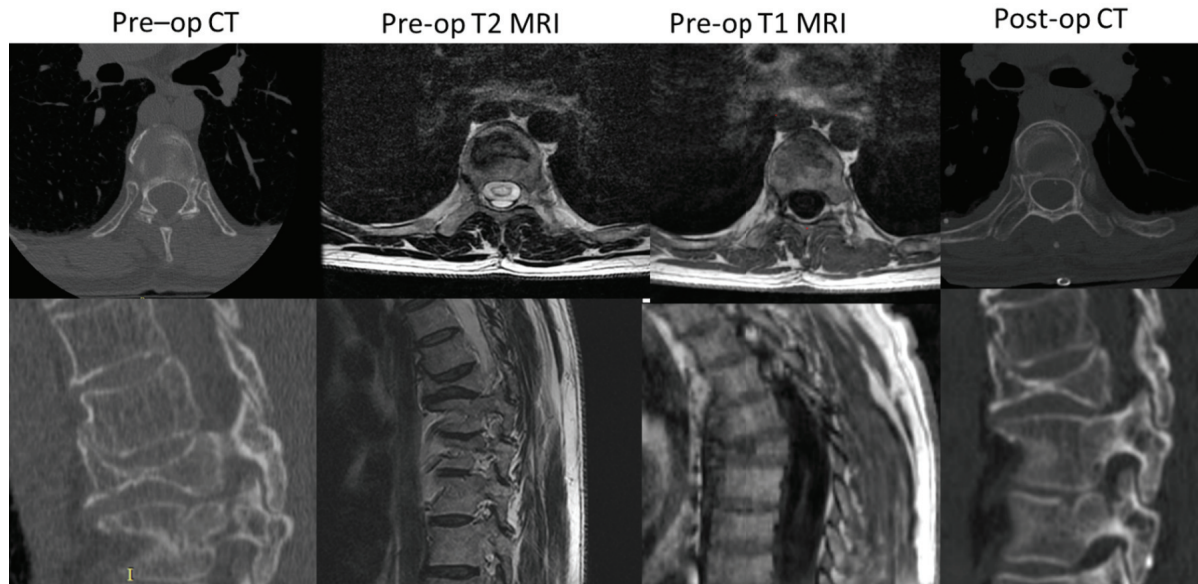
Figure 1.14: Patient 1: Clinical course – Patient with expansile cyst extending from T5 – T11 as visualized on axial and sagittal CT, T2-MR, and T1-MR. Postoperative changes seen on CT.

the spine and 8 Gy/1 fraction to the hip) and stereotactic body radiosurgery (30 Gy/4 fractions to the spine). Current presentation is T3 – T5, T12 – L3, and L4 – L5 metastases with epidural disease in contact with the spinal cord but not causing compression. The patient underwent pre-surgical CT and MRI of the cervical and thoracic spine and was identified as a candidate for separation surgery with subsequent stereotactic body radio-surgery since the primary tumour histology (thyroid) and presentation (bone metastases) were not amenable to local control. Patient underwent partial tumour embolization of the T5 metastasis prior to navigated T1 – T9 laminectomy with bilateral instrumented fusion three levels above and below the lesion (Figure 1.16 & 1.17). Pre-surgical contours of the spinal cord and epidural disease were drawn by a board-certified radiation oncologist to inform the surgeon of the clinical target. For the purposes of navigation, the MRI was fused to the CT prior to surgery. Unfortunately, the high frequency micro-ultrasound system was not available for this surgery.

During surgery, the patient experienced excessive bleeding because of the highly-
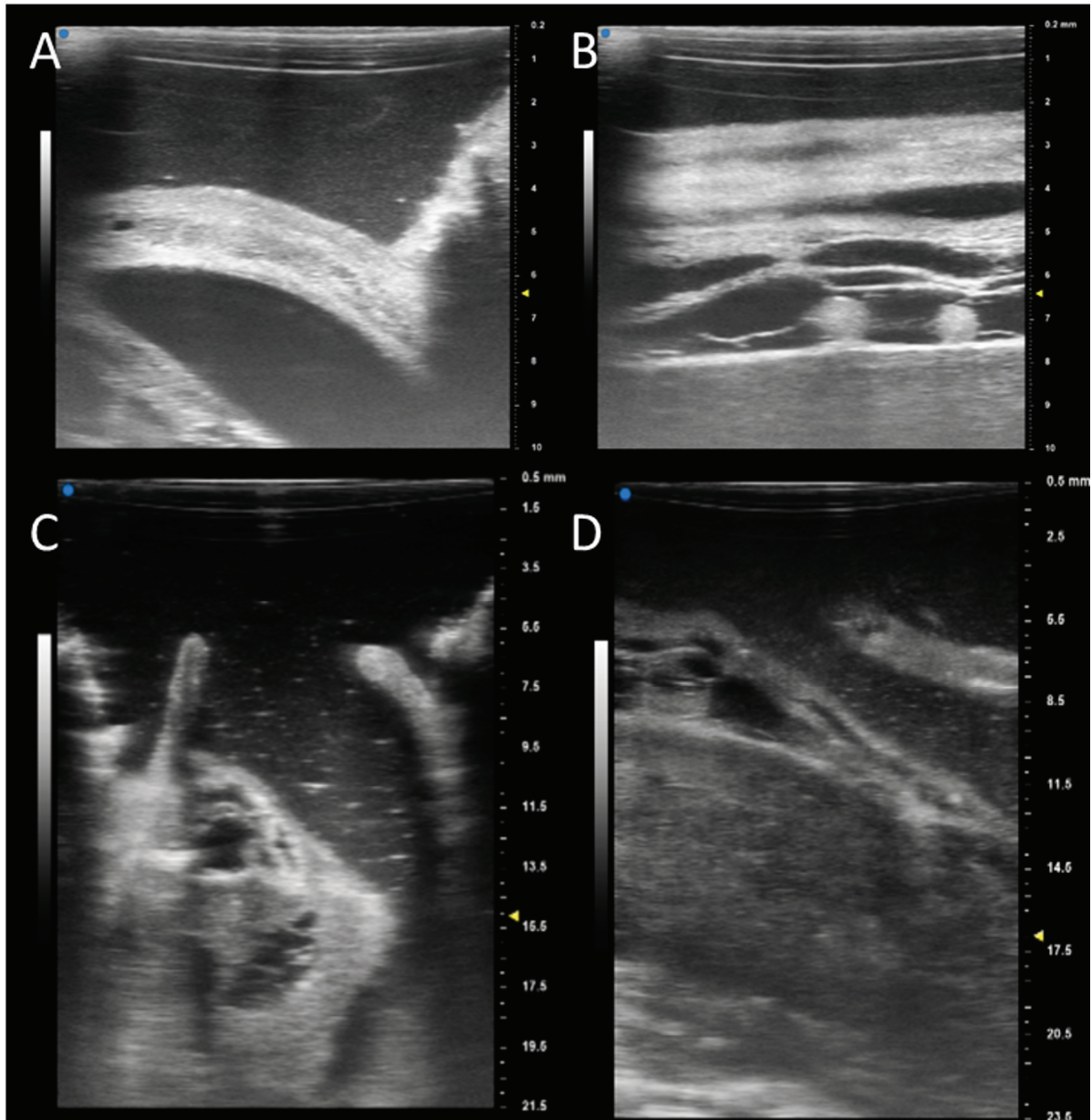
Figure 1.15: Patient 1: Intraoperative ultrasound – A,B) Axial and longitudinal intraoperative high frequency micro-ultrasound images acquired using a 50 MHz central frequency probe. Dura partially intact. C,D) Axial and longitudinal intra-operative high frequency micro-ultrasound images acquired using a 30 MHz central frequency probe. Dura has been removed. Note the trade-off in spatial resolution vs. depth as a function of frequency.
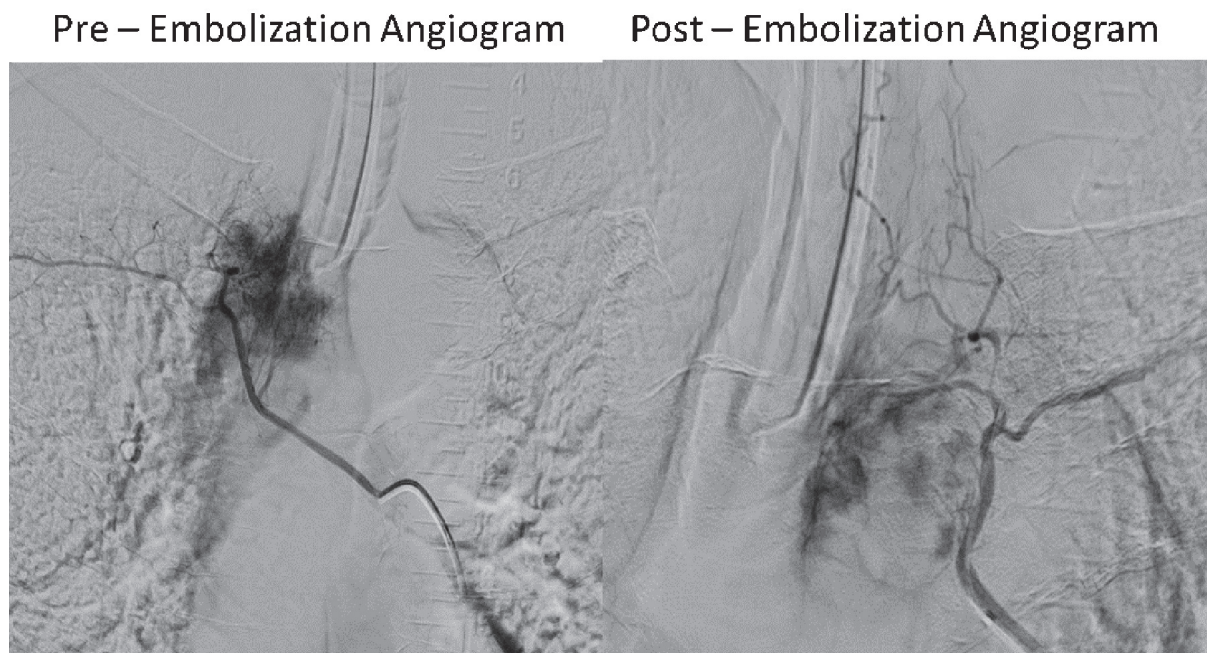
Figure 1.16: Patient 2: Preoperative embolization – Prior to tumour debulking with instrumented fusion, patient underwent partial tumour embolization. Left Panel: Angiogram shows lesion with flow prior to embolization. Right Panel: Angiogram shows partial embolization with reduced flow following procedure.
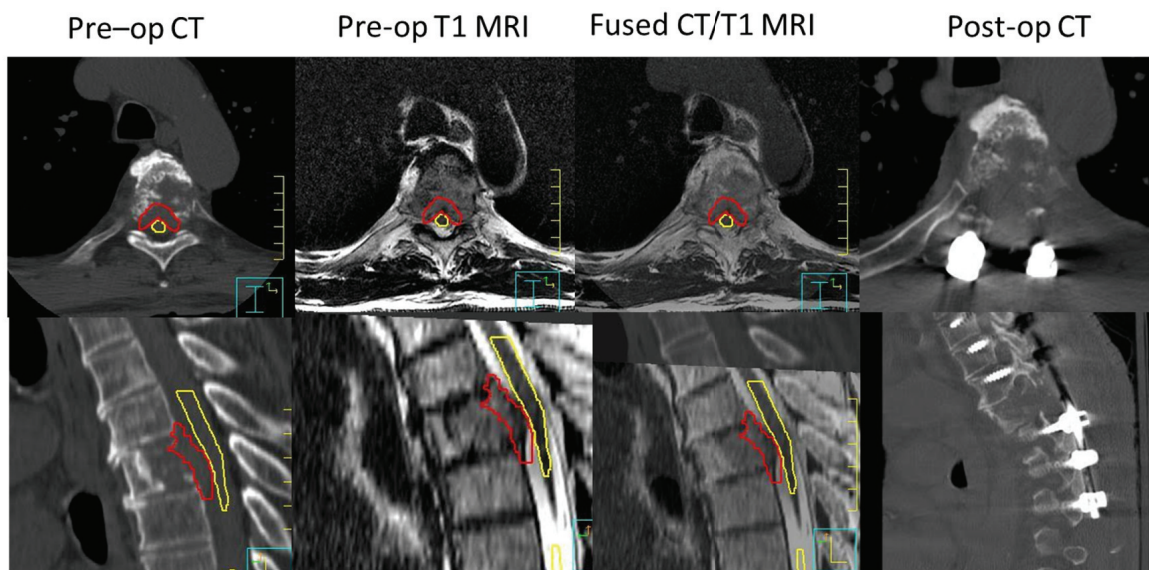
Figure 1.17: Patient 2: Clinical course – Patient with extensive epidural disease causing compression at T5. T1 MRI was fused to CT for navigation. Postoperative changes seen on CT with bilateral instrumented fusion 3 levels above and below and significant decompression achieved. Epidural disease (red) and spinal cord (yellow) were contoured.
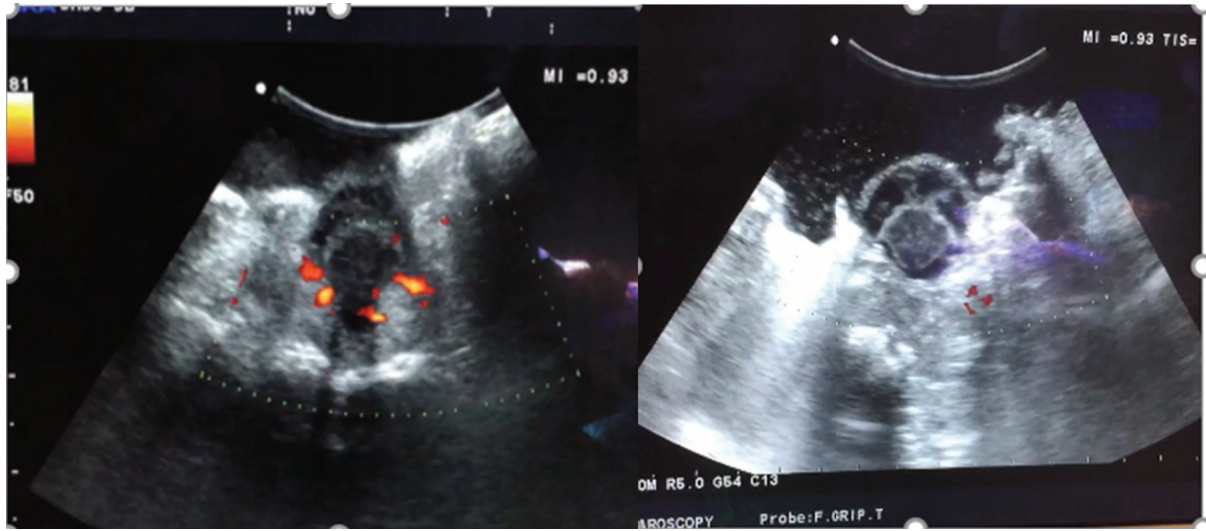
Figure 1.18: Patient 2: Doppler ultrasound images – Doppler ultrasound images show increased blood flow prior to tumour cauterization relative to images acquired post-cauterization. High frequency micro-ultrasound was not available.

vascularized lesion and partial embolization. Therefore, rather than excising the malignant tissue and disturbing the vasculature, the tumour was cauterized while monitoring the spinal cord to ensure safety. Surgical progress was measured using conventional Doppler intraoperative ultrasound to assess whether the tissue remained vascularized (Figure 1.18). One month following successful spinal cord decompression and tumour debulking the residual disease was treated with 30 Gy in 4 fractions.

Patient 3

58 year old female diagnosed with metastatic breast cancer ant T11 circumferential epidural disease (Bilsky score 3). Patient underwent a T8 – T11 bilateral instrumented fusion with laminectomy. Unfortunately, the high frequency micro-ultrasound system was not available for this surgery. During surgery, a sizable portion of the epidural disease was resected and excellent decompression was achieved (Figure 1.19). Surgical progress was measured using conventional intraoperative ultrasound to assess the extent of decompression. (Figure 1.20).
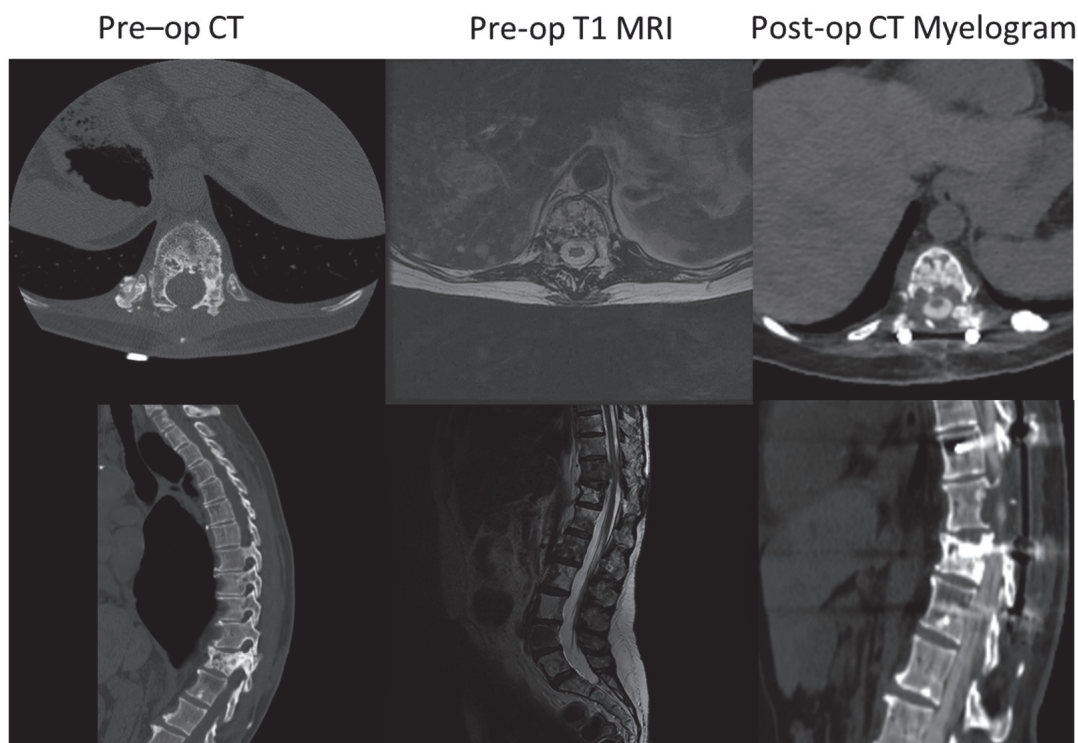
Figure 1.19: Patient 3: Clinical course – Patient with T11 circumferential epidural disease (Bilsky score 3). Preoperative CT and MRI show extensive epidural disease. Postoperative CT myelogram shows T8 – T11 bilateral instrumented fusion with laminectomy with reduction in tumour volume and definition of the spinal cord.

Postoperatively, the patient underwent a treatment planning MRI. While excellent decompression was recognized, significant artifact impeded visualization of the spinal cord. As such the patient required a CT myelogram for treatment planning purposes. One month following successful spinal cord decompression and tumour debulking, the residual disease was treated with 24 Gy in 2 fractions.

Our patient experiences have established feasibility of intraoperative navigated ultrasound. However, in practice a fully integrated navigated ultrasound/dose planning software package is necessary to ensure adoption. Work is currently underway to recognize those goals.
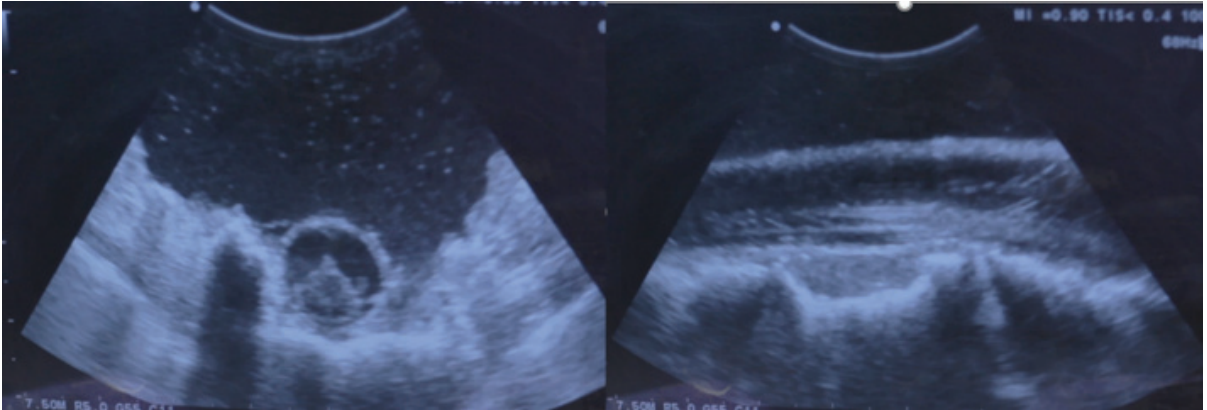
Figure 1.20: Patient 3: Intraoperative ultrasound – Representative ultrasound images acquired using conventional ultrasound.

1.13 Thesis Organization

The objective of this dissertation is to establish the feasibility of image-guided/ dosimetry guided spine separation surgery. Chapter 1 provides background information regarding the incidence and diagnosis of spine tumours and various treatment options (surgery, stereotactic body radiosurgery, combined spine separation surgery) as well as a description of the accuracy requirements of spine pedicle screw fixation, an insight into the accuracy of various neuronavigation systems and the current state of high frequency micro-ultrasound/navigated ultrasound technologies. Chapter 2 presents a study simulating the dosimetric advantage of incremental spine tumour resection entitled "Retrospective Analysis of Combined Surgical Resection with Radiation Treatment Planning of Spinal Tumours". Chapter 3 presents an analysis of the accuracy of the current benchmark surgical navigation systems for spine pedicle screw fixation and comprises a manuscript entitled "Spinal intraoperative three-dimensional navigation: correlation between clinical and absolute engineering accuracy." Chapter 4 presents an analysis of the accuracy of our experimental optical topographical imaging (OTI) navigation system in comparison to the current benchmark navigations systems entitled "High Speed, High Density Intraoperative 3D Optical Surface Topographical Imaging with Efficient Registration to MRI and CT for Craniospinal Surgical Navigation". Chapter 5 presents our initial experiences showing the feasibility of tracked high frequency micro-ultrasound imaging comprising a manuscript entitled "High Frequency Micro-Ultrasound (μUS) Imaging for Spinal Surgery: Initial Experiences. Chapter 6 summarizes and discusses the relevance of these results, presenting limitations and suggestions for future work.

1.14 Dissertation Objectives

Objective 1

The objective of this work is to evaluate the effect of incremental resection of epidural disease on dose. Although treatment failure has been attributed to underdosing of the epidural space and aggressive resection has been shown to improved local control, the relationship between the degree epidural disease resection and dose has yet to be investigated (i.e. how much epidural disease needs to be resected ensure adequate coverage.). This objective is achieved via a retrospective simulation study of ten patients having undergone spinal tumour resection with SBRT to determine the dosimetric advantage for each successive iteration of tumour debulking. This work is discussed in Chapter 2.

Objective 2

The objective of this work is to quantify the absolute application accuracy associated with surgical navigation, particularly for spine surgery. This work established the accuracy of surgical navigation using commercially available benchmark navigation system. This study also explores the correlation between application accuracy and clinical scoring. This work is discussed in Chapter 3.

Objective 3

The objective of this work is to quantify the absolute application accuracy associated with the OTI navigation device in spine and to compare performance with commercially available navigation systems. This objective was achieved by measuring the clinical accuracy, true screw trajectory and entry point error in the axial and sagittal planes using both the OTI navigation system and comparing to the currently available benchmark navigation systems. With regards to cranial applications this work also quantified the absolute application accuracy associated with the OTI navigation device in brain. Further, we established the accuracy in brain following the implementation of an active

calibration protocol to correct for camera drift and compared performance with and without active calibration. This work also quantifies workflow improvement of the OTI navigation device which has the potential to increase adoptobility of neuronavigation amongst surgeons. This work is discussed in Chapter 4.

Objective 5

The objective of this work is to establish the feasibility of image-guided high frequency micro-ultrasound during surgical resection of spinal tumours and the ability of separation surgery to improve surgical margins facilitating improved tumour dose margins while respecting the dose tolerances of the spinal cord. Although we have shown feasibility, this objective is a work in progress. Three patients have undergone tracked surgery. This work is discussed in Chapter 5.

Chapter 2

Surgical Resection with Radiation Treatment Planning of Spinal Tumors

This chapter simulates the dosimetric advantage of incremental spine tumour resection entitled "Retrospective Analysis of Combined Surgical Resection with Radiation Treatment Planning of Spinal Tumours." This work comprises a manuscript that has been submitted to Neurosurgery. The purpose of this chapter is to establish the dosimetric advantage of spine separation surgery on a millimetre by millimetre basis. This chapter provides the basis for the dissertation and is just cause for the extensive engineering analysis of neuronavigation in craniospinal surgeries presented in chapters 3 and 4. Raphael Jakubovic is the primary author for this publication.

This work is important, especially with regards to neurosurgery, as neurosurgeons often lack the requisite knowledge and context to grasp the effect of their surgical margins on the subsequent radiation treatment. This is not limited to spine separation surgery,

but is particularly important in spine where the extent of tumour resection has been shown to impact local control.[15] Therefore, it is imperative that the relationship between the extent of tumour resection and the dosimetric coverage of the disease in the epidural space be quantified so that the neurosurgeon can understand the surgical requirements. This work establishes that relationship, offering supplementary data that can be integrated into the surgical plan and potentially improve surgical outcomes.

The retrospective simulation study consists of 10 patients having undergone spine separation surgery prior to stereotactic body radiotherapy. Patients were included only if preoperative and postoperative/pre-treatment imaging were performed as part of the standard clinical care such that the simulation represented the radiation dose effect on the epidural disease component using the delivered treatment plan. Preoperative images were fused to postoperative, pre-treatment images within the treatment planning system facilitating assessment of the impact of incremental epidural disease resection in the context of the actual delivered radiation dose. A sample size of 10 was calculated to determine whether the correlation co-efficient differed from zero with $\alpha = 0.05$ (type I error), $\beta = 0.2$ (type II error), and an expected Pearsons correlation coefficient of 0.8. [84] Pearson's tests were performed to assess the relationship between amount of tissue resected and delivered radiation dose in a clinically meaningful manner.

Surgical Resection with Radiation Treatment Planning of Spinal Tumors

Raphael Jakubovic MSc[1,2], Mark Ruschin PhD[3], Ana Pejović-Milić PhD[1],Arjun Sahgal MD[3], Victor XD Yang PhD PEng FRCSC[1,2,4]

[1]Department of Physics, Ryerson University, Toronto, Ontario, Canada, M5B 2K3
[2]Department of Neurosurgery, Sunnybrook Health Sciences Centre, Toronto, ON, Canada, M4N 3M5
[3]Department of Radiation Oncology, Sunnybrook Health Sciences Centre, Toronto, ON, Canada, M4N 3M5
[4]Department of Electrical Engineering, Ryerson University, Toronto, Ontario, Canada, M5B 2K

Corresponding author:
Raphael Jakubovic MSc
Department of Biomedical Physics
Ryerson University
350 Victoria St. KHE 331
F Tel: 416-559-2414
Email: rjakubov@ryerson.ca

Conflict of interest, financial disclosures: There are no conflicts of interest to declare.

Significance of the Work This work is the first to quantify the dosimetric advantage of spine separation surgery. In the current clinical context, surgery and radiation treatment planning are performed independently and surgery is executed based on the clinical judgement of the operating surgeon without considering the dosimetric constraints of the spinal cord. Through this work, the relationship between tissue surgically resected and radiation dose has been established, facilitating pre-surgical dosimetric planning.

Abstract

Objective: The clinical paradigm for spinal tumours with epidural involvement is challenging considering the rigid dose tolerance of the spinal cord. One effective approach involves open surgery for tumour resection, followed by subsequent spine stereotactic body radiotherapy (SBRT). Resection extent is often determined by the neurosurgeon's clinical expertise, without considering optimal spine SBRT treatment. Working towards an approach that integrates radiotherapy planning within the operating room, the present study seeks to quantify the effect of incremental resection on tumour coverage in spine SBRT.

Methods: Ten patients having undergone spinal separation surgery with postoperative SBRT and planning including the entire vertebral body/epidural space were retrospectively reviewed. Preoperative diagnostic MRI was coregistered to postoperative planning CT to delineate the preoperative epidural disease gross tumour volume (GTV). The GTV was digitally shrunk by a series of fixed amounts away from the cord simulating incremental tumour resection. The dosimetric effect on simulated GTVs was analyzed using metrics such as minimum biologically effective dose (BED) to 95% volume (D_{95}) and compared to the unresected epidural GTV.

Results: Epidural GTV-D_{95} increased at an average rate of 0.89 ± 0.09 Gy per mm of resected disease for up to 6 mm. Mean D_{95} was 5.2 Gy (31.2%) larger than unresected case. D_{min} and D_{98}, D_{95}, and D_{50} showed strong positive correlations with increasing tumour resection margins (Adjusted R^2: $0.989 - 0.999$, $P < .01$).

Conclusion: Spine separation surgery provides division between the spinal cord and the epidural disease, facilitating better disease coverage for radiotherapy. By quantifying the dosimetric advantage of prior to surgery, targeted surgical planning can be implemented.

Running Title: Dosimetric Benefit of Spine Separation Surgery

Keywords: Radiation Dosimetry; Spine; Spine Separation Surgery; Stereotactic Body Radiosurgery; Surgery; Treatment Planning

2.1 Introduction

The prevalence of spinal metastases has been estimated to occur in over 50% of all cancer patients with $10 - 20\%$ presenting as clinically symptomatic.[7] Metastatic epidural spinal cord compression (MESCC) can arise from intradural, extramedullary metastases in the spine irrespective of any bony involvement.[9] In the United States this translates into approximately 20,000 new cases of MESCC annually.[5] With an aging demographic, increased survival due to more effective treatment of systemic cancers, and better detection of disease, incidence of spinal tumours is expected to rise dramatically.[7,9]

The goal of treatment for spinal tumours is to eradicate the tumour while sparing the surrounding normal tissue. This paradigm is a particular challenge with spine due to the rigid dose tolerances of the spinal cord and associated structures (i.e. thecal sac, cauda equine) and other organs-at-risk (i.e. kidneys, lungs, small bowel, and esophagus), which may result in tumour underdosing.[19] Further, aggressive tumour resection is not possible without inducing spinal instability. Therefore, an open surgery approach referred to as "separation surgery" is employed whereby the tumour is debulked and subsequently treated with stereotactic body radiotherapy (SBRT). This approach increases the margin between the spinal cord and the epidural disease, thus maximizing tumour coverage while reducing the dose to the spinal cord. Although the amount of tissue requiring resection can be estimated based on the extent of epidural disease, this has not been determined in a precise, systematic fashion as to facilitate optimal dosimetry in postoperative SBRT.

SBRT in spine presents a challenge to radiation oncologists and physicists, requiring a high degree of precision and accuracy due to dose constraints of the surrounding tissues and uncertainty introduced by interfraction and intra-fraction organ motion of $\approx$ 1.5 mm as quantified in our previous work.[84] Precision is of particular importance in spine SBRT as a theoretical 3 mm positioning error could potentially result in doubling of the dose delivered to the spine and increase the risk for radiation myelopathy.[30] As

such, typical SBRT plans are generated to maximize the dose gradient occurring from the
margin of the dose limiting structure (i.e. the cord) in order to maximally cover the tar-
get, while minimizing dose to the tissues at risk.[24,25] This is critical when considering
large dose fractions administered using SBRT at our institution (24 Gy/2 fractions, 30
Gy/4 – 5 fractions) as compared to conventional radiotherapy (8 Gy/1 fraction, 20 Gy/5
fractions or 30 Gy/10 fractions).[19, 23, 31] With the advent of technologies capable of
implementing image guided therapy, the use of SBRT has become more widespread due
to its association with improved local control and durable palliation.[41]

Surgical resection of epidural disease prior to SBRT is a logical approach considering
epidural disease progression has been identified as the predominant pattern of failure
after spine SBRT.[17, 34, 41] Surgery serves as an adjunct to SBRT by introducing a
buffer zone of 2 – 3 mm between the tumour and the spinal cord and downgrading the
extent of epidural disease, thus limiting dose to the surrounding tissue.[31, 85] While the
actual effect on the dose distribution has not been studied, this surgical approach with
SBRT has been shown to improve local control.[41,85,86] In this retrospective study and
review, we demonstrate the utility of spine separation surgery with respect to optimizing
dosimetry for spine SBRT with incremental epidural disease resection.

2.2   Methods

This retrospective study approved by our local institutional research board consisted
of a cohort of 10 patients having undergone spinal separation surgery with subsequent
planned stereotactic body radiotherapy (SBRT). Only patients that received pre- and
postoperative and magnetic resonance imaging (MRI) as part of their standard clinical
care were included. Patient demographics comprising tumour histology, age and gen-
der, as well as clinical grades, comprising Spinal Instability Neoplastic Score (SINS) and
Bilsky grading criteria were collected. Briefly, the SINS score assesses tumour related
instability from 0 – 18 based on lesion location, presence and frequency of pain, type
of pain (i.e. mechanical or non-mechanical), lesion characteristics (i.e. lytic, blastic, or

mixed), radiographic spinal alignment, presence and degree of vertebral body collapse and involvement of posterolateral spinal elements. Surgical consideration may be warranted for SINS greater than 7.[13] The Bilsky criteria is a validated 6 point epidural spinal cord compression grading system based on T2-weighted MRI, which has been shown to have high inter-rater and intra-rater reliability.[11] Briefly, the Bilsky grade ranges from 0 – 3, where 0 represents no epidural disease and 1a, 1b, and 1c represent epidural disease impingement, thecal sac deformation, and spinal cord abutment respectively. Bilsky score 2 and 3 represent epidural spinal cord compression without and without CSF effacement.[11]

Clinical Course: Radiation Treatment Planning

Treatment planning comprised CT simulation with slice thickness of 1 mm. Patients underwent thin slice axial T1 (2 mm slice thickness) and T2 volumetric MRI (3 mm slice thickness) focused on the treatment target and extending at least one vertebral body above and below the target. Rigid co-registration of the postoperative treatment planning MR to the postoperative treatment planning CT were performed, using a standard clinical treatment planning system (TPS) (Pinnacle3 v9.2, Philips, Philips Healthcare, Andover, USA). Co-registration was performed manually within the clinical software by aligning the bone-soft tissue interface of the target and adjacent vertebral bodies on MRI to the bony anatomy as visualized on CT. The alignment of the intervertebral space was also considered. Each clinical co-registration was confirmed by the treating radiation oncologist prior to contouring. Gross tumour volumes (GTV) and clinical target volumes (CTV) were contoured by a board certified radiation oncologist. The planning target volume (PTV) comprised the CTV plus a 2 mm uniform expansion. The goal of dose prescription was to maximize the dose to the GTV, CTV, and PTV while minimizing organ at risk (OAR) dose to the spinal cord, esophagus, bowel, liver and kidneys.[87]. In the presence of poor image quality associated with hardware associated artifacts on MRI, a CT myelogram was performed to adequately visualize the spinal cord and associated structures. All patients were treated at our institution with the dose prescriptions based on the discretion of the treating physician and consistent with previously

described guidelines for postoperative/retreatment patients.[19,37,88] Patients were typically treated with 24 Gy in 2 fractions to the PTV with a max point dose tolerance of 17 Gy to the spinal cord PRV. Patients undergoing repeat radiotherapy due to treatment failure were typically treated with 30 Gy in 4 fractions with a max point dose tolerance of 16.2 Gy to the spinal cord PRV. Treatment was delivered via 9 beam intensity modulated therapy (IMRT) with 9 or 11 beam field geometries, or in the case of localized thoracic-lumbar spine vertebra (i.e. one or two levels) and PTV volumes > 40 cc, via dual arc volumetric arc therapy (VMAT).

Retrospective Review: Radiation Treatment Planning

For the purpose of this retrospective study, the preoperative T1 and T2 MRI were fused to the postoperative treatment planning CT using the aforementioned TPS. Following fusion, epidural disease gross tumour volume (Epidural-GTV) and spinal cord planning organ at risk volume (PRV) were contoured by a board-certified radiation oncologist (CLT). Incremental 1 mm contours representing incremental tumour resection up to from 1 – 6 mm were generated to simulate the effect of incremental epidural disease resection. The dose contours were modelled after the surgical approach whereby the surgeon would begin resection at the cord-epidural disease interface with the sole objective to create separation between the spinal cord and the epidural disease as shown in Figure 2.1. Typically, the goal of the surgery is to create a 2 – 3 mm barrier between the disease and the spinal cord allowing for the delivery of high dose of radiation to the target. Generally, this is achieved via laminectomy with instrumented fusion to maintain spinal stability and the epidural disease is resected circumferentially. Although typical surgical margins achieved in spine separation surgery are 2 – 3 mm, exaggerated contours were simulated to evaluate the dosimetric effect of aggressive surgical resection.

The dose volume histograms (DVH) for the simulated resected GTV were generated within the clinically delivered treatment plan. Specifically, the following metrics were extracted from the DVH for each case: D_{min} (minimum dose to the region of interest), D_{98} (dose to 98% of the regions of interest), D_{95}, and D_{50} for epidural-GTV. Biological effec-
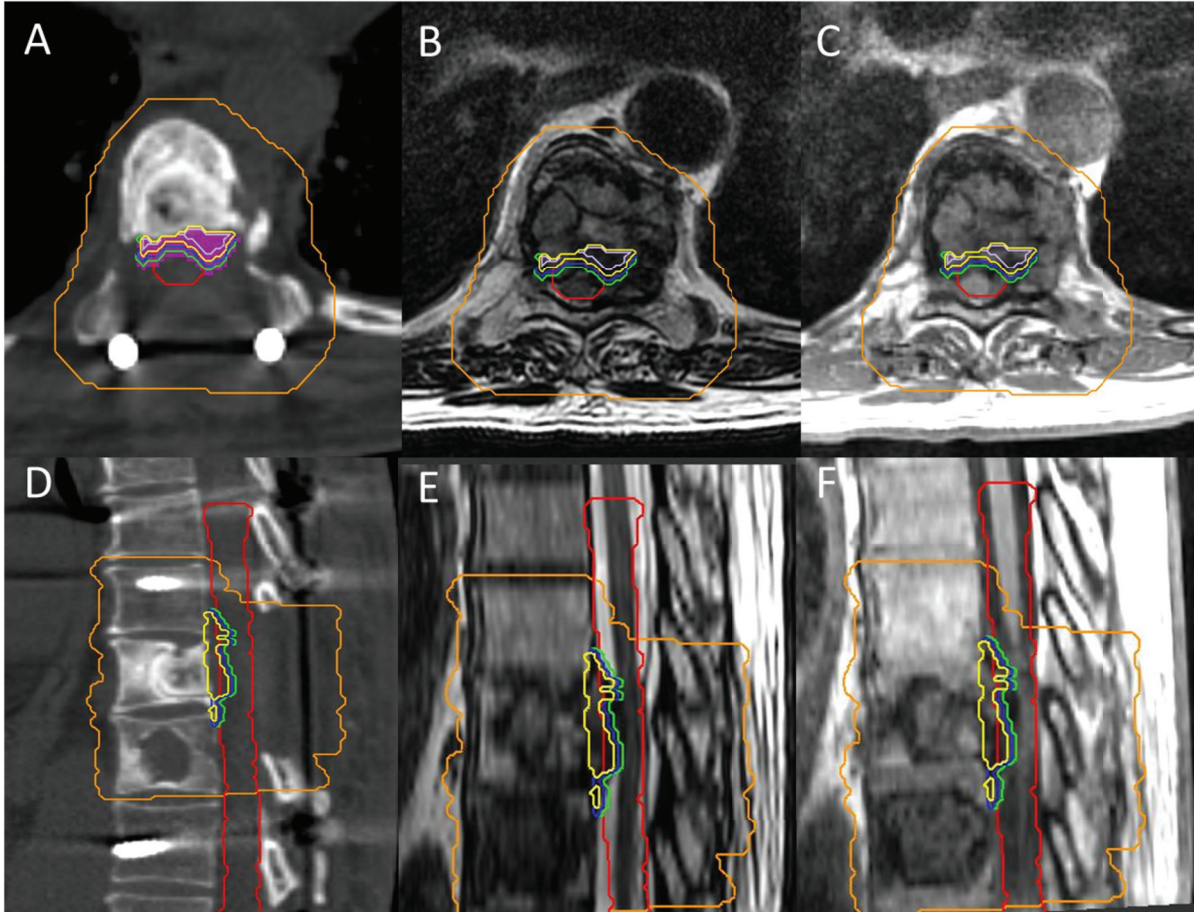
Figure 2.1: Post-surgical Dose Distribution: T9 vertebral body post laminectomy and cord decompression/tumour resection. A,D) Axial and sagittal CT image of the vertebral body with bilateral inserted pedicle screws. Planning target volume encompasses entire vertebral body (orange). Outline of the spinal cord shown in red with epidural-GTV (purple colorwash) and incremental millimeter epidural disease contours (green – 1 mm, blue – 2 mm, yellow – 3 mm, lavender – 4 mm). B,E) T2 MRI image used for fusion and epidural disease contouring. C,F) T1 MRI image used for fusion and epidural disease contouring.

tive dose (BED) was calculated for each metric using α/β equal to 10 for diseased tissue and 2 for the spinal cord late toxicity as published previously.[88,89] A best line linear fit was applied to each set of dosimetric data as a function of resection amount. Pearson's correlations were performed evaluating the relationship between degree of epidural

Patient #	1	2	3	4	5	6	7	8	9	10
Age	62	69	57	57	70	46	70	67	59	58
Gender (M/F)	F	M	F	F	F	M	M	M	M	F
Tumour Histology (%)	Lung	Renal Cell	Breast	Breast	Renal Cell	Renal Cell	Thyroid	Rectal	Squamous Cell	Breast
Prescribed Radiation Dose /Fractions (Gy)	30/5	24/2	24/2	30/4	24/2	30/4	28/2	24/2	25/5	30/5
Prescribed BED (Gy)	48	52.8	52.8	52.5	52.8	52.5	67.2	52.8	37.5	48
Epidural Disease Volume (cm^3)	5.93	4.64	1.60	6.44	4.63	0.64	5.64	3.61	6.39	3.54
Max Radiation Dose to Cord PRV (Gy)	18.6	12.2	12.0	18.1	12.2	16.3	14.6	14.6	13.5	21.8
Max BED to Cord PRV	61.8	49.4	48.0	59.1	49.4	49.5	67.9	67.9	31.7	69.3
Baseline SINS	NA	1	4	8	12	10	NA	NA	NA	NA
Bilsky Grade	NA	2	1C	2	3	1B	NA	2	1C	NA

Table 2.1: Baseline tumour and patient characteristics for 10 patients undergoing spine separation surgery with subsequent stereotactic body radiotherapy.

disease resection and dose for all dosimetric variables. All analyses were performed using SPSS statistics (Version 24; IBM, Chicago, IL, USA). P < .05 was considered significant.

2.3 Results

Baseline tumour and characteristics of the 10 patients reviewed in the present study are summarized in Table 2.1. Four patients were treated with 24 Gy in 2 fractions, two patients were treated with 30 Gy in 4 fractions, and two patients were treated with 30 Gy in 5 fractions. The remaining patients were treated with varying fractionation schemes based on the attending physician's discretion as indicated in Table 2.1. Mean epidural disease volume was 4.16 ± 2.04 cm^3. The mean minimum absolute dose to the epidural GTV of all patients treated with 24 Gy/2 fractions was 9.1 ± 1.5 Gy with a corresponding mean absolute dose of 14.9 ± 1.9 Gy. Epidural GTV in patients receiving 30 Gy/4 fractions had mean minimum absolute dose of 12.1 ± 1.3 Gy with a corresponding mean absolute dose of 17.8 ± 1.7 Gy.

Epidural Gross Tumour Volume and Incremental Dose Margins

The dosimetric data for the epidural disease and each incremental resection margin are shown in Table 2.2. Increased BED coverage of the epidural-GTV was recognized ranging from 3.8 Gy ($\approx$0.6 Gy per millimetre) for D_{min} to 7.8 Gy ($\approx$1.3 Gy per millime-
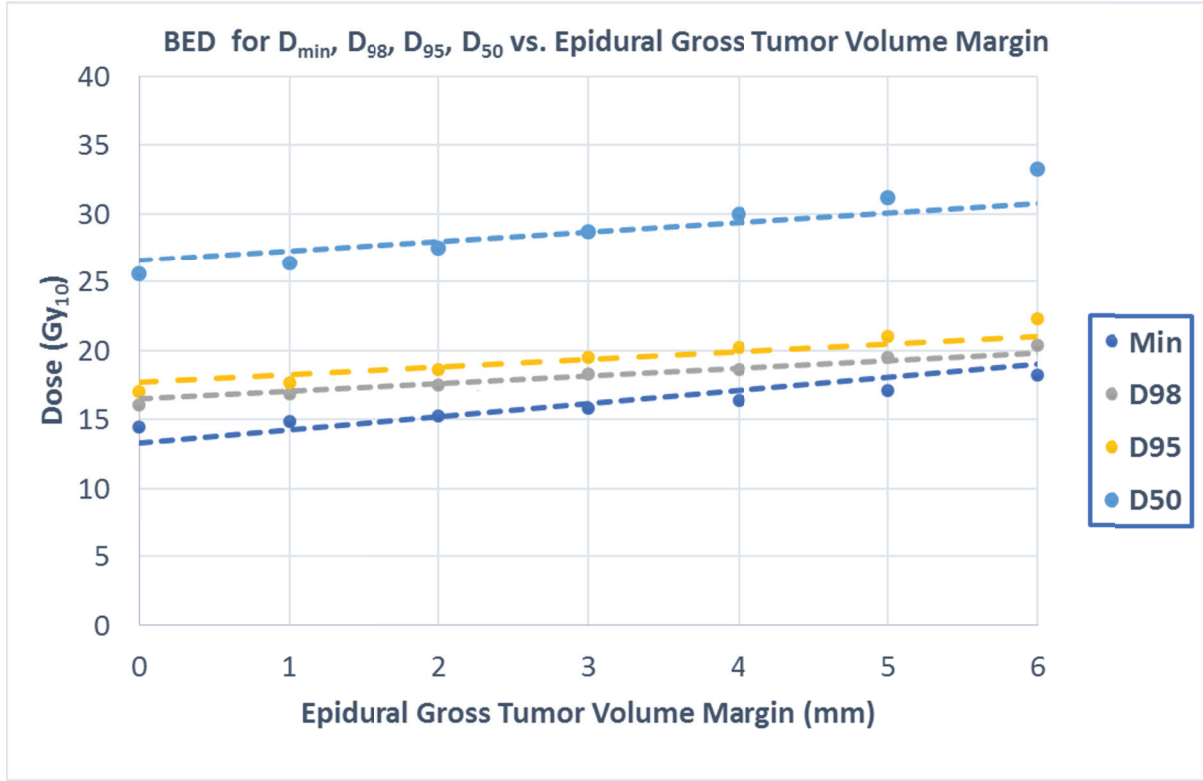
Figure 2.2: BED to D_{min}, D_{98}, D_{95}, D_{50} as a function of millimetre epidural-GTV margins. Linear increases in all parameters with greatest impact on D_{50}.

tre) for D_{50}. Diminishing dosimetric returns were seen with increased tumour debulking beyond 6 mm due to sufficient separation between the epidural disease component and the spinal cord or a minimal residual epidural disease component. All dosimetry metrics exhibited strong positive correlations with increasing tumour resection margins (Adjusted R^2 - 0.989 – 0.999, P < 0.01). BED to D_{min}, D_{98}, D_{95}, D_{50} as a function of millimetre epidural-GTV margins are shown in Figure 2.2. Absolute and percent dose characteristics for all patients are shown in Figure 2.3.
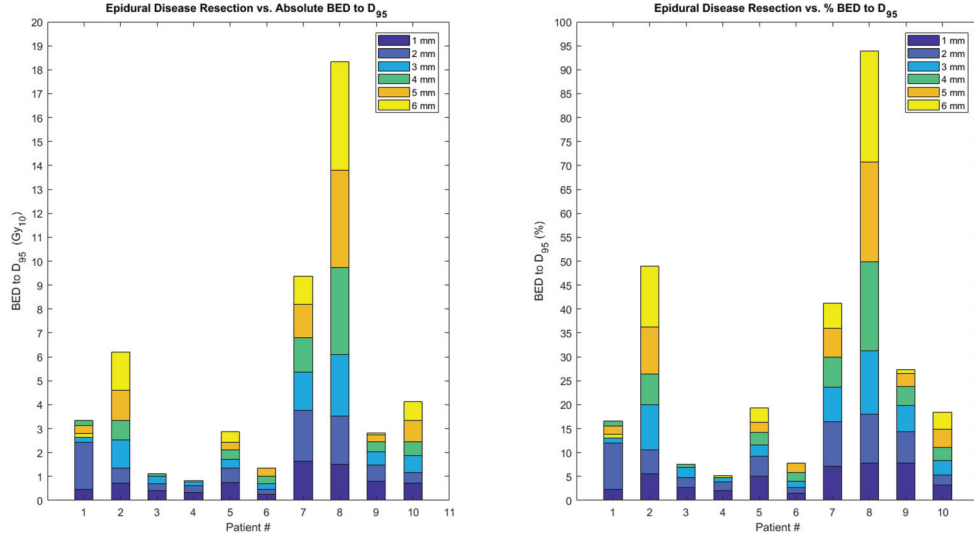
Figure 2.3: Absolute BED to D_{95}(left panel) and % BED to D_{95}(right panel) characteristics for all 10 patients from zero resection to 6 mm resection using simulated 1 mm incremental tumour resection contours.

2.3.1   Representative Study

Patient #1 was a 68-year-old male with multiple osteolytic metastases in the lumbar and thoracic spine including a large T9 lesion extending into the spinal canal and causing cord compression. Primary histology was renal cell carcinoma. Due to vascularity of the T9 lesion the patient underwent a successful embolization prior to laminectomy with bilateral instrumented T8, T11, and T12 fusion with tumour resection. Follow up treatment planning MRI shows nearly complete decompression of the tumour at T9 approximately 1 month after surgery. Patient then underwent SBRT with a PTV prescribed to the entire T9 and T10 vertebral bodies. Treatment planning was performed using the donut configuration described previously by al Omair and colleagues with a dose prescription of 24 Gy in 2 fractions with a max point dose tolerance of 17 Gy to the spinal cord.[41] The BED to D_{min} for the PTV was 15.1 Gy with a corresponding mean dose of 53.4 Gy. At 1 year follow-up MRI, no interval changes were noted and the T9 lesion was classified as stable disease. The epidural-GTV and incremental dose volumes for Patient #1 are shown in Figure 2.1. Increased dose coverage of the epidural-GTV

	$\text{BED} - \text{D}_{min}$ (Gy)	$\text{BED} - \text{D}_{98}$ (Gy)	$\text{BED} - \text{D}_{95}$ (Gy)	$\text{BED} - \text{D}_{50}$ (Gy)
Epidural GTV	14.5	16.1	17.0	25.6
Epidural GTV – 1mm	14.9	16.9	17.7	26.4
Epidural GTV – 2 mm	15.3	17.5	18.6	27.5
Epidural GTV – 3 mm	15.8	18.3	19.5	28.7
Epidural GTV – 4 mm	16.4	18.6	20.2	30.0
Epidural GTV – 5 mm	17.1	19.5	21.0	31.2
Epidural GTV – 6 mm	18.2	20.4	22.3	33.3
Overall Absolute Dose Increase (6 mm)	3.8	4.3	5.3	7.7
Overall % Dose Increase (6 mm)	25.9	26.6	31.2	30.2
Absolute Dose Increase per mm	0.63	0.72	0.89	1.30
% Dose Increase per mm	4.3	4.4	5.2	5.0
R^2	0.983	0.998	0.998	0.992
P Value	$<.01$	$<.01$	$<.01$	$<.01$

Table 2.2: BED for D_{min}, D_{98}, D_{95}, and D_{50} for the epidural-GTV and simulated incremental tumour resection margins.

was recognized ranging from 3.8 Gy (0.6 Gy per millimetre) for D_{98} and 7.8 Gy (1.1 Gy per millimetre) for D_{50}. Dose volume histograms representing the normalized contour volume and absolute epidural disease volume vs. dose are shown in Figure 2.4.
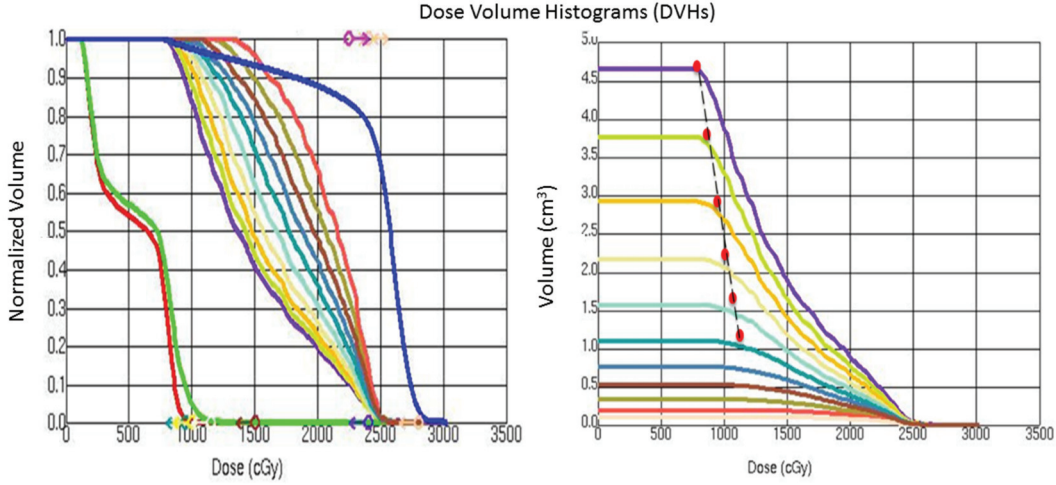
Figure 2.4: Dose volume histograms for Patient 1: Left Panel: Normalized Contour Volume vs. Dose for Cord (Red), Cord PRV (Green), incremental epidural GTV (Purple Orange), and PTV (Blue). Cord and Cord PRV limited to < 1000 cGy. Epidural disease contours show DVH shift from left to right from ≈ 1500 cGy to ≈ 2200 cGy with increasing tumor resection margins indicating increase in deliverable dose. Right Panel: Actual contour volume vs. Dose for incremental epidural GTV. Epidural disease shows DVH shift from left to right with decreasing epidural disease volume indicating increase in deliverable dose.

2.4 Discussion

With this work, we established a definitive relationship between the extent of tumour debulking in spine separation surgery and increased dose coverage of the epidural disease. This data has the potential to change the practice, as the current surgical paradigm does not appreciate the impact of surgical resection on the dosimetric coverage of the target. Further, with the extended survival in patients with metastatic disease secondary to improved systemic therapy, there is a need to optimize the management of patients with spinal metastases. By combining a limited surgery with stereotactic radiosurgery, we can minimize exposure to the surgical wound to decrease complication rates and op-

51

timize local control while sparing the spinal cord from the high radiation dose.[19] This relationship between epidural disease debulking and local control following radiosurgery is highlighted and, when optimal, local control rates of 90% are acheivable.[1, 41] It is plausible to suggest that the increase in local control seen in conjunction with spine separation surgery shown previously by Al-Omair et al.[15] can be attributed to the increase in dose to the epidural disease shown in this work.

Considering that underdosing of the epidural disease has been identified as a possible mode of treatment failure[34], spine separation surgery to remove part of the epidural disease and allow for increased dose coverage is a logical approach. This is intuitive as the spinal cord constraint is rigid, and the dose delivered to the spinal cord is maximized. In this regard, spine SBRT is unique, as conventionally the objective of the dose prescription is to minimize the dose to the OAR rather than to maximize dose to a certain dose tolerance of the organ. Therefore, for spine SBRT when the dose prescription is 24 Gy in 2 fractions and the spinal cord is limited to 17 Gy, the treatment plan is designed to maximize the dose to the spinal cord up to 17 Gy with the secondary objective of maximizing dose prescription coverage to the PTV.[90,91]

As presented in this work, the improvement in dose coverage in the case of a 6 mm tumour debulking is substantial with an increase in BED for D_{min} of ≈ 4 Gy. While these gains appear to be modest, considering a 24/2 Gy regime representing a 52.8 Gy BED, they constitute a mere 1/13 of the total prescribed dose. Therefore, there is reasonable cause that this dose increase could have a profound clinical impact on local control. Specifically, this dose increase in BED ≈ 4 Gy will modify the mechanism of cell damage as it shifts from direct cell death to indirect cell death, which is related to vascular damage via ceramide mediated apoptosis with the delivery of a single 10 Gy dose fraction.[92,93] This is supported by the previous work of our group[94] establishing a relationship between irradiation of the tumour and vascular changes following treatment using MR perfusion and permeability particularly beyond a threshold of 10 Gy in a single fraction.

Previous studies have shown the distinct advantage of spine separation surgery by providing a distinctive barrier between the radiosensitive spinal cord and the gross tu-

mour volume. This approach facilitates improved SBRT by downgrading the extent of epidural disease and, thus, improving local control when compared to SBRT alone or conventional external beam radiotherapy.[24,41] Work by Lovelock et al.[95] and Kumar et al.[96] have shown a correlation between D_{min} and local failure for doses of <15 Gy in 1 fraction and <23.1 Gy in 3 fractions, but little work has been done with regards to establishing the dosimetric impact of spine separation surgery, aside from the expected 10% dose escalation per millimetre of resected tissue.[97] Further, the importance of millimeter precision has been established as a 3 mm positioning error would result in doubling of radiation dose.[30] Our work builds on the prior studies by establishing a definitive dose-resection relationship ranging from 4.3% to 5.2% per millimeter which can inform the surgeon about the extent of surgical decompression required.

The current study is subject to limitations. First, use of a preoperative MRI for delineation of the spinal cord and epidural-GTV fused to a postoperative, pre-treatment CT image is not ideal, particularly in the presence of artifacts attributed to the insertion of surgical hardware and significant anatomical changes attributed to the surgery (i.e. bone removal, tumour debulking etc.).[98, 99] Further, as the spinal cord undergoes decompression, the location of the spinal cord is expected to shift over time and, therefore, the geometric constraints of the cord applied preoperatively are no longer valid. While care can be taken to maintain separation between the cord and the epidural disease by packing the surgical cavity, geometric limitations remain. This cord shift has not been quantified within the context of this study, but previous studies have correlated the extent of decompression, as indicated by the space available for the spinal cord (s/c ratio)[97], with spinal cord posterior shift following laminoplasty in cervical spine.[100] As well, although the dosimetric effect was apparent, the advantage of spine separation surgery may not be impactful in the presence of limited tumour volume or where the epidural disease component is not directly touching the spinal cord (i.e. Patient #3 and #6; Figure 2.3). In contrast, greater benefit was seen in patients with extensive epidural disease (Patient # 8). Therefore, it is crucial that the dosimetric benefit of surgery be provided to the surgeon such that the post-surgical radiotherapy can inform the surgical course.

In conclusion, this retrospective work and review has the potential to further inform

surgical planning in the context of separation surgery, particularly for spinal metastases, a hard to treat cancer where patients have limited life expectancy. Just as important, is the ability to limit the operation once decompression and space generation between tumour and the spinal cord is achieved. The challenge lies in knowing in real time as the decompression is being carried out, if sufficient resection has been performed to optimize the radiosurgery delivery. At present the surgeon is blind to this aspect and having the dosimetry information present may limit the morbidity of the operation by limiting the extent of surgery. This work establishes the dosimetric relationship and is an incremental step forward towards the incorporation of radiation dose planning with surgical planning for spinal tumour resection.

Chapter 3

Application Accuracy of Spinal Intraoperative Three Dimensional Navigation

This chapter evaluates the accuracy of spinal intraoperative, three-dimensional navigation entitled "Spinal intraoperative three-dimensional navigation: correlation between clinical and absolute engineering accuracy." This work builds on the previous chapter, which established the utility of achieving sub-millimetre accuracy during spine separation surgery. This premise is based on the dosimetric advantage conferred by creating a buffer zone between the spinal cord and the epidural disease. This work quantifies the clinical application accuracy of benchmark navigation systems and therefore paves the way towards intraoperative dose guided surgery. This work comprises a manuscript that has been published in The Spine Journal. The manuscript has been included in the dissertation consistent with the guidelines of the publisher. Raphael Jakubovic is a co-first author for this manuscript. Raphael's contribution to this work includes the engineering analysis, co-ordination of the clinical analysis and preparation of the manuscript. Dai-

payan Guha was responsible for the clinical components of the work, assisted with the engineering analysis and prepared the manuscript. The manuscript has been adapted to conform with Ryerson University School of Graduate Studies regulations.

This retrospective review of a prospectively comparative trial comprising 30 patients and 209 inserted cervical, thoracic, lumbar, or sacral screws, evaluates the clinical and engineering accuracy of the commercially available 3D computer assisted navigation devices used for spine surgery. Patients were included in the retrospective review if preoperative and postoperative CT images were acquired at a slice thickness of 0.625 mm. Established clinical classification methods (Heary or 2 mm) were performed for all inserted screws for comparison to engineering accuracy data.[51, 101] Screw placement was graded by five independent reviewers using the Heary grading system and four independent reviewers using the 2 mm grading criteria. Absolute navigation error was quantified based on previously established methodologies by Mathew et al. and Kotani et al., to account for anatomical changes pre- and post-surgery.[63,102] Further explanation of the absolute error quantification is described within the manuscript.

With regards to the analysis, a variety of statistical tests were performed. To assess clinical accuracy of screw placement both the Heary grading system and the 2 mm grading criteria were employed. Inter-rater reliability was measured using the intraclass correlation coefficient (ICC) to evaluate consistency amongst raters and to highlight differences between specialties (i.e. surgeons vs. radiologists) as previously described by Shrout et al.[103] As mentioned in the the manuscript ICC values between 0.60 and 0.74 reflect of moderate agreement, 0.75 to 0.89 good agreement, and 0.90 – 1.00 excellent agreement.[103] An average measures ICC is applicable for evaluation of ordinal variables and appropriate for a fully crossed rater design where each rater rated all screws. Categorical data (i.e. clinically acceptable vs. poorly place screws) was evaluated using a Fisher's exact test and comparisons between paired categorical data (i.e. Heary vs. 2 mm grading scales) was assessed by the McNemar-Bowker test for marginal homogeneity.[104,105] A Fisher's exact test was selected to compare frequencies of categorical data where expected counts may be small (i.e. few poorly graded screws). Further, correlation between absolute navigation error and clinical grading, as well as, between signed translational and angular errors were compared using genarized linear models to assess

agreement between clinical grading and engineering accuracy and to validate our hypothesis of surgical compensation in the presence of entry error. Generalized linear models are appropriate for both continuous and categorical data with continous or dichotomous dependant variables. These statistical tests quantify the clinical application accuracy of the currently available commercial navigation systems with actual clinical context, establishing a benchmark for the novel optical topographical imaging navigation system discussed in Chapter 4.

Spinal intraoperative three-dimensional navigation: correlation between clinical and absolute engineering accuracy

Diapayan Guha MD[1,2,3*], Raphael Jakubovic MSc[3,4*], Shaury Gupta[3], Naif M. Alotaibi MD[1,2], David Cadotte MD PhD[1], Leodante B. da Costa MD[1], , Rajeesh George MBBS MS[5], Chris Heyn MD PhD[6], Peter Howard MD[6], Anish Kapadia MD[7], Jesse M. Klostranec MD PhD[7], Nicolas Phan MD[1], Gamaliel Tan MBBS FRCS[5], Todd G. Mainprize MD[1], Albert Yee MD MSc[8], Victor X.D. Yang MD PhD PEng[1,2,3,9]

[1] Division of Neurosurgery, Department of Surgery, University of Toronto. Toronto, ON, Canada

[2] Institute of Medical Science, School of Graduate Studies, University of Toronto. Toronto, ON, Canada

[3] Biophotonics and Bioengineering Laboratory, Sunnybrook Health Sciences Centre. Toronto, ON, Canada

[4] Department of Biomedical Physics, Ryerson University. Toronto, ON, Canada

[5] JurongHealth, Ng Teng Fong General Hospital. Singapore, Singapore.

[6] Division of Neuroradiology, Department of Medical Imaging, Sunnybrook Health Sciences Centre. Toronto, ON, Canada

[7] Department of Medical Imaging, University of Toronto. Toronto, ON, Canada

[8] Division of Orthopedic Surgery, Department of Surgery, University of Toronto. Toronto, ON, Canada

[9] Department of Electrical and Computer Engineering, Ryerson University. Toronto, ON, Canada

*Authors have contributed equally to this work and hold joint first authorship

Abstract

Background Context: Spinal intraoperative computer assisted navigation (CAN) may guide pedicle screw placement. CAN techniques have been reported to reduce pedicle screw breach rates across all spinal levels. However, definitions of screw breach vary widely across studies, if reported at all. The absolute quantitative error of spinal navigation systems is theoretically a more precise and generalizable metric of navigation accuracy. It has also been computed variably, and reported in fewer than a quarter of clinical studies of CAN guided pedicle screw accuracy.

Purpose: To characterize the correlation between clinical pedicle screw accuracy, based on postoperative imaging, and absolute quantitative navigation accuracy.

Study Design/Setting: Retrospective review of a prospectively collected cohort.

Patient Sample: 30 patients undergoing first-time posterior cervical/ thoracic/ lumbar/ sacral instrumented fusion $\pm$ decompression, guided by intraoperative three-dimensional CAN.

Outcome Measures: Clinical/radiographic screw accuracy (Heary and 2 mm classifications); absolute quantitative navigation accuracy (translational and angular error in axial and sagittal planes).

Methods: We reviewed a prospectively collected series of 209 pedicle screws placed with CAN guidance. Each screw was graded clinically by multiple independent raters using the Heary and 2 mm classifications. Clinical grades were dichotomized per convention. The absolute accuracy of each screw was quantified by the translational and angular error in each of the axial and sagittal planes.

Results: Acceptable screw accuracy was achieved for significantly fewer screws based on 2 mm grade vs. Heary grade (92.6% vs. 95.1%, p $=$ 0.036), particularly in the lumbar spine. Inter-rater agreement was good for the Heary classification and moderate for the 2 mm grade, significantly greater among radiologists than surgeon raters. Mean abso-

lute translational/angular accuracies were 1.75mm/3.13° and 1.20mm/3.64° in the axial and sagittal planes, respectively. There was no correlation between clinical and absolute navigation accuracy.

Conclusions: Radiographic classifications of pedicle screw accuracy vary in sensitivity across spinal levels, as well as in inter-rater reliability. Correlation between clinical screw grade and absolute navigation accuracy is poor, as surgeons appear to compensate for navigation registration error. Future studies of navigation accuracy should report absolute translational and angular errors. Clinical screw grades based on postoperative imaging may be more reliable if performed in multiple by radiologist raters.

Key Words: intraoperative navigation, frameless stereotaxy, image guidance, pedicle screw, registration

Abbreviations: 3D: three-dimensional, CAN: computer assisted navigation

3.1 Introduction

Intraoperative three-dimensional computer assisted navigation (CAN) is used routinely in cranial neurosurgery for the localization of subsurface structures. While not employed as frequently, navigation for spinal procedures may guide implant placement and bony decompression, particularly in minimally invasive and complex deformity correcting procedures where anatomic landmarks are less readily identifiable.[54,106,107]

Modern spinal CAN techniques employ two-dimensional (2D) guidance using "virtual" fluoroscopy, or three-dimensional (3D) guidance based on either preoperative or intraoperative computed tomography (CT) imaging.[108] The accuracy of spinal navigation systems is most easily studied for pedicle screw placement, as instrumentation is reliably localized on postoperative imaging. CAN techniques have been widely reported to reduce pedicle screw breach rates, from $12 - 40\%$ under freehand or fluoroscopic guidance to under 5% with 3D CAN.[53, 59, 109 – 113] Improved instrumentation accuracy is seen across all 3D CAN techniques, in each of the cervical, thoracic, lumbar and sacral regions.[114 – 118]

The clinical accuracy of spinal CAN for pedicle screw placement is variably reported. Up to half of studies assessing pedicle screw accuracy do not define methods of determining screw 'breach', and no consistent grading system is used by those that do.[59,119] The absolute accuracy of spinal navigation systems, quantified most commonly by the target registration error (TRE), has been reported to varying extent in fewer than ten human clinical studies since 2000, while more than forty studies on CAN guided pedicle screw placement have been published in the same period.[63,101,102,115,118,120 – 124] Unsurprisingly, the absolute accuracy requirements of spinal CAN systems, and their relationship to radiographic screw position and clinical outcomes, remain poorly defined.[50]

Here, we therefore review a prospectively collected series of 209 pedicle screws placed with 3D CAN guidance, with clinical accuracy grading using two established scoring systems, as well as quantitation of absolute translational and angular navigation accuracy, to identify any correlation between clinical and engineering accuracies.

3.2 Methods

3.2.1 Patient Selection

Thirty patients enrolled in a prospective comparative trial of our research group's optical topographic 3D CAN system (to be published separately) against two commercially available 3D CAN systems, were retrospectively reviewed. All patients underwent posterior cervical/thoracic/lumbar/sacral instrumented fusion with pedicle screw constructs, with or without decompression, for predominantly traumatic, degenerative, or neoplastic pathologies. Procedures were performed at Sunnybrook Health Sciences Centre by a single surgeon (VY), with or without trainee assistance, from May 2014 – February 2015.

3.2.2 Intraoperative Navigation

All screws were placed with 3D CAN guidance using either the Nav3/3i (Stryker; Portage, MI, USA), registered to preoperative imaging with point-matching followed by surface refinement, or the StealthStation S7 (Medtronic Sofamor Danek; Memphis, TN, USA), registered to intraoperative imaging using the O-Arm^{TM} (Medtronic). Preoperative CT scans were performed at a slice thickness of 0.625 mm, on a GE LightSpeed VCT scanner. All patients underwent postoperative CT imaging of the instrumented region, using the same scanner at a slice thickness of 0.625 mm.

3.2.3 Clinical Grading

Clinical grading of pedicle screw accuracy was performed on postoperative CT imaging using two established methods, the Heary and 2 mm classifications.[51,101] Sum-

Grade	Definition
1	Shaft + tip contained entirely within pedicle
2	Shaft violates lateral pedicle, but tip entirely contained within vertebral body
3	Tip penetrates anterior or lateral vertebral body
4	Shaft breaches medial or inferior pedicle wall
5	Tip or shaft violates pedicle or vertebral body, and endangers spinal cord, nerve root(s) or great vessels, requiring immediate revision

Table 3.1: Heary classification for pedicle screws, on postoperative CT imaging

Grade	Definition
1	Shaft contained entirely within pedicle
2	Shaft violates pedicle cortical wall by <2 m
3	Shaft violates pedicle cortical wall by 2-4mm
4	Shaft violates pedicle cortical wall by >4mm
5	Tip or shaft violates pedicle or vertebral body, and endangers spinal cord, nerve root(s) or great vessels, requiring immediate revision

Table 3.2: 2 mm grading system for pedicle screws

maries of each scoring system are shown in Tables 3.1 and 3.2, respectively.

Heary grading was performed for all screws independently by one neurosurgeon (DC), two orthopedic surgeons (RG, GT) and two radiologists (CH, PH). 2 mm grading was performed for all screws independently by two neurosurgeons (NMA, DG) and two radiologists (AK, JMK). Reviewers for each scoring system were blinded to the results of the other.

Clinical grades were dichotomized as acceptable (Heary grade ≤ 2, or 2 mm grade ≤ 2) or poor (Heary grade >2, or 2 mm grade >2), as has been previously reported.[51,101,119,]

3.2.4 Absolute Navigation Accuracy

Absolute navigation accuracy was measured by comparing the final screw position, on postoperative CT imaging, to a screenshot of the planned screw entry point and trajectory, as seen by the navigation system intraoperatively. Translational and angular deviation from the planned entry point and trajectory were than quantified, in both the axial and sagittal planes, using multiplanar reformatting of both pre- and postoperative CT imaging. The method of absolute navigation error quantification is adapted from those described by Mathew et al. and Kotani et al. (Fig. 3.1).[63,102] In the axial plane, positive translational deviations denote a lateral deflection of the entry point, and positive angular deviations denote a more lateral trajectory. In the sagittal plane, positive translational deviations denote a superior deflection of the entry point, and positive angular deviations denote a more cranial trajectory.

All image processing and measurements were performed using an Osirix 64-bit workstation (version 10.9.5; PIXMEO SARL, Switzerland).

3.2.5 Statistical Analysis

Inter-rater reliabilities (IRR) of Heary and 2 mm grades were computed using two way consistency average measures intraclass correlation coefficients (ICC), appropriate for a fully crossed design.[103] As an approximation, ICC values between 0.60 and 0.74 were reflective of moderate agreement, 0.75 to 0.89 good agreement, and $0.90 - 1.00$ excellent agreement.[125] Frequencies of categorical data were analysed using Fisher's exact tests. For paired categorical data, including the frequencies of poor grade screws on both Heary and 2 mm grading scales, McNemar-Bowker tests of marginal homogeneity were used. Correlation of clinical grading with absolute navigation errors were performed by independent samples t-tests as well as generalized linear regression models. Regression models were first tested for nonlinearity with three cubic splines, with subsequent elimination of all nonsignificant nonlinear terms from the final model. Significance levels for all tests were set at < 0.05.
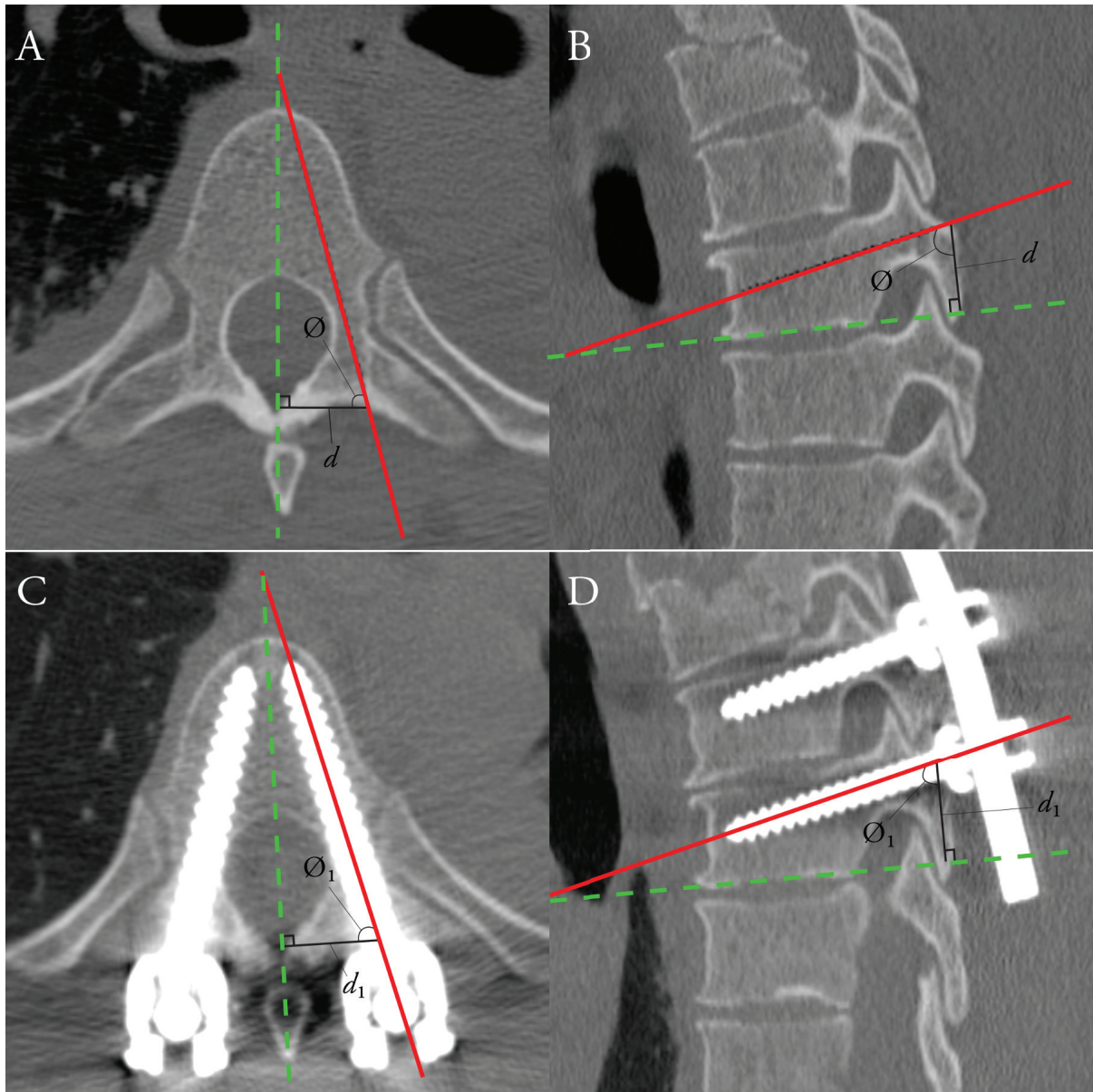
Figure 3.1: Absolute navigation accuracy: Measurement of absolute navigation accuracy, in the axial (A+C) and sagittal (B+D) planes. Comparison is made between intra-operative navigation screenshots of planned entry points and trajectories (A+B), to final screw placement on post-operative CT (C+D). Reference lines (dashed) are drawn, in the axial plane, in the mid-sagittal line (bisecting the vertebral body, spinal canal and spinous process) and, in the sagittal plane, along the inferior endplate. Translational error is computed as $(d_1\text{-}d)$; angular error is computed as $(\phi_1\text{-}\phi)$

All statistical analyses were performed in SPSS Statistics (version 21; IBM, Chicago, IL, USA).

3.2.6 Literature Review

A search of the English language literature from 2000 – present was performed, in June 2016, to identify articles reporting absolute navigation accuracy. MEDLINE, Web of Science and Scopus databases were searched using the terms ("spine" AND "navigation" AND ("error" OR "accuracy")). Abstracts were reviewed by a single author (DG) to identify human clinical in vivo studies; the full texts of eligible abstracts were reviewed to identify parameters and measurement methods of absolute navigation error.

3.3 Results

A total of 209 pedicle screws from 30 patients were included in our analysis. 3 screws were placed in the cervical spine (all at C7), 138 in the thoracic spine, 64 in the lumbar spine, and 4 in the sacrum (all at S1).

3.3.1 Clinical Accuracy

Of 209 screws, with 932 combined Heary grades from five independent reviewers, 95.1% were rated as acceptable. On the 2 mm grading scale, from four independent reviewers assessing the same dataset, significantly fewer screws were rated as acceptable, at 92.6%. These differences did not persist when thoracic screws were analyzed independently, however the Heary grading system was significantly more generous in the lumbar spine. Cervical and sacral screws were not analyzed independently due to inadequate sample size. A summary of clinical grades is presented in Table 3.3.

	Heary Grade (# of ratings)	2mm Grade (# of ratings)	Difference (absolute value)	Significance
All screws				
Acceptable	886 (95.1%)	774 (92.6%)	2.48%	p = 0.036*
Poor	46 (4.9%)	62 (7.4%)		
Thoracic screws				
Acceptable	584 (93.4%)	509 (92.2%)	1.23%	p = 0.43
Poor	41 (6.6%)	43 (7.8%)		
Lumbar screws				
Acceptable	272 (98.6%)	240 (93.8%)	4.80%	p = 0.005*
Poor	4 (1.4%)	16 (16.2%)		

(*) denotes significance at $\alpha < 0.05$

Table 3.3: Clinical grades of 209 pedicle screws, using the Heary and 2 mm grading systems

The intraclass correlation coefficient, a measure of inter-rater reliability, was 0.763 (95% CI 0.665 – 0.809) for Heary grade, 0.428 among the three surgeon raters and 0.781 among the two radiologist raters. For the 2 mm grade, overall ICC was 0.611 (95%CI 0.517 – 0.690), 0.21 among the two surgeon raters and 0.678 among the two radiologist raters.

3.3.2 Absolute Navigation Accuracy

The absolute translational and angular errors of all screws in our cohort, in both axial and sagittal planes, are shown in Fig. 3.2. For all screws, axial and sagittal translational errors were (1.75 ± 3.57 mm) and (1.20 ± 1.15 mm), respectively, while axial and sagittal angular errors were ($3.13 \pm 2.90°$) and ($3.64 \pm 3.48°$), respectively (mean $\pm$ SD). Axial angular errors were greater in the lumbar vs. thoracic spine (mean 3.74° vs. 2.64°, respectively; p = 0.018); all other errors were equivalent across spinal regions.
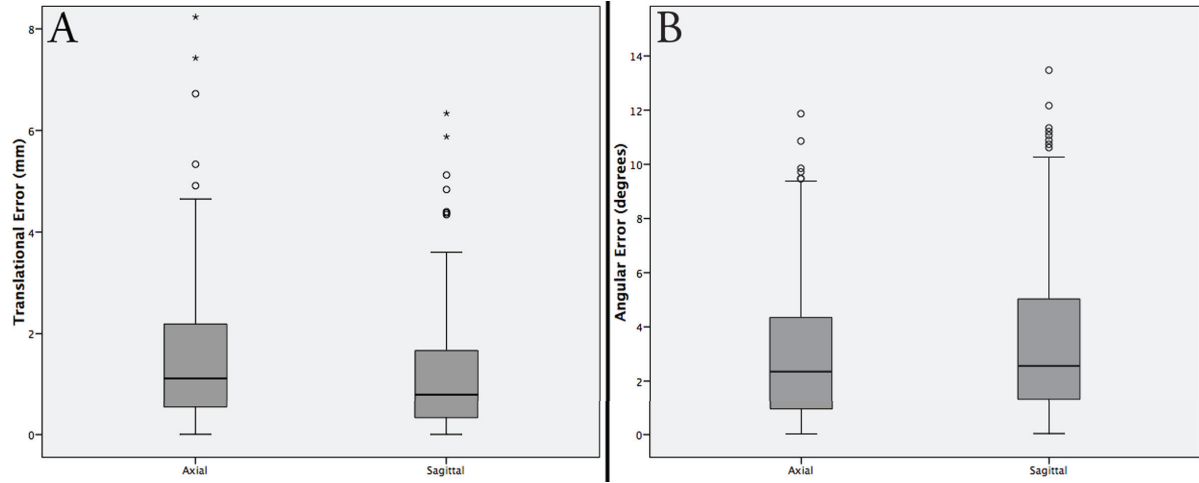
Figure 3.2: Translational and navigational error: Boxplots demonstrating the translational (A) and angular (B) absolute navigation errors in axial and sagittal planes. Boxplot height corresponds to interquartile range (IQR), whiskers correspond to 1.5xIQR, circular points are those outside 1.5xIQR, asterisked points are those outside 3xIQR.

3.3.3 Clinical Engineering Correlation

In a generalized linear regression model, there was no correlation between any absolute navigation error parameter, and the mean Heary grade across all raters (Fig. 3.3). Comparison of absolute navigation errors between 'poor' and 'acceptable' dichotomized Heary grades also revealed no significant differences.

Similarly, no correlation was observed between absolute navigation errors and the mean 2 mm grade (Fig. 3.3). Comparison of absolute navigation errors between 'poor' and 'acceptable' dichotomized 2 mm grades revealed no significant differences.

3.3.4 Surgeon Compensation for Navigation Error

We theorized that the lack of observed correlation between clinical screw grade and absolute navigation accuracy may be due, in part, to surgeon compensation for perceived misalignment of virtual and anatomic intended screw entry points, based on surgeon vi-

sualization and knowledge of anatomic landmarks. For instance, a 'perfect' entry point as shown by the navigation system, that is felt by the surgeon to be excessively lateral based on anatomic knowledge, may lead the surgeon to compensate by medializing their screw trajectory (Fig. 3.4). In this situation, the signed axial translational error is expected to be positive, with a corresponding negative axial angular error.

Linear regression models were therefore generated between signed translational and angular errors, in the axial and sagittal planes, respectively. Negative linear correlations were observed for both axial ($p < 0.001$) and sagittal ($p < 0.001$) errors, suggestive of surgeon compensation occurring in both planes, greater in the axial than sagittal plane (Fig. 3.5).

3.4 Discussion

The primary purported benefit of CAN for spinal procedures is improved instrumentation accuracy and, in theory, minimization of complications from breached screws. Clinical sequelae of screw breach include, acutely, neurologic and vascular injury and, in the longer term, pseudoarthrosis due to poor osseous purchase and load bearing.[30] As CAN techniques evolve, from 2D-fluoro to 3D-fluoro to intraoperative CT based registration, from surgeon manipulated to robotically actuated instruments, the body of literature on navigation accuracy is rapidly expanding. In an era of fiscally responsible health care, the cost effectiveness of various CAN techniques, in relation to their purported accuracy, is also being explored.[127,128]

The grading systems used to quantify navigation accuracy for pedicle screw insertion remain highly heterogeneous.[119] Some, such as the 2 mm grading system, are based on screw shaft relation to the pedicle wall alone, while others, such as the Heary classification, include the relation of the screw tip to the vertebral body.[51,129] Similarly, while most scales quantify only the amount of pedicle wall breach, others have demonstrated the importance of directionality, with lateral breaches less likely to be clinically
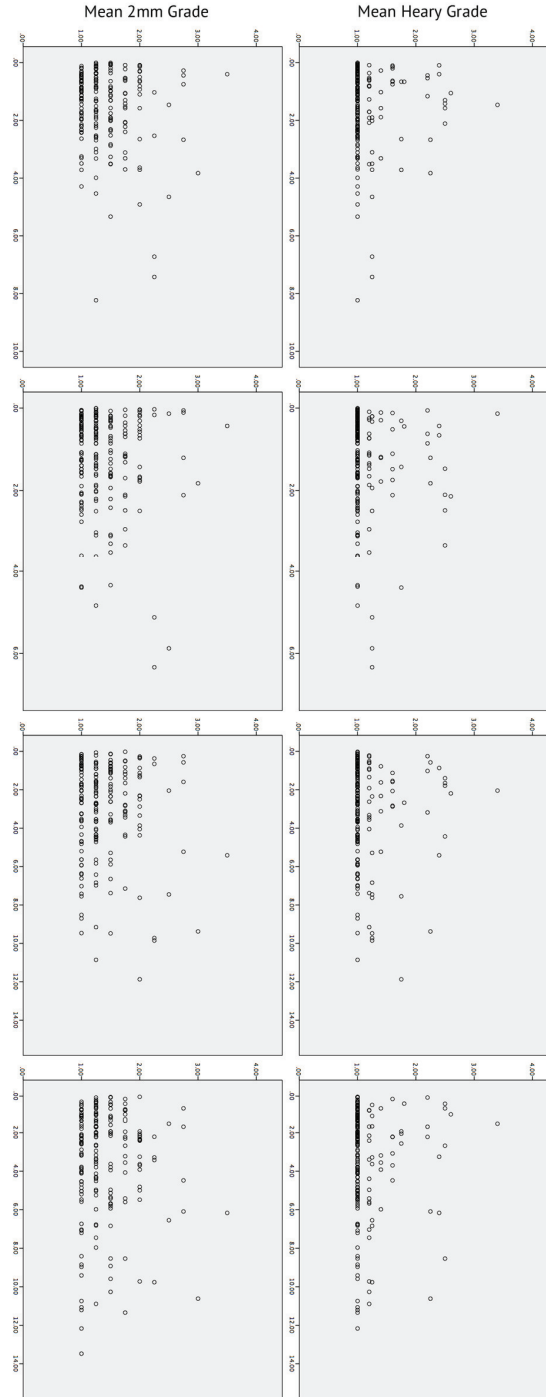
Figure 3.3: Scatterplots of mean Heary grade (top row) and mean 2mm grade (bottom row), vs. each of axial and sagittal translational and angular errors. No correlation is seen between Heary grade or 2mm grade, and any absolute navigation error parameter.
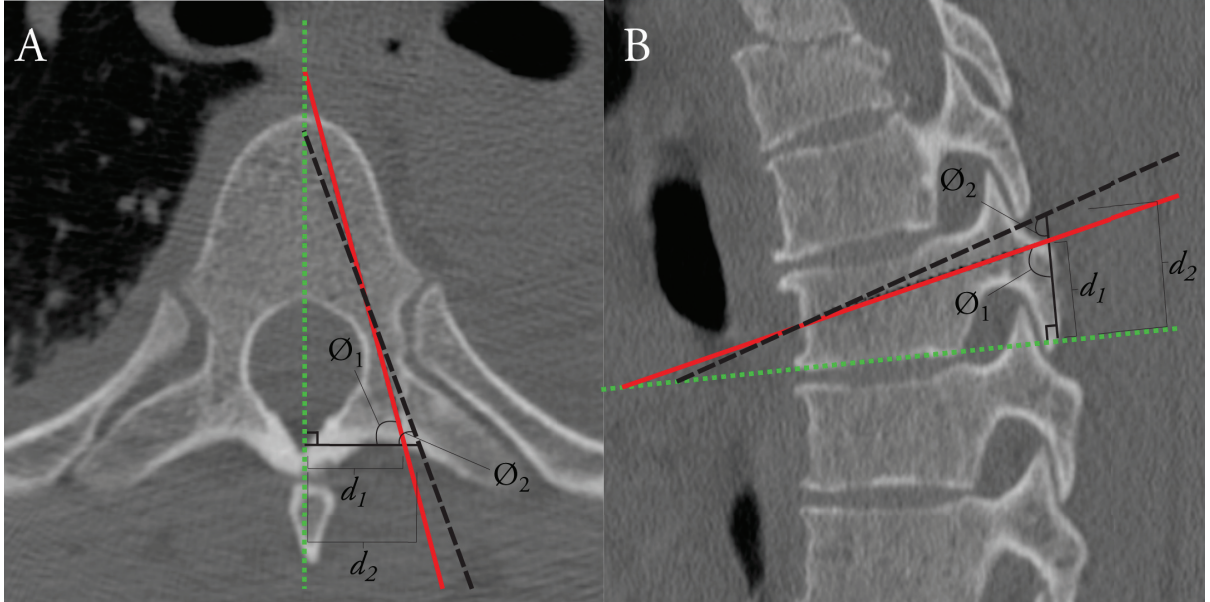
Figure 3.4: Visualization of potential mechanism of surgeon compensation for perceived navigation registration error. In the axial plane (A), a lateral translational error may lead the surgeon to medialize the screw trajectory, leading to inversely-signed translational and angular errors ($d_2 - d_1 > 0$; $\phi_2 - \phi_1 < 0$). In the sagittal plane (B), a rostral translational error may lead the surgeon to direct the screw more caudally, with similar inversely-signed translational and angular errors.
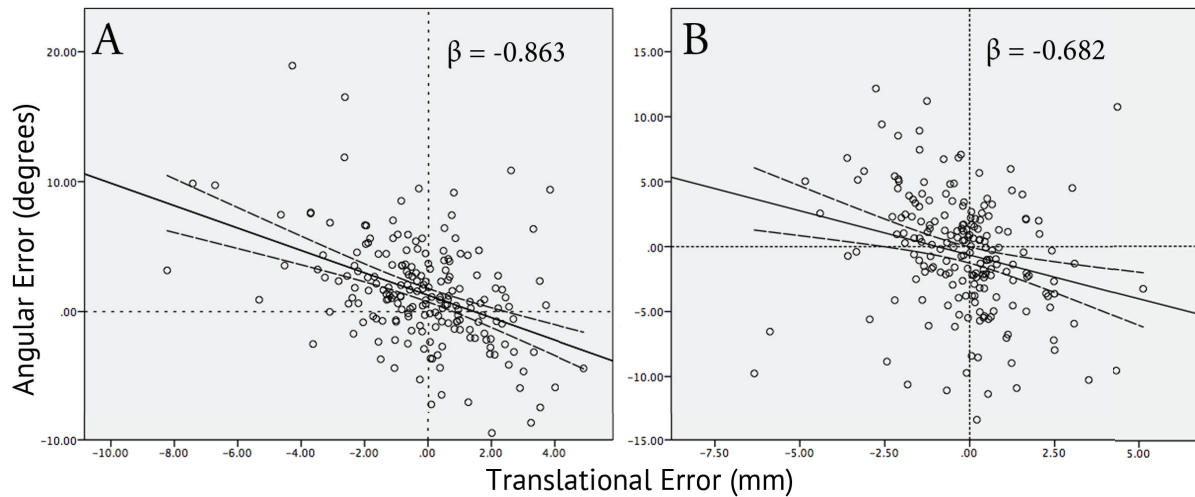
Figure 3.5: Scatterplots of angular vs. translational errors in the axial (A) and sagittal (B) planes. Least-squares regression lines (solid) and 95% confidence intervals (dashed) are shown, along with regression coefficients (β).

significant.[130,131] As assessments of in vivo screw accuracy are based on postoperative CT imaging, metallic artefact may also contribute to the reliability of accuracy ratings, though the type of screw material has been shown not to impact inter-rater reliability.[132]

The commonest grading system in current use is the 2 mm classification, with variations in the grade cutoffs ranging from > 4 mm breach to > 6 mm breach for Grade IV screws.[129,131] The increasingly popular Heary classification accounts for tip position relative to the vertebral body, and emphasizes medial/inferior breaches over less clinically relevant lateral breaches, regardless of magnitude. In our series, the Heary classification was significantly more conservative than the 2 mm grade in identifying poorly placed screws, but only among lumbar pedicle screws. While the Heary grade was developed for thoracic pedicle screws and has not formally been validated in the lumbar spine, it can reasonably be expected to perform similarly as its emphasis is to prioritize breaches more likely to be symptomatic.[51] Anterior, medial and inferior perforations are given greater weight in the Heary classification due to risk of injury to the esophagus/trachea/lungs, spinal cord and nerve roots, respectively, in the thoracic spine. In the lumbar spine, per-

forations in similar directions may injure the iliac vessels/bowel, conus medullaris/cauda equina, and nerve roots, respectively. Therefore, the relatively aggressive identification of poor grade screws by the 2 mm grading system in the lumbar spine, is likely reflective of the larger pedicles and screw diameters relative to the thoracic spine. A breach of 2 mm for a 7 mm diameter lumbar pedicle screw is far more likely to be tolerated by a surgeon than the same 2 mm breach for a 4.5 mm diameter thoracic screw. While the 2 mm increment in this classification is appropriately justified, and the grade cutoffs in our study are those used most commonly in the literature, adjustment of grade cutoffs may be required across spinal levels.[101,120,129,132 – 134] For instance, 'Grade IV: > 4 mm breach' may be appropriate for the thoracic spine, while 'Grade IV: > 6 mm breach' may be more appropriate in the lumbar spine, as described originally by Gertzbein and Robbins.[129]

Good inter-rater agreement was demonstrated in our series for the Heary classification, and moderate agreement for the 2 mm scale. For both scales, inter-rater reliability was significantly higher amongst radiologists than surgeons. For the 2 mm system, using the same grade cutoffs as our study, ICC has been reported to vary from 0.45 to 0.69, in concordance with our results.[135 – 138] To our knowledge, this is the first study reporting on inter-rater reliability of the Heary classification. It is also the first to compare IRR between radiologist and surgeon raters. Given the difficulty in distinguishing metallic screw artefact from pedicle cortex on CT imaging, it is unsurprising that radiology trained raters are more consistent. It may therefore be prudent for future studies of navigation accuracy to employ multiple radiologists for rating clinical screw accuracy, rather than a single rater as has been done in more than half of studies to date.[119]

Absolute navigation accuracy, commonly quantified as the target registration error (TRE), likely represents the most generalizable method of reporting navigation accuracy. The TRE of novel navigation techniques is commonly quantified ex vivo using specialized fiducial implanted phantoms.[139,140] However, in vivo absolute navigation accuracy has been reported in only seven human clinical studies since 2000 (Table 3.4). Quantitation of absolute accuracy in these studies is highly variable, with the majority reporting only angular error. Given that surgeons employing CAN intraoperatively modulate both the position and angulation of their instruments, in both the axial and sagittal planes based

on in plane views on the navigation display, error tolerances in each of these parameters should be reported in future studies of navigation accuracy.

We have shown here furthermore that clinical grading, on two commonly used scales, does not correlate with absolute quantitative navigation accuracy. Using a novel technique of measuring both translational and angular error in axial and sagittal planes, we have also demonstrated quantitatively for the first time that surgeon compensation may lead to clinically acceptable screw placement despite navigation registration error. While the absolute accuracy requirements for surgical navigation systems remain uncertain, in trained hands they are likely to be less stringent than the submillimeter tolerances suggested by rigid mathematical models.[50] Conversely, while CAN is a useful intraoperative adjunct, it cannot and should not replace dedicated subspecialty training, which affords the experience and anatomic knowledge required to identify and compensate for navigation registration errors.

Given the heterogeneity and inter-rater discordance in clinical grading scales, along with their lack of correlation with engineering accuracy, reporting of absolute navigation accuracy along with a summary of clinical sequelae may be a reasonable standard for future studies of navigation accuracy. Acute neurovascular injury from breached screws are rare events, however, and long term pseudoarthrosis related complications are difficult to attribute specifically to breached screws.[118] Clinical screw grading based on postoperative imaging will therefore continue to be of value in identifying breaches likely to cause significant sequelae.

Author, Year	Spinal Levels	CAN Technique	Quantitative Parameters
Kleck et al., 2016	Thoracic, lumbar	Imaging: Intra-operative CT (Medtronic O-Arm) Navigation: Medtronic StealthStation S7	3D translation and angulation of screw tip from intended position
Mathew et al., 2013	Lumbar	Imaging: Intra-operative CT (Medtronic O-Arm) Navigation: Medtronic StealthStation S7	Axial and sagittal angular error
Oertel et al., 2011	Thoracic, lumbar, sacral	Imaging: Intra-operative CT (Medtronic O-Arm) Navigation: Medtronic Treon Plus	Axial angular error
Scheufler et al., 2011	Cervical, thoracic	Imaging: Intra-operative CT (Siemens SOMATOM) Navigation: BrainLab iCT	Axial and sagittal angular error
Scheufler et al., 2011	Thoracic, lumbar	Imaging: Intra-operative CT (Siemens SOMATOM) Navigation: BrainLab iCT	Axial and sagittal angular error
Kotani et al., 2007	Thoracic, lumbar	Imaging: preoperative CT Navigation: Medtronic StealthStation	Axial angular error, with comparison to 'ideal' pedicle axis from preoperative CT
Haberland et al., 2000	Thoracic, lumbar, sacral	Imaging: Intra-operative CT (Philips Tomoscan M) Navigation: Philips EasyGuide, or Zeiss Surgical Tool Navigator (STN)	3D translation at screw entry point and screw tip

Table 3.4: Summary of the literature from 2000-2016, of human in vivo studies of CAN accuracy for pedicle screw placement, with reporting of absolute navigation accuracy

75

3.5   Conclusions

Radiographic grading scales of pedicle screw accuracy are highly heterogeneous, with variability in performance across spinal levels, as well as in inter-rater reliability. Correlation between clinical screw grade and absolute navigation accuracy is poor, in part due to surgeon compensation for navigation error. Future studies of navigation accuracy should therefore report absolute translational and angular navigation accuracy, along with relevant clinical sequelae of any placed screws. If used, clinical screw grades based on postoperative imaging should ideally be generalizable, validated, and include the directionality of breach, and may be more reliable if performed in multiple by radiologist raters. Navigation systems are not intended to replace quality surgical training, which affords the experience and anatomic knowledge required to identify and compensate for navigation errors.

3.6   Acknowledgements

3.7   CONFLICTS OF INTEREST DECLARATION

VY is co-founder and Chief Scientific Officer of 7D Surgical Inc., a company licensing the optical topographic navigation technology developed by our research group. VY, DC and LdC are minority shareholders in this company. 7D Surgical Inc. and its technology have not had any influence on the conduction of this study, and all patients included in this analysis have been treated with guidance from commercially available navigation

systems.

Chapter 4

Validation of Experimental Optical Topographical Imaging System

This chapter presents an evaluation of the accuracy of spinal and cranial intraoperative three-dimensional navigation entitled "High Speed, High Density Intraoperative 3D Optical Topographical Imaging with Efficient Registration to MRI and CT for Craniospinal Surgical Navigation". This work builds on the previous chapter which established the application accuracy of the current state of the art benchmark navigation systems. This chapter addresses what is considered a significant barrier towards the adoptability of surgical navigation; namely the workflow restrictions that result in increased operating time. This work validates the clinical application accuracy of our novel experimental optical topographical imaging system as comparable to the benchmark navigation with significant improvement in surgical timing. This work comprises a manuscript that was submitted for publication in Nature Photonics. The manuscript is included in the dissertation consistent with the guidelines of publisher. The manuscript has been adapted to conform with Ryerson University School of Graduate Studies regulations.

This work comprises an analysis of our novel optical topographical imaging naviga-

tion system for both cranial and spinal applications. This analysis is comprehensive, encompassing the evolution of the technology from initial cadaver experimentation to proof-of-principle validation in animals to the implementation of a multiphase surgical trial. Absolute navigation error (axial/sagittal; translation/angular) was quantified in a similar manner to the methodology employed in Chapter 3 for animal and human trials, based on previously established methodologies by Mathew et al. and Kotani et al. [63,102] With regards to human trials, all screws were graded using the criteria proposed by Heary et al.[51] A total of 71 thoracic and lumbar pedicle screws were analyzed in the animal cohort and 183 cervical (C7), thoracic, lumbar, and sacral screws were analyzed in the human trials. 208 cranial screws were also analyzed, measuring the Euclidian (3D) translational error via comparison of the postoperative location of fixed cranial screws to intraoperative screw location reported by the experimental navigation system. Direct comparison was achievable in the cranial cohort through postoperative to preoperative image registration of the bony anatomy (mutual information).

With regards to the analysis, a variety of statistical tests were performed. To assess clinical accuracy of screw placement the Heary grading criteria was used. Seven board certified physicians (neuroradiologists, neurosurgeons, and orthopeadic surgeons) graded all clinically placed screws. Inter-rater reliability was measured using the intraclass correlation coefficient to evaluate consistency amongst raters as previously described by Shrout et al. [103] and dichotomized data was evaluated by the Fleiss Kappa test. Univariate and multivariate analysis (Kruskal-Wallis and generalized linear models) were performed to identify predictors of application error. For cranial applications Mann-Whitney univariate analysis was perform to assess whether integration of an active calibration protocol during surgery improved accuracy. Further comparisons of timing data were performed to assess timing improvement using the experimental navigation system. These statistical tests establish the clinical application accuracy of the our novel optical topographical imaging navigation system against the benchmark commercial navigation systems with a significant improvement in workflow. This workflow improvement is integral for integration of this technology with high frequency micro-ultrasound and dosimetric parameters discussed in chapter 5.

High Speed, High Density Intraoperative 3D Optical Surface Imaging with Efficient Registration to MRI and CT for Craniospinal Surgical Navigation

Raphael Jakubovic MSc[1,2†], Daipayan Guha MD[2,3,4†], Shuarya Gupta [2,3], Michael Lu[2], Jamil Jivraj MASc[2,5], Beau A. Standish PhD[2], Michael K. Leung MSc[2], Adrian Mariampillai PhD[2], Kenneth Lee PhD[2], Peter Siegler PhD[2], Patryk Skowron BSc[2], Hamza Farooq BEng[2,5], Nhu Nguyen BEng[2,5], Joseph Alarcon BEng[2,5], Ryan Deorajh BEng[2,5], Michael Ford MD, FRCSC[6], Peter Howard MD,FRCSC[7,8], Nicolas Phan MD, FRCSC[3], Leodante B. da Costa MD[3], Chris Heyn MD, PhD, FRCPC[7,8], Gamaliel Tan MBBS, FRCS[9], Rajeesh George MBBS, MS[9], David Cadotte MD, PhD[3], Todd Mainprize MD, FRCSC[3], Albert Yee MD, MSc, FRCSC, DABOS[6] & , Victor XD Yang MD, PhD, PEng[2,3,4,5*]

[1]Department of Biomedical Physics, Ryerson University, Toronto, ON, Canada

[2]Biophotonics and Bioengineering Laboratory, Ryerson University/Sunnybrook Health Sciences Centre, Toronto, ON, Canada

[3]Division of Neurosurgery, Department of Surgery, University of Toronto. Toronto, ON, Canada

[4]Institute of Medical Science, School of Graduate Studies, University of Toronto. Toronto, ON, Canada

[5]Department of Electrical and Computer Engineering, Ryerson University, Toronto, ON, Canada

[6]Division of Orthopedic Surgery, Department of Surgery, University of Toronto. Toronto, ON, Canada

[7]Division of Neuroradiology, Department of Medical Imaging, Sunnybrook Health Sciences Centre, Toronto, ON, Canada

[8]Department of Medical Imaging, University of Toronto. Toronto, ON, Canada

[9]Jurong Health, Ng Teng Fong General Hospital, Singapore, Singapore

Corresponding Author:
Victor XD Yang, MD PhD PEng FRCSC
Canada Research Chair, Biophotonics and Bioengineering Laboratory
Division of Neurosurgery/Brain Sciences Program
Sunnybrook Health Sciences Centre/Sunnybrook Research Institute

University of Toronto/Ryerson University

2075 Bayview Avenue, Toronto, Ontario, M4N 3M5, Canada

Tel: 416-803-9320

Email: victor.yang@sunnybrook.ca

† Authors have contributed equally to this work and hold joint first authorship.

Abstract

Intraoperative image-guided surgical navigation for craniospinal procedures has significantly improved accuracy by providing an avenue for the surgeon to visualize underlying internal structures corresponding to the exposed surface anatomy. Despite the obvious benefits of surgical navigation, surgeon adoption remains relatively low due to long setup and registration times, steep learning curves, and workflow disruptions. We introduce an experimental navigation system utilizing optical topographical imaging (OTI) to acquire the 3D surface anatomy of the surgical cavity, enabling visualization of internal structures relative to exposed surface anatomy from registered preoperative images. Our OTI approach includes near instantaneous and accurate optical measurement of >250,000 surface points, computed at >52,000 points-per-second for considerably faster patient registration than commercially available benchmark systems without compromising spatial accuracy. Our advancements provide the cornerstone for widespread adoption of image guidance technologies for faster and safer surgeries without intraoperative CT or MRI scans. This work represents a major workflow improvement for navigated craniospinal procedures.

4.1 Introduction

Intraoperative surgical navigation has become the standard-of-care in cranial neurosurgery for the localization of subsurface structures. Applications include tumour resection, vascular lesion identification and, more recently, targeting of electrical implants to specific nuclei. While not as ubiquitous, navigation for spinal surgery has undergone significant evolution over the past decade. This technological advancement has been driven by need, as the direct and indirect annual costs associated with back pain in the United States have been estimated at approximately \$50 billion.[44] 410,000 spinal fusion procedures were performed in the United States in 2008; with an aging population, this number is expected to rise significantly over the next decades.[52,143] While instrumentation is often used to facilitate osseous fusion, breach of screws outside the intended trajectory occurs in 12 – 40% of screws (Figure. 4.1).[53,109 – 111] This may result, acutely, in neurovascular injury and, in the longer term, mechanical construct failure, causing potentially life or limb-threatening complications which may require costly revision surgery.[126,127] Computer-assisted navigation has been developed to improve the accuracy of screw placement at all spinal levels, reducing breach rates to under ten percent.[109,112,113,144] We demonstrate a new surgical navigation technology, developed in our Biophotonics and Bioengineering Laboratory (BBL), using optical topographical imaging (OTI) to create virtual 3D surfaces of open surgical cavities, allowing surgeons to visualize internal structures relative to exposed surface anatomy. Our system completes full bony surface registration using graphics processing units (GPU) considerably faster than current systems, with comparable spatial resolution, sparing the patient from additional radiation exposure, reducing operating room time and costs, and minimizing disruption to surgical workflow.

Our experimental navigation system consists of a small camera gantry integrated with surgical lighting. The camera gantry is composed of two cameras, a digital micromirror device pico-projector and an infrared optical tracking system (Figure. 4.2A-B). The projector illuminates a patterned light of known structure and periodicity (e.g. grids, repeating bars) that is recorded by the cameras and used to reconstruct the 3D surface of the patient (Figure. 4.3A).[147] The patterns enable image correspondence between the stereo cameras to be established. With calibrated cameras, the stereo images allow
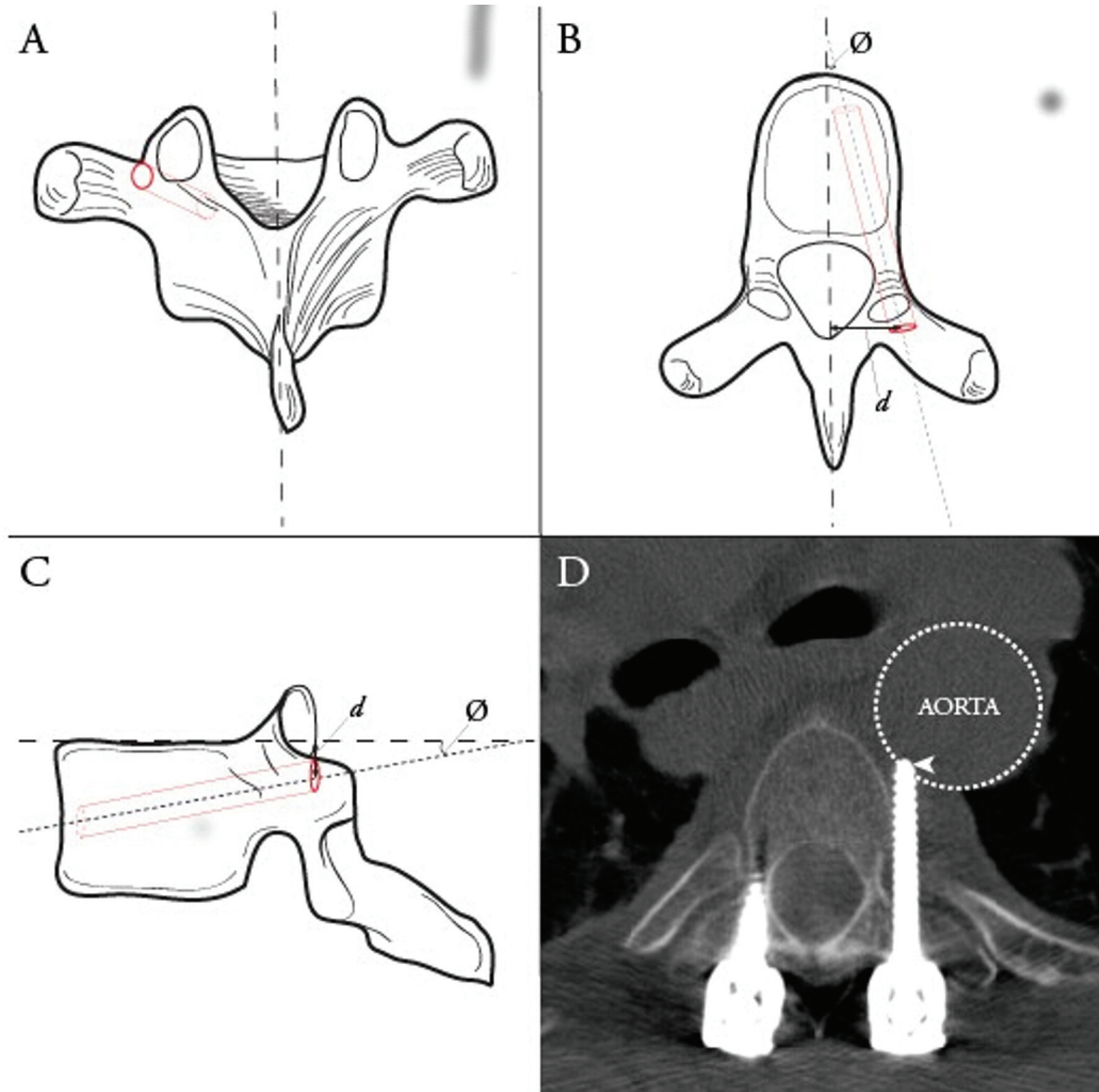
Figure 4.1: Ideal thoracic pedicle screw entry point (dark circle) and trajectory (dashed cylinder) in the coronal (A), axial (B) and sagittal (C) planes. Ideal entry point distance (d) and trajectory angle (ϕ) shown on axial and sagittal planes. Example of a misplaced thoracic pedicle screw via freehand technique (D), Heary Grade V, with tip (arrowhead) abutting the aorta.

for 3D mapping of the surface correlating to the various height disparities. The experimental navigation system registers the acquired 3D-point cloud to pre-acquired imaging data (i.e. CT, MRI) using a surface registration algorithm that is based on the iterative closest point (ICP) algorithm (Figure. 4.3C-D). The experimental navigation system also utilizes an infrared (IR) tracking system containing two IR cameras surrounded by IR LEDs to illuminate the tracking volume. The IR system is currently used to track surgical tools using passive-reflective markers (Figure. 4.3B).

Despite the apparent benefit of spinal surgical navigation in reducing breach rates, adoption of navigation as standard of care has been slow due to lengthy setup/registration times, steep learning curves, and interruption of surgical workflow.[148] Contemporary benchmark navigation systems employ a 'matched-point' registration protocol relying on surgeons to drag a pointed probe across exposed bony anatomy to map to a preoperative computed tomography (CT) scan. These protocols have steep learning curves and take three to five-fold longer per screw than traditional fluoroscopy, necessitating additional anesthetic and operating room time.[115,149,150] Current registration protocols are unable to account for variances in spinal anatomy due to changes in patient positioning from CT gantry to operating table, critical in trauma and deformity cases. While this may be overcome with intraoperative 3D fluoroscopy or CT, it is at the cost of significantly increased radiation to the patient, particularly with multilevel fusions, and adds substantial set up time.[47,151] Our experimental navigation system confers significant benefit over the currently available navigation systems, implementing a simple point picking protocol and ultrafast optical imaging registration to fuse the intraoperative surface anatomy with the preoperative CT. Rapid repeat registration allows for sequential segmental registration, minimizing intersegmental deviation from preoperative imaging to intraoperative positioning.
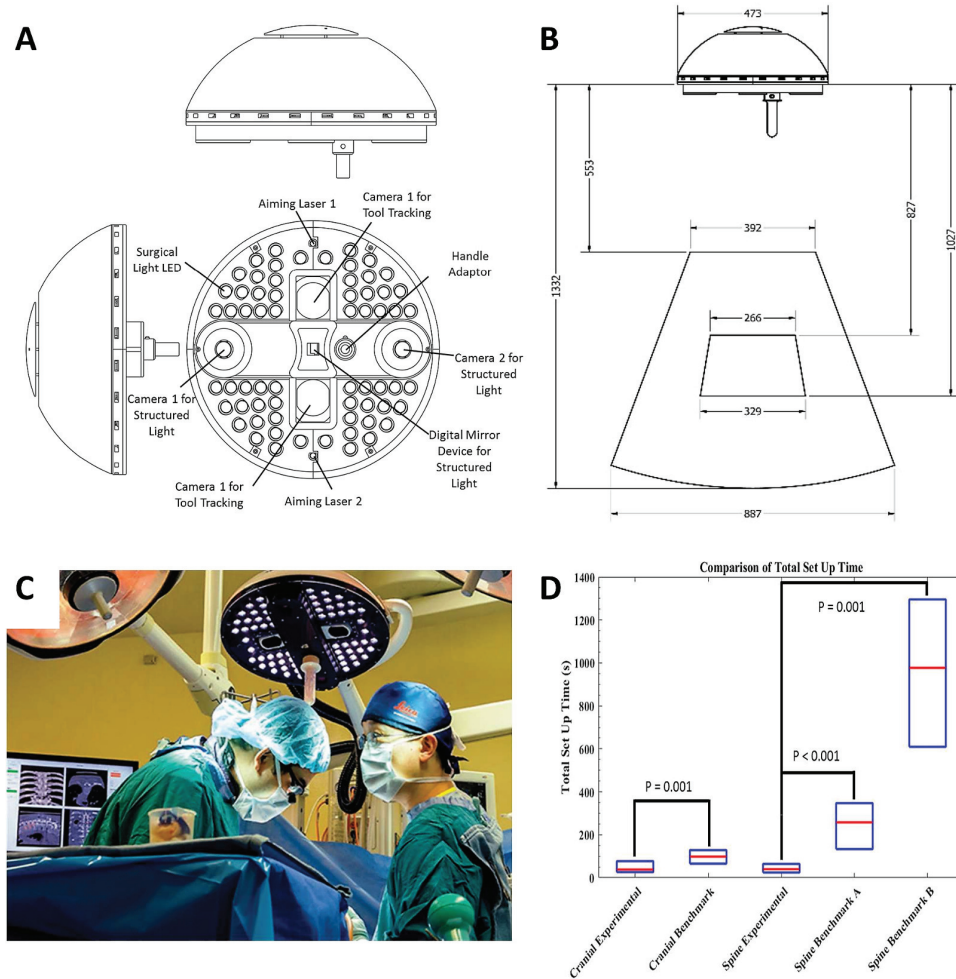
Figure 4.2: Clinical prototype of the experimental navigational system. A) Design model of the surgical light head with embedded navigation. Designed to inconspicuously serve as traditional boom-supported surgical light head comprised of 64 high intensity surgical light LEDs to provide standard lighting with minimal spectral overlap with the navigation optics. Binocular infrared cameras utilizing provide real-time tracking of passive-reflective markers mounted on surgical tools. A digital mirror device centered around binocular structured light cameras forming an epipolar baseline provide intra-operative topographical imaging for registration to the pre-operative images. Co-ordinates of the tracked tools are easily matched to the acquired structured light topographical image. B) Design model of the surgical light head with embedded navigation: Technical specifications: Field of view of the infrared tracking volume (outer pyramid) and the structured light imaging volume (inner pyramid). All measurements are in millimeters. C) Prototype navigation system in clinical use. D) Comparison of total setup time (median and IQR) for cranial and spine applications of experimental and benchmark navigation systems (cranial: StealthStation; spine A: Nav3/3i; spine B: O-arm).
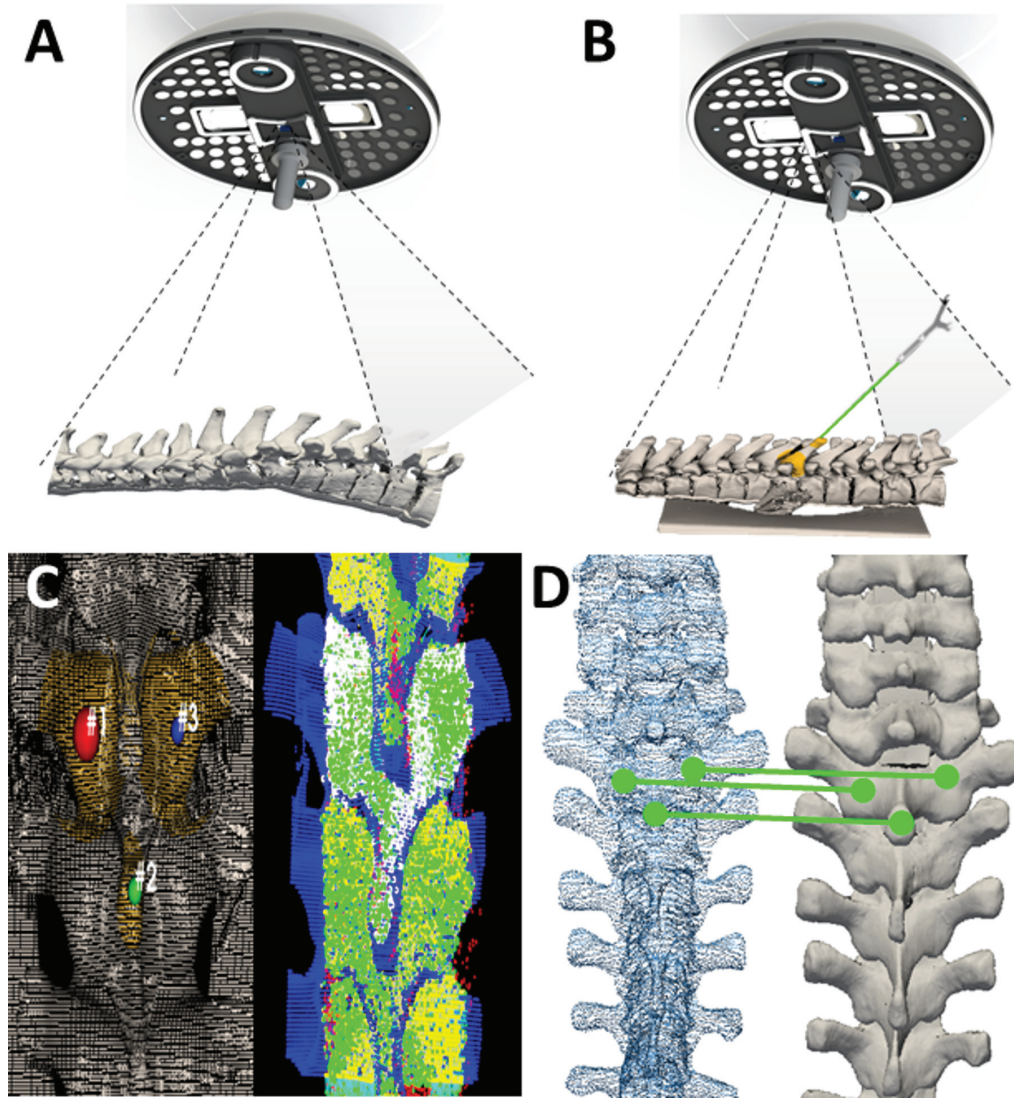
Figure 4.3: Conceptual design of optical topographical imaging (OTI) experimental navigation system. A) Structured light patterns projected into the open surgical field. Structured light patterns deflect and deform upon reaching the surface of the target. Pattern deformations reflect height variations (along the optical axis) of the surface. B) Registered reconstructed surface data to pre-acquired imaging data with tool tracking capabilities. Verification of the system's accuracy is conducted by sliding a passively tracked probe along boney landmarks of the anatomy and confirming the system is reporting the tool's spatial location correctly. C) Registration of the acquired 3D-point cloud to pre-acquired imaging data (i.e. CT, MRI, OTI) using an iterative closest point (ICP) algorithm based on a three-point picking protocol. D) Grey-scale stereoscopic cameras acquire topographical images. Images are captured as the light patterns are projected onto the surface. 3D reconstructed and thresholded point-cloud representing the bony surface of the spine.

4.2 Results

Ex-vivo feasibility of our experimental optical navigation technology was studied in 6 adult human cadavers, resulting in the integrated design of navigation with surgical lighting. In- vivo proof-of-principle validation of OTI was performed on 10 anaesthetized ventilated adult swine models, where interference between optical illumination for surgical lighting and OTI, both in the visible spectrum, were studied and minimized. Optical imaging of subperiosteal dissection planes between and bony tissues, cluttered by bleeding and carbonization effects from electro-cautery using standard surgical techniques, was performed to demonstrate pre-clinical applicability and establish required specifications for 3D imaging speed (< 0.5 second to acquire entire operative field using standard surgical suction to clear pooling blood) and for maximal tolerated animal anatomy movement speed (< 2 mm/second) using IR tracking. To study navigation accuracy, 71 thoracic and lumbar pedicle screws were inserted and quantified by comparing intraoperative trajectory data to true screw placement based on postoperative CT imaging. Median (95%) translational and angular error of the experimental navigation system in the adult swine model was 1.67 mm (5.12 mm) and 4.37° (12.95°) in the axial plane and 1.63 mm (7.81 mm) and 6.50° (17.76°) in the sagittal plane. Following engineering optimization based on the cadaver and swine data, human clinical trials were commenced for cranial and spinal surgical procedures. At the time of writing, 171 human craniospinal surgical procedures have been performed using our experimental navigation system, including a lead-in phase of optical topographical imaging and registration only, a validation phase of using benchmark navigation systems for surgical guidance and experimental system to measure guidance trajectories, a cross-over phase of using experimental navigation system for surgical guidance and benchmark system to confirm guidance accuracy, and finally using the experimental navigation system only for surgical guidance with postoperative imaging analysis. Accuracy for craniotomy procedures was quantified following implantation of cranial plates by placing the tracked probe on cranial screws fastening the plates and comparing the reported position of the tooltip to the coordinates of the screw on a postoperative CT scan. Relative displacement drift between stereo-cameras over time was found to degrade navigation accuracy during the validation phase, aggravated by larger thermal expansion coefficients of 3D printed plastic material used in the experimental system. An active calibration protocol was developed to account for camera

drift which showed statistically improved cranial screw coordinate measurements. Accuracy for spinal procedures was benchmark against two commercial navigation systems – the NAV3/3i (Stryker; Portage, MI, USA), and the O-arm/StealthStation S7 (Medtronic Sofamor Danek; Memphis, TN, USA). The complete set-up processes of all three systems were timed in order to quantify the operative time used to enable navigation. Clinical and engineering analysis of screw placement accuracy for spine procedures was conducted on preoperative and postoperative CT imaging. Refer to Methods section for analysis methodologies (Figure 4.4).

In regards to cranial accuracy, Euclidean (3D) translational error was quantified based on the location of a fixed cranial screw as measured postoperatively relative to the intraoperative screw head location as reported by the experimental system. Median (95%) 3D translational errors for all cranial screws (N = 216 screws, 19 patients) was 2.49 mm (5.53 mm) with 1.18 mm (3.16 mm), 1.11 mm (3.95 mm), 1.15 mm (4.32 mm) in the X, Y, and Z directions respectively. Significant improvements in all axes were seen following software integration of the active calibration algorithm to account for camera drift over time (P < 0.001), reducing the median (95%) 3D translational error from 4.01 mm (5.99 mm) (N = 102 screws, 8 patients) without active calibration to 1.89 mm (3.40 mm) (N = 114 screws, 11 patients) with active calibration. Similarly, integration of the active calibration algorithm reduced the X, Y, and Z translations from 1.54 mm (4.08 mm), 1.97 mm (4.79 mm) and 1.65 mm (4.81 mm) to 0.89 mm (2.37 mm), 0.89 mm (2.19 mm), and 0.82 mm (2.13 mm). The short (4 – 5 mm) cranial screws did not allow reliable angular deviation measurement. Engineering analysis of screw placement accuracy for cranial procedures was conducted on preoperative and postoperative CT imaging. Refer to Methods section for analysis methodologies (Figure 4.5).

In regards to spinal surgical accuracy, previous work for spinal image-guided navigation techniques has focused on anatomic screw location (screw grading) rather than true *in-vivo* quantification of error (translational or angular deviations of the true screw trajectory vs. the intraoperative trajectory). In this study, translational and angular deviations were quantified for both the benchmark navigation systems and the experimental navigation system in the axial and sagittal planes (Figure 4.4). Absolute error measurements were quantified based on postoperative CT scans of implanted pedicle screws,
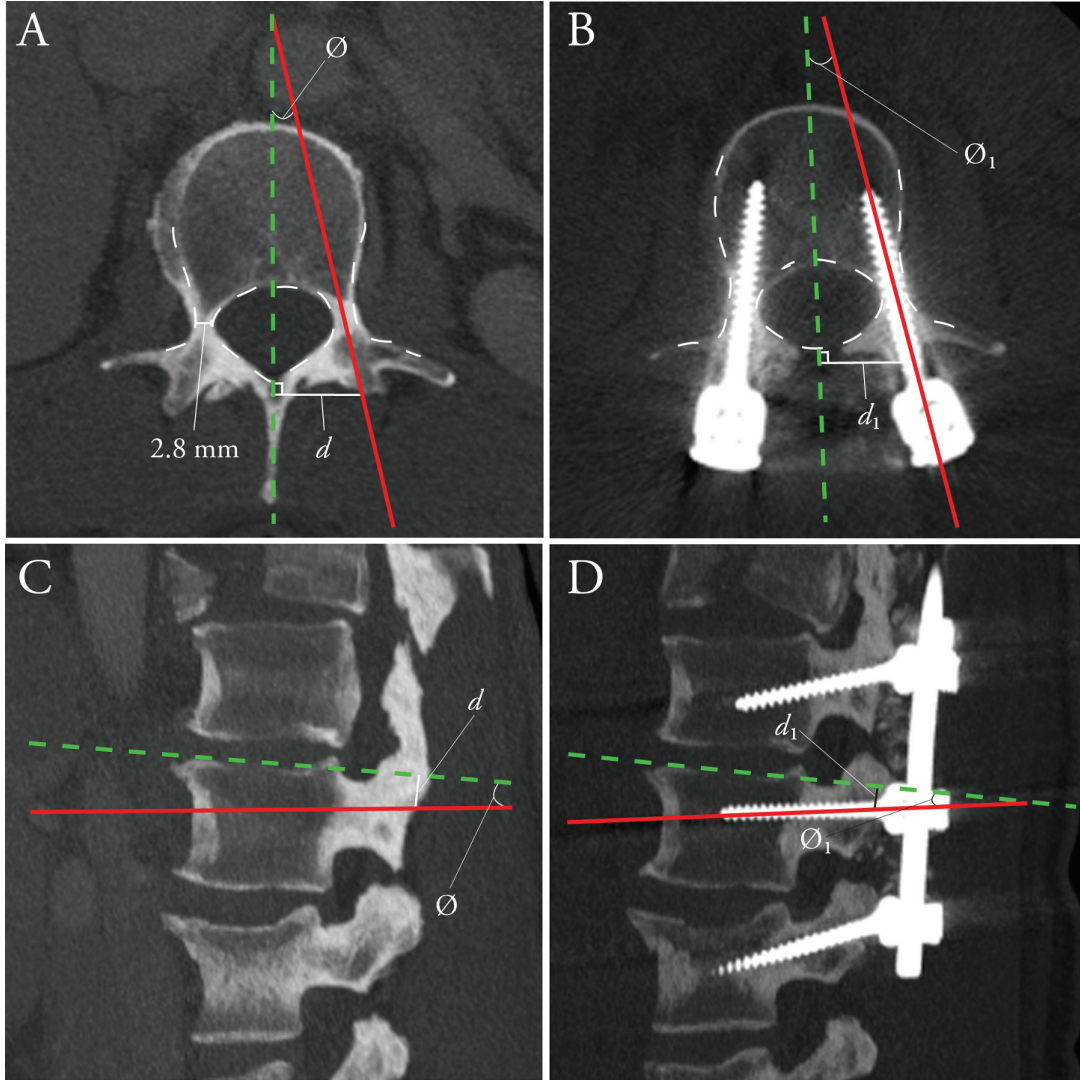
Figure 4.4: Engineering analysis quantifying absolute translational and angular deviation in the axial and sagittal planes. Example shown of a patient with hypoplastic pedicles at L2. A) Intraoperative predicted screw trajectory (red) as visualized on a pre-operative axial CT. B) Post-operative actual screw trajectory (red) as visualized on a multiplanar reformatted post-operative CT. Axial distances (d) were measured at 90° relative to midsagittal axis (green line). Angle (ϕ) represents corresponding trajectory angles. C) Intraoperative predicted screw trajectory (red) as visualized on a pre-operative sagittal CT. D) Post-operative actual screw trajectory (red) as visualized on a multiplanar reformatted post-operative CT. Sagittal distances (d) were measured at 90° relative to the inferior or superior sagittal endplate (green line). Angle (ϕ) represents corresponding trajectory angles. Errors in each plane were calculated as d_1 - d (translational) and ϕ_1 - ϕ (angular).

90

ranging from 4.5 – 6.5 mm in diameter. Metallic CT artefacts amplify variation in absolute error measurements, particularly from large-diameter pedicle screws appropriate for our thoracolumbar series. The true engineering accuracy of the experimental navigation system is therefore underestimated. Clinical grading of screws, using the established Heary grading system, [51] was performed independently by two neuroradiologists (CH, PH), three neurosurgeons (DWC, NP, LC) and two orthopedic spine surgeons (RG, GT) (Table 4.1). Average clinical major breach (Heary III-IV) rates of 5.7% for all navigated screws were reported, with strong intraclass correlation (ICC: 0.725; $P < 0.001$) and fair inter-rater agreement (Fleiss Kappa (95% CI): 0.248 (0.243 – 0.254); $P < 0.0001$). Furthermore, there were no significant differences in major screw breaches rates between the experimental and benchmark systems (6.8% vs. 5.3%, $P = 0.99$). For more details, refer to Methods section.

In human clinical trials for spinal procedures, median (95%) translational and angular errors for benchmark systems (209 screws) were 1.14 mm (3.92 mm) and 2.43° (8.97°) in the axial plane and 0.83 mm (3.62 mm) and 2.60° (10.06°) in the sagittal plane, vs. 1.21 mm (3.42 mm) and 2.15° (8.14°) and 1.13 mm (4.25 mm) and 2.33° (8.59°) for the experimental navigation system (162 screws) (see Figure 4.6). More benchmark system navigated screws were inserted prior to use of experimental system to ensure surgical teams proficiency in using existing commercial systems and reduce bias in the comparison. Without active calibration for spinal screw navigation (N = 50), the median (95%) translational and angular errors were 1.27 mm (3.03 mm) and 1.88° (7.62°) in the axial plane and 1.60 mm (4.39 mm) and 2.33° (8.16°) in the sagittal plane, vs. 0.99 mm (3.37 mm) and 2.28° (8.09°) and 0.94 mm (2.56 mm) and 2.48° (7.79°) for navigation with active calibration (N = 79). These differences did not reach statistical significance.

Univariate analysis, accounting for age, gender, surgical navigation method (i.e. benchmark navigation, experimental navigation) and screw location (cervical, thoracic, lumbar, sacrum) identified age as a predictor for increased axial distance error, and sacral screw location as a predictor of increased axial angle error vs. thoracic and lumbar spine. Generalized linear regression confirmed sacral screw location as a predictor of increased axial angle error ($P = 0.009$; Table 4.2) and advanced age as an indicator of increased axial distance error ($P = 0.005$). Surgical workflow improvement, as measured by setup
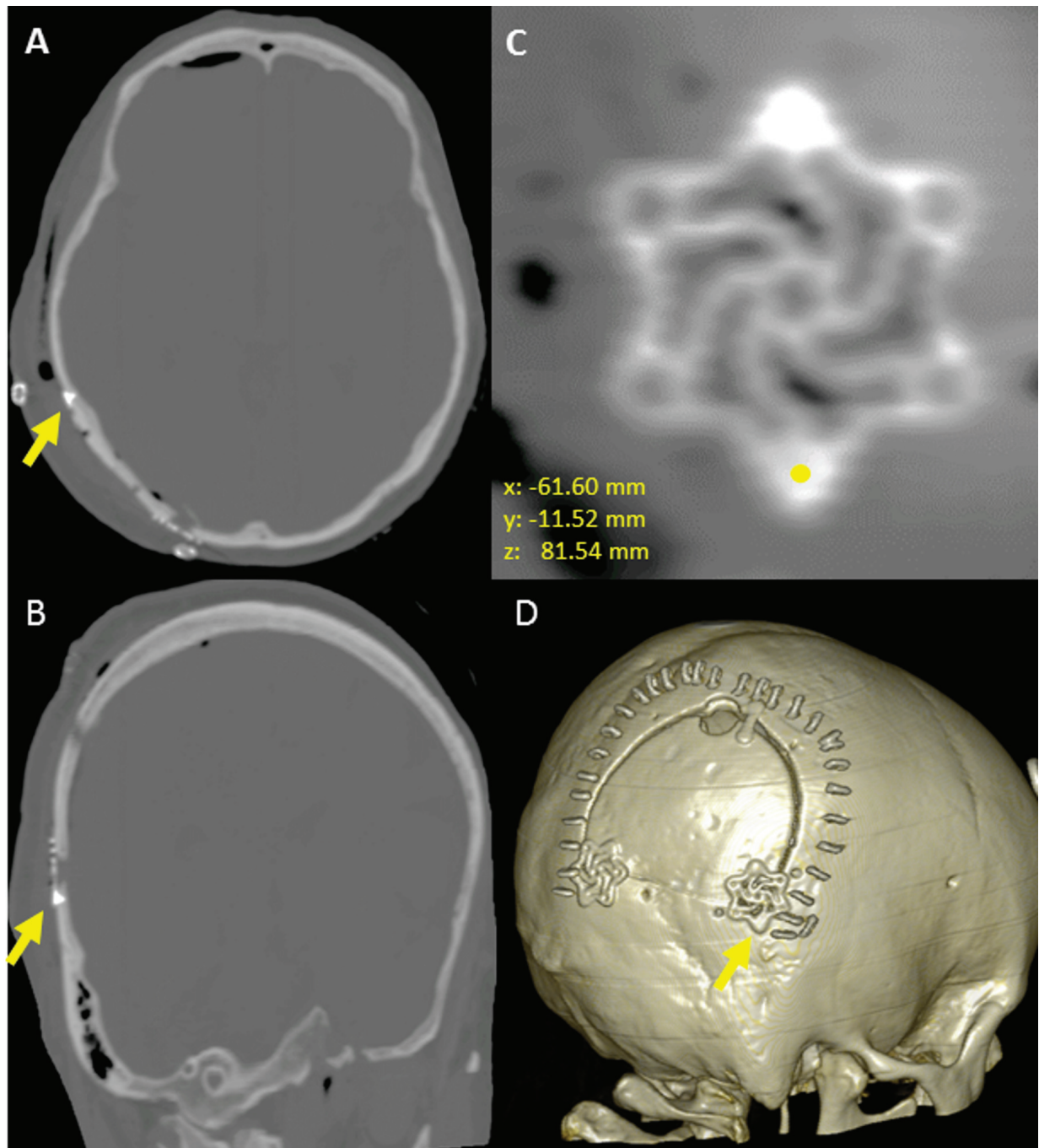
Figure 4.5: Engineering analysis quantifying cranial translational error. Comparison of postoperative cranial screw co-ordinates to intraoperative co-ordinates base on the location of the tracked probe. A) Axial CT representation, B) Coronal CT representation C) Multiplanar reformatted CT image (2 cranial fixation screws), (D) 3-dimensional volume rendered CT.

Grade	Reviewer 1	Reviewer 2	Reviewer 3	Reviewer 4	Reviewer 5	Reviewer 6	Reviewer 7
1	284 (98.3%)	266 (92.0%)	243 (84.1%)	220 (76.1%)	269 (93.1%)	259 (89.6%)	223 (77.2%)
2	4 (1.4)%	5 (1.7%)	32 (11.1%)	39 (13.5%)	7 (2.4%)	20 (6.9%)	36 (12.5%)
3	0 (0.0)%	7 (2.4%)	6 (2.1%)	15 (5.2%)	7 (2.4%)	2 (0.7%)	11 (3.8%)
4	1 (0.3)%	11 (3.8%)	8 (2.8%)	15 (5.2%)	6 (2.1%)	7 (2.8%)	2 (6.6%)

Table 4.1: Clinical Heary grading of all navigated screws by 7 independent reviewers (two radiologists, three neurosurgeons, and two orthopaedic surgeons (RG & GT). Grade I denotes the screw is entirely contained within pedicle; Grade II the screw violates lateral pedicle but screw tip is contained within the vertebral body; Grade III indicates the screw tip penetrates anterior or lateral vertebral body Grade IV indicates a medial or inferior breach of the pedicle; No Grade V screws were scored. No screw revisions were required.

Axial Distance
Benchmark vs. Experimental

A

Axial Angle
Benchmark vs. Experimental

B

Sagittal Distance
Benchmark vs. Experimental

C

Sagittal Angle
Benchmark vs. Experimental

D

· Benchmark · Experimental
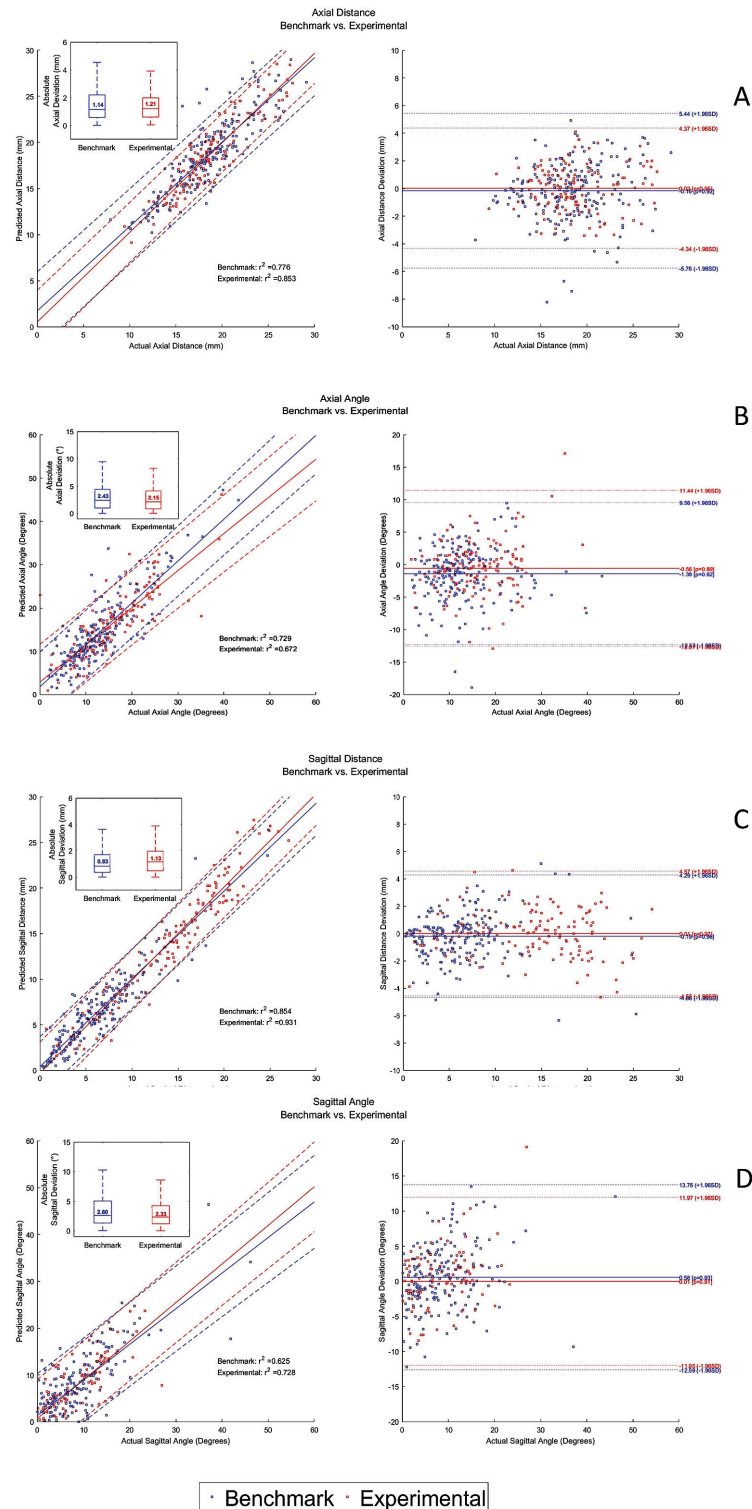
Figure 4.6: Bland Altman analysis. Left Panel: Correlation plots with corresponding boxplots comparing predicted intra-operative screw trajectory with actual post-operative screw trajectory for benchmark (blue) and experimental (red) navigation systems. Inset subpanels represent median (IQR) comparison between benchmark (blue) and experimental (red) navigation systems. Right Panel: Bland-Altman plots comparing actual screw trajectory with distance and angular deviations for A) Axial Distance, B) Sagittal Distance, C) Axial Angle, D) Sagittal Angle. No statistically significant differences were found.

and registration time to enable navigation, was compared between the experimental and benchmark systems. For cranial procedures, the median total setup and registration time interquartile range (IQR) for the experimental navigation system was 38s (26 − 76) vs. 96s (65 − 120) for the benchmark system (P = 0.001). For spinal procedures, experimental navigation system median (IQR) time was 41s (25 − 68) vs. 258s (143 − 355) for matched-point based (P < 0.001) and 794s (609 − 1136) intraoperative CT based benchmark systems (P = 0.001) (Figure 4.2D). This suggests that intraoperative navigation confers significant accuracy benefit compared to freehand and fluoroscopy techniques, and that the remarkable gains in surgical workflow facilitated by the experimental navigation system do not come at the expense of surgical accuracy. Such benefit was enabled by the efficient GPU algorithm, as demonstrated by the computation time for optical image acquisition and registration at 5.07±1.83 seconds measured over 476 craniospinal registrations, each consisting of over 250,000 surface points, with average throughput of over 52,000 points per second. This was orders of magnitude faster than current point-matching registration techniques employed by existing benchmark navigation systems, typically with throughput of 30 to 100 points over a few minutes. Therefore, this study represents an improvement on the current clinical paradigm, whereby spatial accuracy is maintained while vastly improving registration time and workflow.

4.3 Discussion

This work represents a major shift in the current surgical paradigm through the introduction of ultra-fast optical topographical imaging and registration. We have demon-

Clinical Variables		P - Values			
		Axial Distance Error	Axial Angle Error	Sagittal Distance Error	Sagittal Angle Error
Age* Median(IQR)	57 (48 − 66)	0.332	0.846	0.019*	0.032*
Gender* Male (%)	36 (60)	0.214	0.260	<0.001*	0.505
Screw Location:* (# of screws) Cervical Thoracic* Lumbar* Sacral	13 242 133 4	0.172	<0.001*	0.011*	0.306
Navigation Method:* (# of screws) Non-navigated* Benchmark Experimental	21 209 183	0.367	<0.001*	0.003*	<0.001*

*P < 0.05 is considered significant; Non-navigated: freehand or fluoroscopy

Table 4.2: Generalized linear model. Generalized linear model of axial distance, axial angle error, sagittal distance error, and sagittal angle error as a function of age, gender (male, female), screw location, (cervical, thoracic, lumbar, and sacral) and navigation method (freehand, fluoroscopy guided, benchmark navigation, experimental navigation). There were no statistical differences in accuracy between the benchmark and experimental systems. Advanced age was predictor for worsening sagittal distance and angular error. Screw location predicted increased axial distance error from thoracic to lumbar to cervical spine and increased sagittal distance error from thoracic/lumbar to cervical spine. Freehand or fluoroscopy guidance predicted increased angular and sagittal distance error.

strated the implementation of an optical topographical imaging modality in craniospinal surgery, with thorough clinical and engineering data analysis to ensure surgical accuracy. By using optical imaging based surface point acquisition and GPU based parallel computing processing, we perform registration of intraoperative anatomy to preoperative MRI or CT imaging at speed orders of magnitude faster than current point-matching navigation systems. The form factor of our experimental surgical navigation system has been designed to integrate into the existing operating room environment, with the benefit of performing imaging and registration tasks considerably faster than existing technologies. We believe these significant innovations eliminate the workflow restrictions that have traditionally led some surgeons to forgo navigation in favour of freehand approaches.

While the utility of the present study is apparent in the context of craniospinal procedures, the same optical topographical imaging technology is suitable for a variety of applications. In particular, rapid optical topographical imaging allows for frequent repeat registrations, minimizing the significant target registration errors seen with existing neuronavigation technologies as a result of progressive brain shift during the procedure.[152] Frameless stereotactic navigation is also employed routinely in otolaryngology, with growing applications in orthopedic, abdominal, and craniomaxillofacial procedures.[153 – 155] The utility of optical topographical imaging techniques is evident in these non-neurosurgical applications, particularly in those with significant soft-tissue manipulation or deformation, where rapid repeat registration is required to maintain accurate correlation to preoperative imaging. High frequency re-acquisition of intraoperative optical images also lends itself well to augmented-reality, with co-registered images overlaid onto operating microscopes or other displays employed commonly in multiple surgical disciplines.

The salient findings of our study are, first, that intraoperative navigation based on OTI is accomplished significantly faster than existing technologies. These differences are particularly pronounced when compared to newer-generation devices employing intraoperative CT scanning, relative to techniques requiring point-matching registration to preoperative imaging (Figure 4.2D). Second, for spinal procedures, absolute translational and angular accuracy of intraoperative navigation is comparable to benchmark technologies (Figure 4.6). The accuracy measured in this study is the total surgical application

accuracy, stacking the navigation systems accuracy with the surgeons ability to utilize 3D navigation data in placing pedicle screws, where surgeons experience and anatomical knowledge also contribute.[156]

Comparison of screw accuracies between experimental and benchmark systems was adjusted for age, gender, surgeon and surgical technique, in multivariate regression models. Absolute navigation accuracy is more critical in the upper to mid thoracic spine, where pedicle diameters are narrower. The distribution of instrumented spinal levels was equivalent between experimental and benchmark groups. Patient height, weight and ethnicity have also been associated with pedicle diameter, and hence the accuracy requirements of intraoperative navigation systems; these data were not available to us at the time of analysis for inclusion in multivariate models.[157,158]

For cranial applications, the speed advantage of OTI relative to benchmark systems remains albeit less pronounced than in the spine. Multiple techniques for frameless stereotactic patient-to-image cranial registration have been developed, including surface-based or point-matching using anatomic landmarks, skin adhesive markers or bone-implanted fiducials. The accuracy of the OTI system in our cranial cohort is on par with that achieved using bone-implanted skull fiducials by current frameless navigation systems, and superior to the accuracy obtained using more common registration techniques such as surface or point matching on the scalp.[66] Remarkably, the accuracy of OTI is also on par to that reported for frame-based stereotactic localization, the current gold-standard for cranial navigation, which ranges from 2.5 – 3.5 mm in 3D error in both phantom and *in-vivo* studies.[64,65,159] With the introduction of software improvements of the active calibration protocol adjusting for camera drift over time, a significant improvement in median (95%) 3D accuracy from 4.01 mm (5.99 mm) to 1.89 mm (3.40 mm) was seen, without using bone-implanted fiducial screw based registration[66] which would disrupt existing surgical workflows.

The introduction of active calibration protocol is crucial as it facilitates rapid intraoperative re-registration without exposing the patient to additional radiation. While the exact cause of camera drift is unknown, several possible factors have been identified including thermal expansion of the aluminum and acrylonitrile butadiene styrene (ABS)

camera housing due to heat produced by the LED surgical lights, optical drift occurring within the cameras, and torsion stemming from the structural design of the experimental system and various screw connection sites. These inaccuracies, while still present in the spine, are more prominent in cranial applications where a significant time lag between registration and screw placement exists, during which surgical steps such as mechanical drilling, cutting, musculocutaneous flap traction, and patient movement can all introduce navigation error due to relative displacement between the patient's cranium and the navigation reference. The active calibration protocol obviates the need for additional intraoperative imaging while maintaining the required surgical accuracy. While the current analysis comprises the experience of a number of surgeons, the majority of screws navigated with the experimental system were either directly placed or supervised by one surgeon (V.X.D.Y.), representing a single-surgeon influence. Larger studies, involving multiple surgeons, are therefore underway to fully evaluate the evolution of a novice user to a skilled operator using the experimental navigation system, with multicenter studies representing the subsequent logical progression.

4.4 Methods

4.4.1 Human, Cadaver, and Animal Research

This work comprises cadaver validation (REB #260 – 2011), animal studies (AUP#13 – 512), and human trials including prospective and retrospective analysis of pedicle screw placement and cranial surgery using neuronavigation (REB #177 – 2013, #309 – 2014, #086 – 2015, #004 – 2015). Informed consent was obtained for all human subjects.

4.4.2 Human trials

Following engineering optimization based on our swine data, human clinical trials were commenced for craniospinal procedures. Human trials were benchmark against two

commercial point matching-based navigation systems – NAV3/3i (Stryker; Portage, MI, USA), and StealthStation S7 (Medtronic Sofamor Danek; Memphis, TN, USA) for cranial procedures using either point merge and surface tracer protocols. For spinal procedures, benchmark systems consisted of NAV3/3i using point merge and surface tracer protocols, or StealthStation S7 in conjunction with O-arm for intraoperative imaging. 3D Navigation was used to guide thoracolumbar spinal pedicle screw insertion, and map the skull projections of intracranial lesions to optimize craniotomy boundaries.

To maximize safety, the clinical trials begin with a lead-in phase where the experimental system was used to obtain optical topographical imaging and perform registration only, followed by a validation phase where the benchmark navigation system provided surgical guidance while the experimental system measured established guidance trajectories, a cross-over phase where the roles of the benchmark and experimental systems were switched, and finally using experimental navigation system only for surgical guidance with postoperative imaging analysis to verify accuracy. At the time of writing, 171 craniospinal surgical procedures have been performed using our experimental optical navigation system comprising 476 registrations.

4.4.3   Engineering and Clinical Analysis

Experimental Navigation System – Animal Cohort

Translational and angular deviation in the axial and sagittal planes were analyzed for 71 thoracic and lumbar pedicle screws. Screws were placed using the experimental navigation system.

Experimental Navigation System – Cranial Cohort

Accuracy was quantified by placing a tracked probe on the screws of fixed cranial plates and comparing the reported position of the tooltip to the coordinates of the

cranial screws on a postoperative CT registered to the preoperative image. Data was obtained for 216 cranial screws. Subsequent to the integration of an active calibration algorithm utilizing a known geometry to apply appropriate transformations, cranial screws were dichotomized into active calibration (N = 102) vs. non-active calibration (N = 114).

Image Post-Processing

Postoperative CT images were co-registered to preoperative CT using an iterative closest point (ICP) algorithm. The location of the cranial screw was determined as the point where the center of the screw comes into contact the skull. The screw location recorded by the OTI system was compared to location of the centre of the screw on postoperative CT. The postoperative actual screw location was located using an OSIRIX 64 bit workstation (Version 10.9.5, PIXMEO SARL, Switzerland). Comparisons of intra- and postoperative screw locations were performed using the Mann-Whitney univariate test.

Engineering Analysis

For the experimental navigation system, application accuracy was compared between screws that were inserted with and without active calibration using a Mann-Whitney univariate test. P-value < 0.05 was considered statistically significant.

Benchmark Navigation System – Clinical Spine Cohort

Translational and angular deviation in the axial and sagittal planes were computed for 209 cervical, thoracic and lumbar pedicle screws. Screws were placed using commercially available navigation systems. All screws were graded clinically using the Heary Grading System.

Experimental Navigation System – Clinical Spine Cohort

After the lead-in phase (which included freehand or fluoroscopy guided screws, N = 21), translational and angular deviation in the axial and sagittal planes were measured for 162 screws, which were placed using commercially available benchmark navigation or OTI navigation.

Image Post-Processing

Pre- and postoperative CT images were resliced to 0.3 mm thickness and dynamically resliced using multiplanar reconstruction corresponding to the axial and sagittal co-ordinates of the intraoperative and postoperative screw trajectories. For benchmark spine screws, the corresponding axial and sagittal co-ordinates were localized manually using distinct anatomical landmarks. The entry point of the screw was determined as the point where the center of the screw comes into contact with the vertebral body. The distance from the axis of symmetry perpendicular to the point of entry was recorded on the pre- and postoperative axial and sagittal multiplanar reconstructions. As well, the angle between the screw trajectory and the perpendicular distance of the entry point was recorded on the pre- and postoperative axial and sagittal multiplanar reconstructions. All measurements were performed using an OSIRIX 64-bit workstation (Version 10.9.5, PIXMEO SARL, Switzerland).

Heary Grading

All screws were graded clinically using the method introduced by Heary et al.[51] where Grade I denotes the screw is entirely contained within the pedicle pedicle; Grade II the screw violates lateral pedicle but screw tip is contained within the vertebral body; Grade III indicates the screw tip penetrates anterior or lateral vertebral body; Grade IV indicates a medial or inferior breach of the pedicle; Grade V involves a violation of the pedicle or vertebral body endangering the spinal cord, nerve root, or great vessels. Clinical grading was performed independently by two neuroradiologists (CH & PH), three

neurosurgeons (DWC, NP, & LC), and two orthopaedic spine surgeons (RG & GT). Heary grades were assessed for inter-rater reliability using the intra-class correlation coefficient. Clinical grades were dichotomized into no breach/minor breach (Heary Grade ≤ 2) vs. major breach (Heary Grade >2) and reliability of agreement was measured using the Fleiss Kappa test.

Engineering Analysis

Engineering analysis was performed as previously outlined by Jakubovic et al.[160] Translational and angular deviation in the axial and sagittal planes in the benchmark spine cohort were compared with the corresponding deviations in the experimental navigation system spine cohort. Statistical analysis was not performed on the lead-in phase as the experimental navigation system was not used for guidance. Translational and angular deviations were compared using the Kruskal-Wallis test, visualized on Bland-Altman plots (Figure 4.6) and tested using a generalized linear model (Table 4.2). Age, gender, screw location, and guidance method (navigation, fluoroscopy, or freehand), were considered as covariates. P-value <0.05 was considered statistically significant. All statistical analyses were performed using IBM SPSS 17.0 statistical software.

Chapter 5

Navigated High Frequency Micro - Ultrasound Imaging

This chapter presents a study case report establishing our first experiences with intraoperative high frequency micro - ultrasound (μUS) imaging tracked by our optical topographical imaging device. This work establishes the feasibility of intraoperative spine separation surgery and features the ultra-fine resolution conferred by μUS. This work builds on the previous chapters which established the dosimetric advantage of each millimetre of diseased tissue removed during spine separation surgery and confirmed the millimetre application accuracy of the existing neuronavigation systems and our optical topographical imaging navigation system. Integration of the high frequency μUS system with navigation capabilities is essential if real-time dosimetric feedback is required. This work comprises a manuscript that has been submitted for publication in Ultrasound in Medicine and Biology (UMB). The manuscript is included in the dissertation consistent with the guidelines of publisher. The manuscript has been adapted to conform with Ryerson University School of Graduate Studies regulations.

High Frequency Micro - Ultrasound (μUS) Imaging for Spinal Surgery: Initial Experiences

Raphael Jakubovic MSc[1,2], Joel Ramjist[2], Daipayan Guha MD[2,3] Shuarya Gupta [2], Arjun Sahgal MD [5], Stuart Foster PhD[6] & , Victor XD Yang MD, PhD, PEng[2,3,4*]

[1]Department of Physics, Ryerson University, Toronto, ON, Canada, M5B 2K3

[2]Biophotonics and Bioengineering Laboratory, Ryerson University/Sunnybrook Health Sciences Centre, Toronto, ON, Canada

[3]Department of Neurosurgery, Sunnybrook Health Sciences Centre, Toronto, ON, Canada, M4N 3M5

[4]Department of Radiation Oncology, Sunnybrook Health Sciences Centre, Toronto, ON, Canada, M4N 3M5

[5]Department of Physical Sciences, Odette Cancer Research Program, Sunnybrook Research Institute, Toronto, ON, Canada, M4N 3M5

[6]Department of Electrical Engineering, Ryerson University, Toronto, ON, Canada, M5B 2K3

Corresponding Author

Victor Yang

Department of Neurosurgery

Sunnybrook Health Sciences Centre

University of Toronto

2075 Bayview Avenue, Toronto, Ontario, M4N 3M5, Canada Tel: 416-803-9320

Email: victor.yang@sunnybrook.ca

Running Head: High Frequency Micro - Ultrasound Imaging for Spinal Surgery

Conflict of interest, financial disclosures: Dr. Victor Yang's research laboratory has developed the surgical navigation technology, which was licensed to 7D Surgical that provided equipment for this study.

Abstract

High frequency micro - ultrasound (μUS) transducers with central frequencies up to 50 MHz facilitate dynamic visualization of the patient anatomy with minimal disruption of the surgical workflow. μUS improves spatial resolution over conventional ultrasound from millimeter to micrometer, but compromises depth penetration. This trade-off is mitigated by removing bone such that the probe can be placed directly into the surgical cavity. By fusing μUS with preoperative imaging, and tracking the probe intraoperatively using our optical topgraphical imaging technology, we can provide dynamic feedback during surgery. We present our initial experience using μUS during spinal procedures for

four patients (3 tumor resections, 1 cystic synovial mass). During surgery, the μUS probe was registered to the preoperative CT and MR images. μUS delineated exquisite detailing of the spinal anatomy including white/gray matter differentiation and nerve root visualization, allowing accurate assessment of decompression/tumor resection progress. Thus, tracked μUS conferred significant improvement over conventional ultrasound.

5.1 Introduction

Intraoperative imaging has gained prominence in the field of image guided surgery with recent advancement in various regional or whole body imaging modalities. Intraoperative imaging aides the physician in visualizing patients' anatomy to make real-time decisions about their surgical plan based on the current state of the patient. Adoption of current imaging modalities into a neurosurgical setting, especially in spine, has been limited due to concerns with speed, ease of use, cumbersome size, sterility, and/or increased exposure to radiation.[47,54,151] In contrast ultrasound technologies enjoy widespread use within cranial neurosurgery as it provides a fast, non-ionizing method to visualize the patient anatomy without causing major disruption of the surgical workflow.[161] While use of ultrasound has not yet become prevalent for spinal surgeries distinct advantages have been shown particularly during spinal tumour resection.[81]

High frequency micro - ultrasound (μUS) offers a distinct resolution advantage over conventional ultrasound while compromising with reduced penetration depth.[69] Considering the resolution necessary for neurosurgical applications (within 2 mm of accuracy), a higher-resolution system such as that offered by a μUS is necessary to track and update margins during the surgery, potentially improving surgical outcomes. μUS has been used in a variety of applications including the monitoring of arteriovenous fistulas, [70] pediatric vascular development,[71] hand transplantation,[72] and intima and

medial thickening for a variety of indications.[73 – 77] Integration of these probes into the operating room will enable dynamic intraoperative imaging capable of delineating white matter tracts, nerve roots, vascular networks, and tumor margins with micrometer resolution. μUS is particularly suited for spinal procedures as the depth requirements are minimal considering the bone is quite often removed and the ultrasound probe can be advanced directly into the surgical bed. Three high frequency micro - ultrasound transducers are available for this study (UHF 22, UHF 48, and UHF 70) with central frequencies of 15 MHz, 30 MHz, and 50 MHz with axial resolutions of 100 μm, 50 μm and 30 μm respectively. This resolution advantage is particularly beneficial in neurosurgery considering the precision required for many neurosurgical procedures.

In this work, we present the first experiences fusing our novel optical topgraphical imaging surgical navigation system with μUS intraoperatively. Further, we have established that navigated high frequency micro - ultrasound can provide real-time feedback which can then be incorporated into the surgical plan and potentially guide clinical course.

5.2 Methods

Four patients were recruited into our existing research ethics board approved spine navigation study (004 – 2015) at Sunnybrook Health Sciences Centre. Informed consent

was obtained from each participant in the study. High frequency micro - ultrasound imaging (VevoMD Imaging Platform, FUJIFILM VisualSonics, Inc, Toronto, Canada) was performed during surgery through the Health Canada Special Access program. Inclusion criteria comprised patients scheduled to undergo spinal decompression with laminectomy and tumor resection. Surgical procedures were not altered in any way and were performed according to the established standard of care. Briefly, the current standard practice spinal surgery involves bony exposure and subsequent bone removal with or without x-ray imaging confirmation. This is followed by inspection of the surgical incision site with ultrasound imaging. The surgical cavity was filled with saline and the sterile ultrasound probes were inserted into the cavity to image using a sterile sheath and proper reprocessing protocol. The surgical target was imaged first by a standard ultrasound imaging platform prior to being imaged by the μUS probes. Preoperative MRI was fused to the preoperative CT using a semi-automatic rigid body registration prior to surgery using Anaylze 12.0 medical imaging software (AnalyzeDirect Inc., Kansas, United States). During surgery, the μUS probe was registered to the preoperative CT and MR images using an in-house designed infrared (IR) ultrasound tracker and our novel optical topgraphical imaging system using an iterative closest point (ICP) algorithm (Figure 5.1). The optical topgraphical imaging system utilizes structured light to obtain a 3-dimensional point cloud of the surface anatomy. The camera pod is mounted onto an articulating arm and contains 2 white light cameras, 2 IR cameras and a projec-
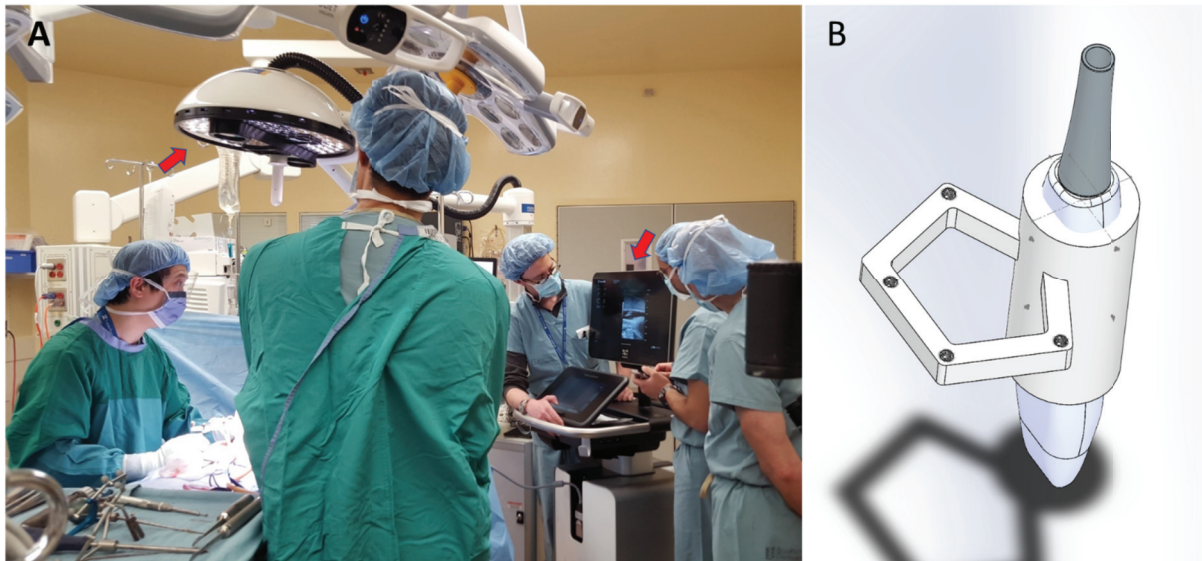
Figure 5.1: A) Intra-operative navigated ultrasound: Optical topographical imaging system and high frequency ultrasound system are present in the operating theater (red arrows). B) Computer-aided design (CAD) of a tracked high frequency ultrasound probe.

tor. The projector illuminates the surface and the image is reconstructed by the cameras based on the depth distortions of the projected pattern. Following image acquisition, the topgraphical image is registered to the pre-acquired CT or MR and the ultrasound probe is tracked. This facilitates IR tracking of the ultrasound probe during surgery. μUS probe selection was based on the discretion of the surgeon.

5.3 Results

Images obtained comprised 4 spinal decompression surgeries (3 tumor resections, 1 hemorrhagic synovial mass). μUS images obtained during spine surgery delineated exquisite detailing of the spinal anatomy including delineation of white matter and grey matter tracts and nerve roots and allowed accurate assessment of the extent of decompression/tumor resection. Intraoperative navigation enabled real-time tracking of the imaging field with respect to preoperative imaging. Our patient experience is described below.

5.3.1 Patient 1

69 year old female with a diagnosis of a hemangioma with epidural extension and cerebrospinal fluid effacement causing spinal cord compression. The patient underwent preoperative CT and MRI of the thoracic spine and was identified as a candidate for separation surgery with the potential for subsequent stereotactic body radiosurgery to alleviate symptoms associated with cord compression (Figure 5.2). Patient underwent complete tumor embolization of the T7 lesion prior to navigated unilateral spinal fusion one level above and below the lesion. During surgery, the surgeon achieved spinal cord decompression with tumor debulking of approximately 3 mm. Tracked axial and longitudinal μUS images were obtained intraoperatively at a central frequency of 30 MHz (Figure
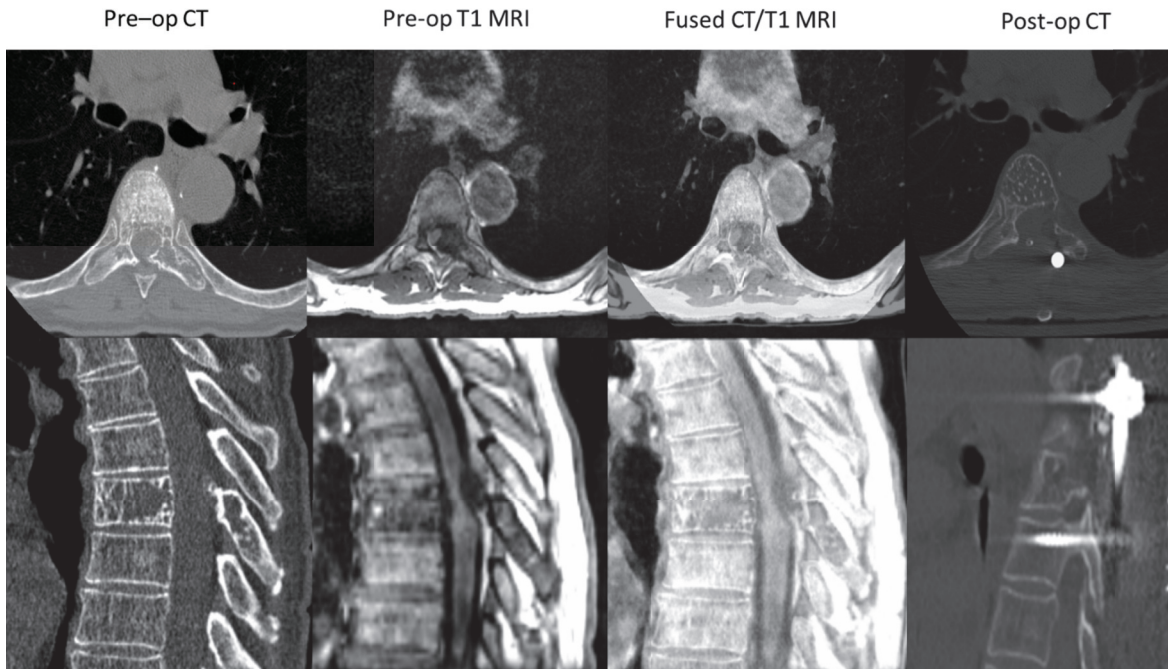
Figure 5.2: Patient 1: Clinical course – Patient with hemangioma with epidural extension and cerebrospinal fluid effacement causing spinal cord compression. T1 MRI was fused to CT for navigation. Postoperative changes seen on CT with unilateral instrumented fusion.

5.3). The acquired μUS images allowed the surgeon to gauge the extent of decompression during the surgery. Patient symptoms improved post-surgery such that radiation therapy was deemed unnecessary.

5.3.2 Patient 2

69 year old male with a left S1-S2 cystic, hemorrhagic synovial mass with suspicion of metastatic pathology due to prior history of prostate cancer. Patient underwent a L5-S2
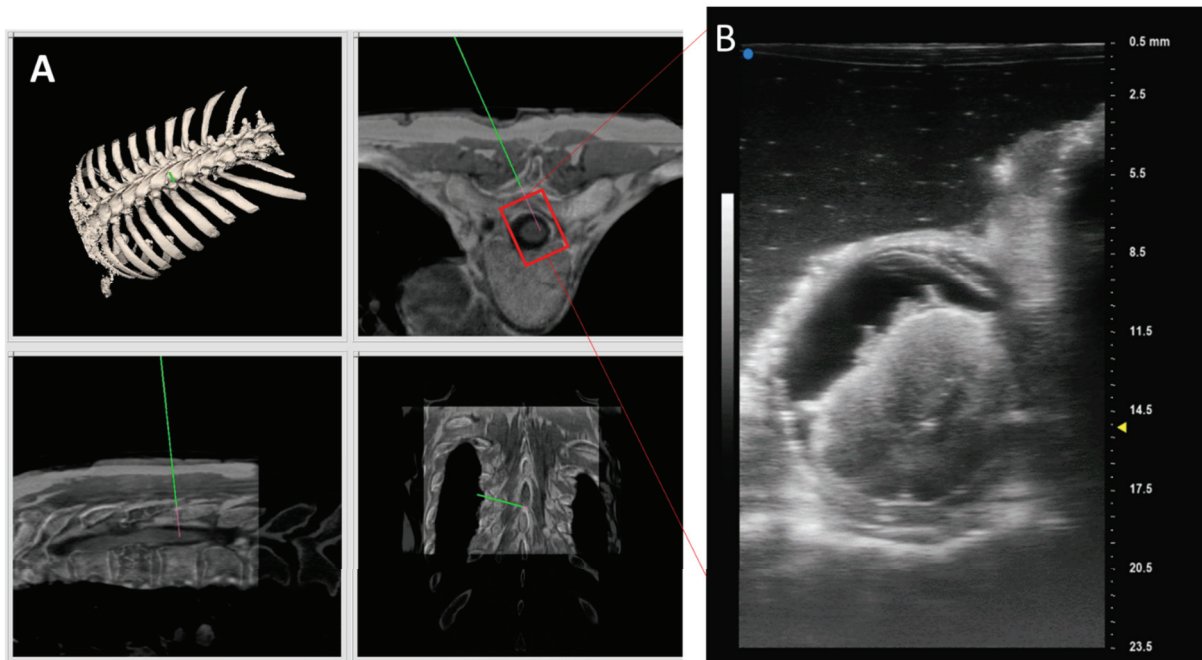
Figure 5.3: Patient 1: Tracked axial intraoperative high frequency μUS images acquired at 30 MHz. A) Tracking information – field of view (Red Box) and trajectory (Green Line) of the ultrasound probe as tracked by the navigation system. B) Representative μUS axial image.

bilateral laminectomy with navigation and ultrasound for incisional biopsy. Exposure of the thecal sac and the cystic wall of the lesion was achieved, thus facilitating cystic wall resection and decompression. Tracked intraoperative μUS and Doppler imaging with a central frequency of 30 MHz facilitated visualization of the lesion and surrounding vascular network (Figure 5.4). μUS identified the lesion as hemorrhagic and was able to delineate the location of the cyst and vascular networks with micrometer resolution (Figure 5.4). Following surgery pathology confirmed a synovial cyst rather than metastatic disease.

Figure 5.4: Patient 2: Tracked axial and longitudinal intraoperative high frequency µUS images acquired at 30 MHz. A) Tracking information – field of view (Yellow Box) and trajectory (Green Line) of the ultrasound probe as tracked by the navigation system. B,C) Representative axial and longitudinal µUS images. D) Intraoperative Doppler imaging for vessel delineation.

5.3.3 Patient 3

76 year old male with a soft tissue mass located on the left C6-C7 neural foramen without destruction of the adjacent bone. Patient presented with progressively worsening left arm and left leg weakness and was confined to a wheelchair. The patient underwent CT and MRI of the cervical spine and a CT angiogram of the head and neck to visualize the proximity of the tumour to the left vertebral artery. The C6-C7 intradural, extramedullary mass was presumed to be a meningioma occupying the spinal canal, extending into the epidural space and causing severe rightward displacement and compression of the spinal cord. Patient underwent a posterior C5-C7 laminectomy and resection (Figures 5.5). Intraoperative µUS was used to locate and the C6 tumour and assess surgical progress. µUS identified the lesion and was able to delineate white matter tracts, nerve roots, and vascular networks with micrometer resolution (Figures 5.6). Tracked µUS was not available for this case. Patient symptoms improved post-surgery and the patient was ambulating with a crutch six-weeks post-surgery.

5.3.4 Patient 4

73 year old male with a recurrent L2 T cell lymphoma previously treated with multiple rounds of chemotherapy and radiation. Most recent presentation was a L2 mass measuring 11 cm. Treatment of 20 Gy/ 5 fractions shrunk the tumour to 5 cm. Substan-
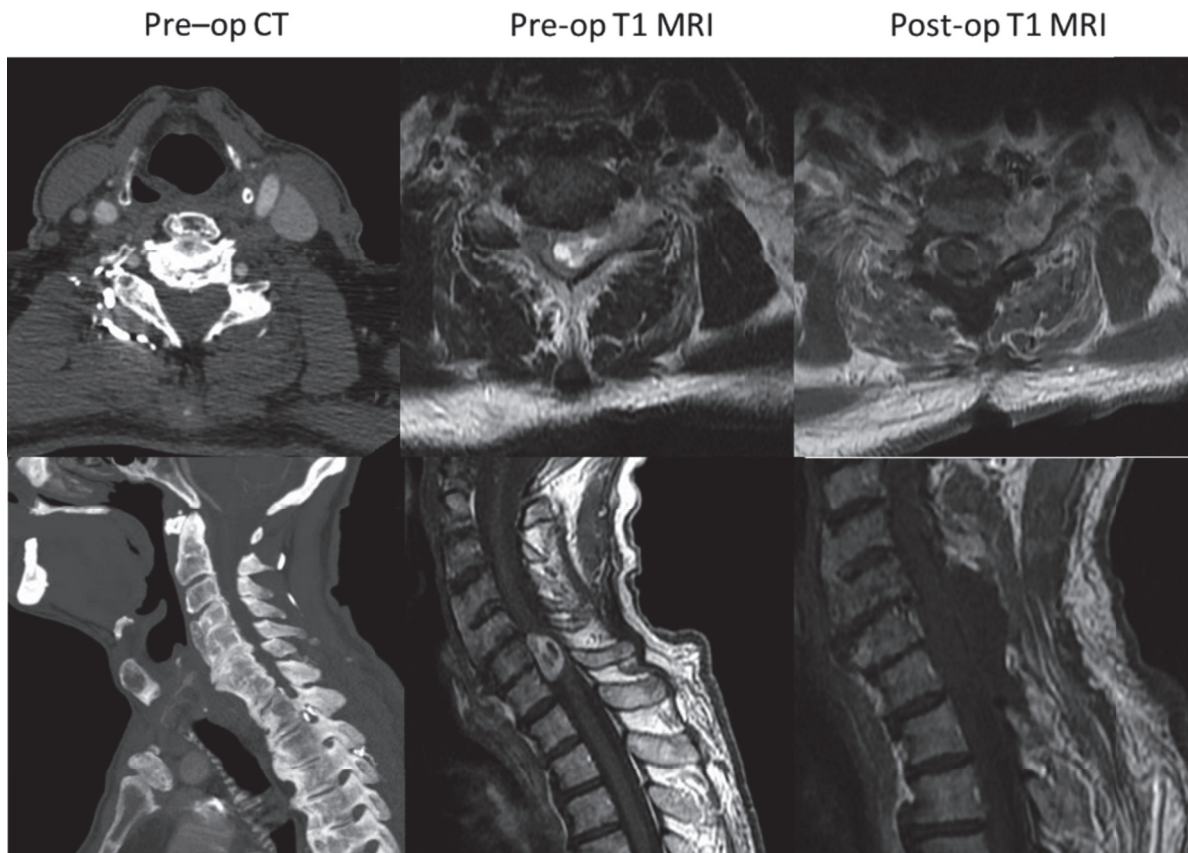
Figure 5.5: Patient 3: Clinical course – Patient with C6-C7 intradural, extramedullary mass occupying the spinal canal, extending into the epidural space and causing severe rightward displacement and compression of the spinal cord. Visualized on CT angiogram and T1 MRI. Postoperative debulking seen on T1 MRI.
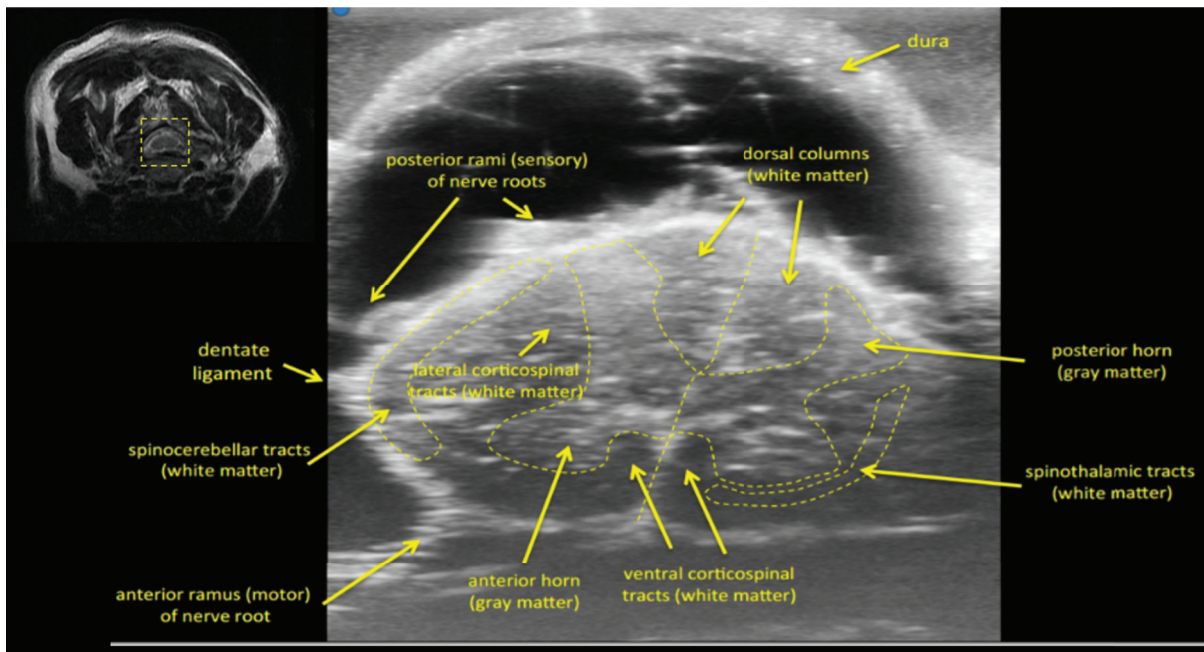
Figure 5.6: Spine decompression surgery: MRI (millimeter) to high frequency μUS (micrometer) comparison shows clear definition of the spinal cord with clear delineation of white matter tracts, nerve roots, and vascular networks with micrometre resolution.
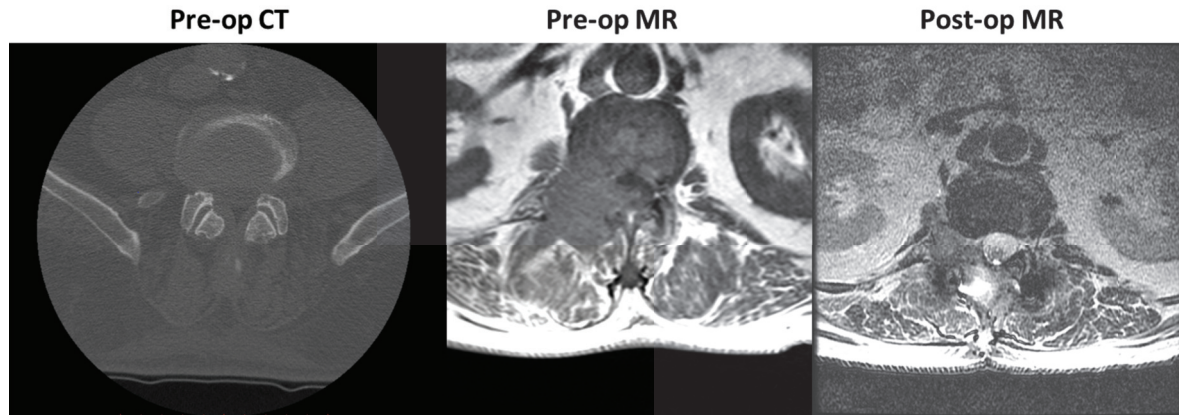
Figure 5.7: Patient 4: Clinical course – Patient with L2 mass measuring 11 cm. Pre-operative MRI shows soft tissue lesion extending into the L2 spinal vertebral body and obliterating the R L2 pedicle. Postoperative changes seen on MRI with right semicircular epidural disease with minimal compression on the thecal sac.

tial epidural extension obliterating the right L2 pedicle, occupying the epidural space, and traversing nerve roots was observed, causing L2 radiculopathy and other neurological symptoms (Figure 5.7). Patient underwent L2 laminectomy and epidural decompression the tumor with L1-L3 instrumented fusion. No hardware was placed at L2. Following bone removal, since visualization was difficult due to the tumor being enmeshed in the dura superior to the exiting L2 nerve root, only limited resection was achievable. Tracked axial and longitudinal μUS images were obtained intraoperatively at a central frequency of 30 MHz (Figure 5.7). The acquired μUS images allowed the surgeon to evaluate the extent of decompression of the L2 nerve roots and proceed with resection without causing additional neurological damage (Figure 5.8).

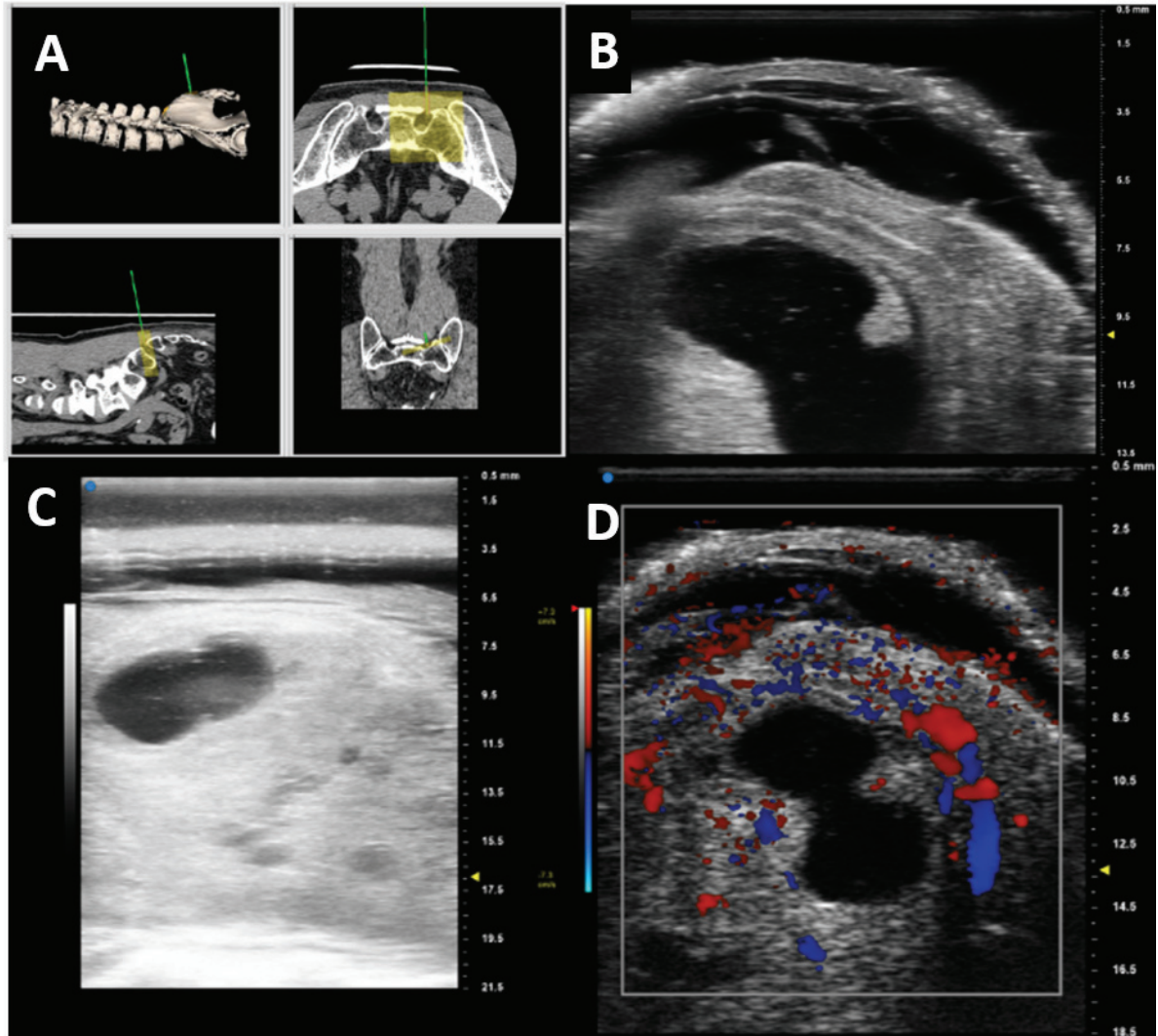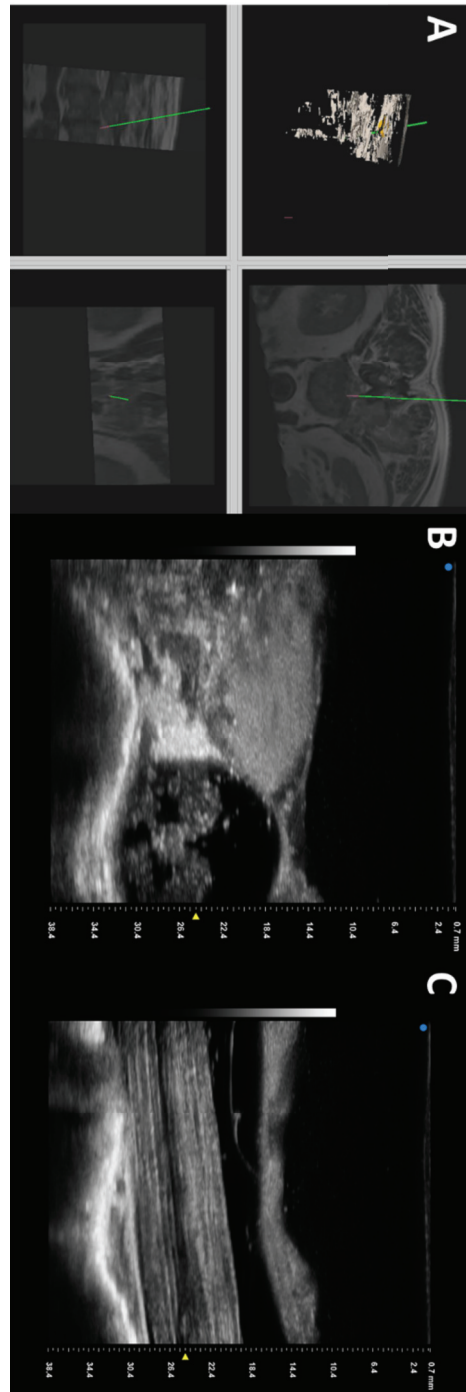Figure 5.8: Patient 4: Tracked μUS – Tracked axial and longitudinal intraoperative high frequency μUS images acquired at 30 MHz. A) Tracking information and trajectory (Green Line) of the ultrasound probe as tracked by the navigation system. B,C) Representative axial and longitudinal μUS images.

5.4   Discussion

In this study, we present our first experiences with tracked intraoperative μUS imaging using our novel optical topgraphical imaging technology. Intraoperative ultrasound is well established in brain using optical tracking technologies to register ultrasound data to pre-surgical CT or MRI and track surgical tools during surgery.[78,79] This facilitates dynamic intraoperative imaging unattainable with traditional preoperative CT/MRI without exposing the patient to additional radiation. However, while the feasibly of tracked intraoperative ultrasound in spine has been established, use of ultrasound during spinal tumour resection has been limited.[78,80] This lack of clinical acceptance has been attributed to ultrasound probes that may be larger than the surgical field, poor contrast particularly in the presence of bleeding, and clinicians unaccustomed to using ultrasound.[81] Further, in regards to tumour resection and depending on the tumour histology, distinguishing tumour margins from perifocal edema using ultrasound presents a challenge considering the limited resolutions of traditional ultrasound probes.[82] As such, significant opportunity exists for the use of high frequency ultrasound which confers spatial resolution on the order of micrometers especially in the context of an open surgical field where depth limitations are minimal.

Intraoperative three dimensional ultrasound has been used to provide continuous, real-time tracking of spinal tumors during surgery and is effective in determining the

location and size of the tumor.[78,80,81] The ultrasound probe is generally guided by an optical tracking device eliminating the need for registration to the pre-acquired CT or MRI during surgery.[78,81] Further, ultrasound is a low-cost imaging modality and has limited effect on surgical workflow especially when compared to intraoperative CT or MRI. Therefore, by fusing intraoperative optical tracking and μUS with CT and MRI for spinal metastases resection dynamic imaging feedback can be provided during surgery and essentially guide the surgeon with improved precision. This advantage is highlighted in the cases reported here as μUS facilitated exceptional visualization of the surgical exposure to not only gauge the extent of decompression and resection but to also delineate white matter tracts, nerve roots, and vascular networks with micrometer resolution.

Integration of optical tracking and μUS with CT and MRI into the operating theatre is compelling in patients with spinal tumors particularly in the context of spinal instability. The current clinical paradigm is such that spinal instability precludes removal of the entire tumor and treatment with radiotherapy is limited by the rigid dose tolerances of the spinal cord.[162] Treatment often involves a combined treatment approach coined "spine separation surgery" where minimal tumor resection is performed in order to create a separation between the spinal cord and the diseased tissue such that spinal stability can be maintained (with instrumented fusion if necessary) without damaging the spinal cord during subsequent stereotactic body radiotherapy.[43,162] In this regard,

we have shown the utility of tracked μUS considering the imaging results achieved in this report. Thus, in the case of spinal tumor resection where millimeter precision is required, dynamic imaging feedback can be provided during surgery and essentially guide tumor resection with a higher degree of precision. Considering that the registration accuracy of our navigation system is submillimeter and our application accuracy is on the order of 1-2 mm (in press), navigated μUS would facilitate this approach.

Moreover, the combination of this approach with the ability to integrate radiation dose planning with spinal tumor resection surgical planning, would facilitate real-time intraoperative dose planning allowing the surgeon to remove the precise amount of tumoral tissue to maximize dose coverage of the diseased tissue and remain within the dose tolerances of the spinal cord. This has the potential to provide real-time intraoperative feedback inform the surgeon the extent of tumor resected and the dose advantage, thus facilitating a true dynamic intraoperative dose planning feedback loop.

5.5   Conclusions

Our patient experiences have established feasibility of intraoperative navigated micro - ultrasound. Considering the distinct resolution advantage over conventional ultrasound imaging systems, navigated μUS has the potential to improve surgical precision and

impact patient outcomes. However, in practice a fully integrated navigated μUS/dose planning software package is necessary to ensure adoption. Work is currently underway to achieve those goals.

Chapter 6

Future Works and Conclusions

6.1 Future Works

6.1.1 Intraoperative Ultrasound for Spine Separation Surgery

The objectives achieved in this dissertation represent the key components of a large-scale program aimed at establishing true dynamic intraoperative dose planning feedback loop for spinal tumour resection. This work is essential, as it has proven the dosimetric advantage of spine separation surgery, established the accuracy of neuronavigation, and shown that the resolution of intraoperative high frequency micro-ultrasound imaging is sufficient for visualization of debulking progress. This will allow the surgeon to know the extent of tumour resected during surgery and facilitate true dynamic intraoperative dose planning feedback loop.

A shift in the paradigm of treatment is warranted. The current standard of clinical care is to surgically resect the tumour prior to radiotherapy. The objective of the surgery is to perform minimal surgical resection such that the dose objectives of radiotherapy can be achieved. This approach is logical since surgical resection is an open procedure with high rates of morbidity and mortality, and radiotherapy is limited by the dosimetric constraints of the spinal cord. Further, with the evolution of technology facilitating advances in radiation delivery, surgical navigation, and photodynamic therapy (PDT), disease targeting therapeutics sparing the surrounding healthy tissues are preferred. A large-scale program integrating image guided surgical planning, tumour resection, radiotherapy, and PDT would achieve this objective, creating a new standard for treating spinal tumours.

6.1.2   Intraoperative 3-dimensional Ultrasound for Spine Separation Surgery

Intraoperative three dimensional ultrasound has been used to provide continuous, real-time tracking of spinal tumours during surgery and is effective in determining the location and size of the tumour.[79,81] The ultrasound probe is generally guided by an optical tracking device eliminating the need for registration to the pre-acquired CT or

MRI during surgery.[79] Further, ultrasound is a low cost imaging modality and does not interfere with the surgical workflow especially when compared to intraoperative CT or MRI.

Therefore, future work focusing on the fusion of optical topographical data with CT, MR and ultrasound is imperative. This would provide dynamic imaging feedback during surgery and guide tumour resection with a high degree of precision. The combination of this approach with the ability to integrate radiation dose planning with spinal tumour resection surgical planning would facilitate real-time intraoperative dose planning. Essentially, a dosimetry guided, surgically navigated solution would provide specific real-time assistance enabling precise tumour resection until the dosimetric objectives are achieved. This can only be accomplished through the integration of 3-dimensional ultrasound imaging and fusion, with automatic volumetric segmentation of the residual tumour volume, such that intraoperative dose planning can be achieved.

6.1.3 Spine Photodynamic Therapy

Due to the constraints of the current therapeutic paradigm, there has been considerable interest in adopting novel adjunct therapies in the context of spinal metastases. The current treatment paradigm for spinal metastases is variable, but for the most part

treatment involves surgery, radiotherapy or a combination of surgery and radiotherapy. Combination therapy is required since surgical resection introduces spinal instability and radiation therapy alone is not effective due the rigid dose constraints of the spinal cord. By amalgamating surgical resection and SBRT a buffer is created between the spinal cord and the epidural disease allowing for increased dose delivery to the tumour and increasing local control.[15]

An alternative approach to sparing the spinal cord is photodynamic therapy (PDT). PDT is an effective, targeted treatment that destroys precancerous and cancer cells without harming surrounding tissue. PDT employs a light sensitive photosensitizing substance that accumulates in neoplastic cells and is activated with the application of low power light. Since PDT activation requires the application of a wavelength specific light, clinical applications have traditionally been limited to anatomically accessible lesions. Due to recent advances in minimally invasive surgery (MIS) PDT can now be employed in bone using targeted light application. Feasibility has been established in pre-clinical mouse experiments and safely translated clinically in a cohort of 5 patients. [163,164] Further, pre-clinical models have established PDT as effective, providing synergistic effects with bisphosphonate and radiation therapy treatments.[164]

Therefore, future work establishing PDT as an adjunct to spine separation surgery

specifically in patients with severe spinal instability precluding extensive tumour de-bulking is imperative. This approach would utilize the synergistic effect of PDT with radiation therapy to maximize the effect of treatment on the tumour while sparing the spinal cord and associated structures from superfluous radiation dose. This would augment the current therapeutic approach, further enhancing local control and facilitating the treatment of hard to treat metastatic spinal tumours. This would further enhance our ability to deliver safe and effective treatment of metastatic spinal tumours.

6.1.4 Gamma Knife Radiotherapy/Deep Brain Stimulation

While much of this dissertation dealt with surgical accuracy and established the sub-millimetre requirements for in spine, this work is easily translatable to applications in brain including stereotactic radiosurgery (SRS) and deep brain simulation (DBS). Both make use of a stereotactic frame and although the accuracy of the stereotactic frame has been shown to be on the order of $2.5 - 3.5$ mm[65,66,165], submillimetre accuracy is still preferred and the $1 - 2$ mm application accuracy afforded by our cranial navigation system with active calibration would be appropriate for both SRS and DBS. Further integration of tracking with millimetre precision would potentially facilitate frameless procedures.

The standard Gamma Knife radiosurgery and DBS treatments consist of a dose plan-

ning stage and a treatment stage. The dose planning stage uses pre-acquired MR images to determine the soft tissue characteristics of the target. On the day of the procedure, an appropriate stereotactic frame (Leksell, Gill-Thomas-Cosman (GTC), Cosman-Roberts-Wells (CRW), Browns-Roberts-Wells (BRW), etc.) is placed on the patient using percutaneous pins with the lesion optimally situated in the centre of the frame. The patient then undergoes CT imaging with the fixed stereotactic frame to establish the co-ordinate system for treatment planning. The MR is fused to the CT in order to localize the target with respect to the stereotactic co-ordinate system and the patient treatment is planned. The stereotactic frame must remain fixed to the patient during treatment planning and for the duration of the treatment.

Although effective immobilization can be achieved using the stereotactic frame, the fixation of the percutaneous pins and the stereotactic frame are considerably uncomfortable for the patient. Therefore, significant work has been done particularly in the field of radiotherapy to effectively immobilize the patient and reduce the invasiveness of immobilization by introducing various bite block or thermoplastic mask variations.[166,167] Further, various imaging systems have been used to track patient movement during treatment using optical topographical imaging and infrared tracking, but have not been able to track sudden, random intra-fraction motion with sufficient spatial and temporal resolution for Gamma Knife radiosurgery.[168,169] Implementation of a real-time, non-ionizing

Figure 6.1: Left Panel: "Rando" anthropomorphic head phantom with Leksell stereo-tactic frame attached. Right Panel: Experimental set-up for acquisition of optical topographical image.

image guided system that can maintain millimetre level positional accuracy as has been

shown in this dissertation is required and would represent a major breakthrough in DBS

and Gamma Knife radiosurgery (Figure 6.1 & Figure 6.2).
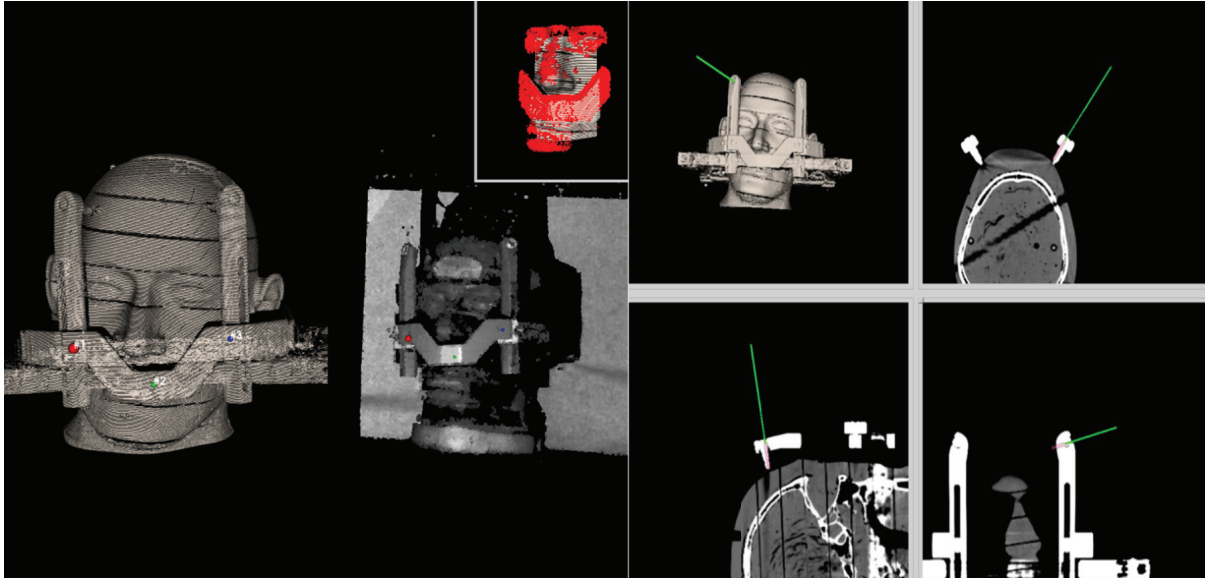
Figure 6.2: Registration and tracking of the Lesksell stereotactic frame. Left panel: Stereotactic Frame was attached to the "rando" anthropomorphic head phantom. Optical topographical image was registered to pre-acquired CT of the head. Note the alignment of the frame and facial features in the subpanel. Right Panel: Following registration tool tracking is enabled.

6.1.5 Optical Topographical Imaging Tracking for SRS

With regards to stereotactic radiosurgery (SRS) the fundamental principle is to deliver a dose of radiation that is high enough to control the lesion and concentrated enough to avoid undesired side effects in the surrounding tissues. Therefore, SRS is a high precision, high dose radiation, treatment utilizing a multiple beam geometry and creating a conformal beam to the chosen target. This ultimately destroys the tumour while minimizing damage to the adjacent tissues.[22] A number of treatment modalities are available for SRS facilitating treatment with photons (i.e. Gamma Knife, or linear accelerator (LINAC)) or charged particles (e.g. protons). While each particular modality has its

own distinct benefit, Gamma Knife is particularly suited for brain tumours considering the rigid fixation of the patient within a stereotactic frame, and the ability to deliver radiation with uncertainties on the order of $0.2 - 0.4$ mm as compared to 1 mm for its LINAC counterpart.[170 – 172]

Delivery of treatment with the Gamma Knife is fundamentally distinguishable from other radiosurgery systems as the source remains stationary and the target is directed towards a fixed beam of radiation. Therefore, the accuracy of treatment depends on the ability to localize the target in three dimensions and vary the position of the target at the focal point of the Gamma Knife such that complex treatment plans can be achieved. Recent technological advances and the introduction of submillimeter accuracy automatic positioning systems have facilitated this approach, allowing for the delivery of highly conformal dose distributions to the tumour site while minimizing dose to surrounding normal tissue structures and organs at risk (OARs).

Further, the capabilities of the Gamma Knife now include head repositioning, and the use of bite block within the head frame has shown the ability to increase repositioning accuracy and reduce head movement during treatment.[166] However, while various studies using frameless stereotaxy in the context of Gamma Knife and LINAC SRS have confirmed increased setup accuracy by using various masks and/or a bite block, these

techniques do not account for variations in internal bony anatomy relative to the bite block or mask. The current gold-standard for set-up is therefore pre-treatment CT with a frame or CBCT without a frame.[166,167] Further, while use of thermoplastic masks and bite blocks are less invasive than the stereotactic frame, patient compliance is compromised due to discomfort, claustrophobia and potential skin reactions due to the presence of electron build-up from the mask material.

The additional use of on-line image guided radiation therapy (IGRT) can further improve patient set-up accuracy. Three dimensional image guidance using cone beam computed tomography (CBCT) is the current standard for pre-treatment image guided radiotherapy and provides clinically useful bony and soft tissue contrast in the head and neck region with sub-millimetre resolution for accurate verification of patient set-up.[173] However, while both 3D-CT imaging techniques are well established for pre- and post-treatment set-up verification, the inherent process of image acquisition, reconstruction and registration necessitate long verification times (1 – 3 minutes) that are impractical for tracking real-time intra-fractional motion.[174] Intra-fractional validation is a possibility using real-time kilovoltage radiographs but the resulting images provide only 2D tracking and necessitate additional radiation dose.

The ability to track sudden, random intra-fraction motion is of particular importance

for long single fraction treatment courses with tight treatment margins typical of Gamma Knife radiosurgery. For example, treatment of patients without an immobilization mask would necessitate real-time feedback to catch large sudden patient motion (i.e. sneezing, twitching) that falls outside of the prescribed safety margins. Incremental gains have been made towards eliminating the stereotactic frame with the introduction of the Leksell Gamma Knife® Icon™ with CBCT, facilitating use of a modified thermoplastic mask with infrared (IR) tracking of a patient nose marker. This system has been validated as an adjunct to CBCT to monitor intra-fraction motion with the assumption that IR marker movement is correlated with infraction motion.[168] To reduce the footprint of the thermoplastic mask, implementation of a real-time, non-ionizing image guided system that can maintain millimetre level positional accuracy is required and would represent a major breakthrough in Gamma Knife radiosurgery considering since the PTV margin limit is typically $3 - 5$ mm for intracranial applications.[168]

In the radiotherapy setting, the use of OTI could potentially allow for real-time acquisition of the patient anatomy enabling the tracking of any movements in the region of interest. OTI improves on IR navigation methods as it enables real-time tracking of both the patient nose marker and the actual patient anatomy. Introducing robust, real-time topographical imaging will reduce radiation exposure and eliminate the set-up CT or CBCT prior to treatment. Accuracy requirements can be maintained by registering

the OTI image of the stereotactic frame to pre-acquired CT or MR images. Moreover, by using on-line OTI positioning information as feedback to a radiation delivery device, detection of positional deviations beyond a pre-determined action level could interrupt beam delivery until the patient reverts to a baseline position. Intra-fraction monitoring could be achieved without subjecting the patient to any additional ionizing radiation exposure, thereby providing the basis for true maskless radiation therapy. Therefore, integration of OTI into the Gamma Knife radiosurgery workflow can be used to provide real-time patient monitoring of intra-fraction motion. Expanding this approach, OTI can be adapted to track distinct anatomical features to reduce the thermoplastic mask from full face to partial face and ultimately eliminate the need for immobilization masks. This innovative approach would deem the use of a stereotactic frame, patient specific mask, and pre-treatment CT or CBCT verification irrelevant, introducing a new paradigm in radiosurgery.

6.1.6 Optical Topographical Imaging Tracking for SRS: Preliminary Data

Preliminary OTI surfaces were obtained for the "rando" anthropomorphic head phantom shown in Figure 6.3. Using the current (non-optimized) system, preliminary assessment the OTI monitoring system for monitoring for Gamma Knife Radiosurgery was

Actual Translation Distance	OSI Detected Translation	Translation Error
1.0 mm Lateral	0.57	-0.43
1.5 mm Lateral	1.16	-0.34
2.0 mm Lateral	2.18	0.18
5.0 mm Lateral	5.43	0.43
1.0 mm Longitudinal	0.69	-0.31
1.5 mm Longitudinal	1.53	0.03
2.0 mm Longitudinal	1.69	-0.31
5.0 mm Longitudinal	5.20	0.20

Table 6.1: Lateral and longitudinal deviation relative to translation stage.

performed using a calibration cube (Pentaguide). The calibration cube was placed on a translation stage for imaging and registered to a reference 3D reconstructed CT. A representative OTI image is shown in Figure 6.4. The stage was translated laterally and longitudinally. At each translation, a surface image was obtained and registered to the reference surface image using an iterative closest point (ICP) algorithm. The registration algorithm minimizes the point-to-surface distance in two steps. First, an initial registration is performed at 3 pre-defined points of interest to arrive at a first approximation. Next, the algorithm performs a global registration over the entire imaging surface to arrive at a final solution. Mean rigid translations were quantified and compared to actual translations. Mean (standard deviation) translation shifts relative to the actual shifts were 0.279 ± 0.137 mm are shown in Table 6.1 and Figure 6.5, which is within the required sub-millimeter accuracy of typical intracranial Gamma Knife Radiosurgery.
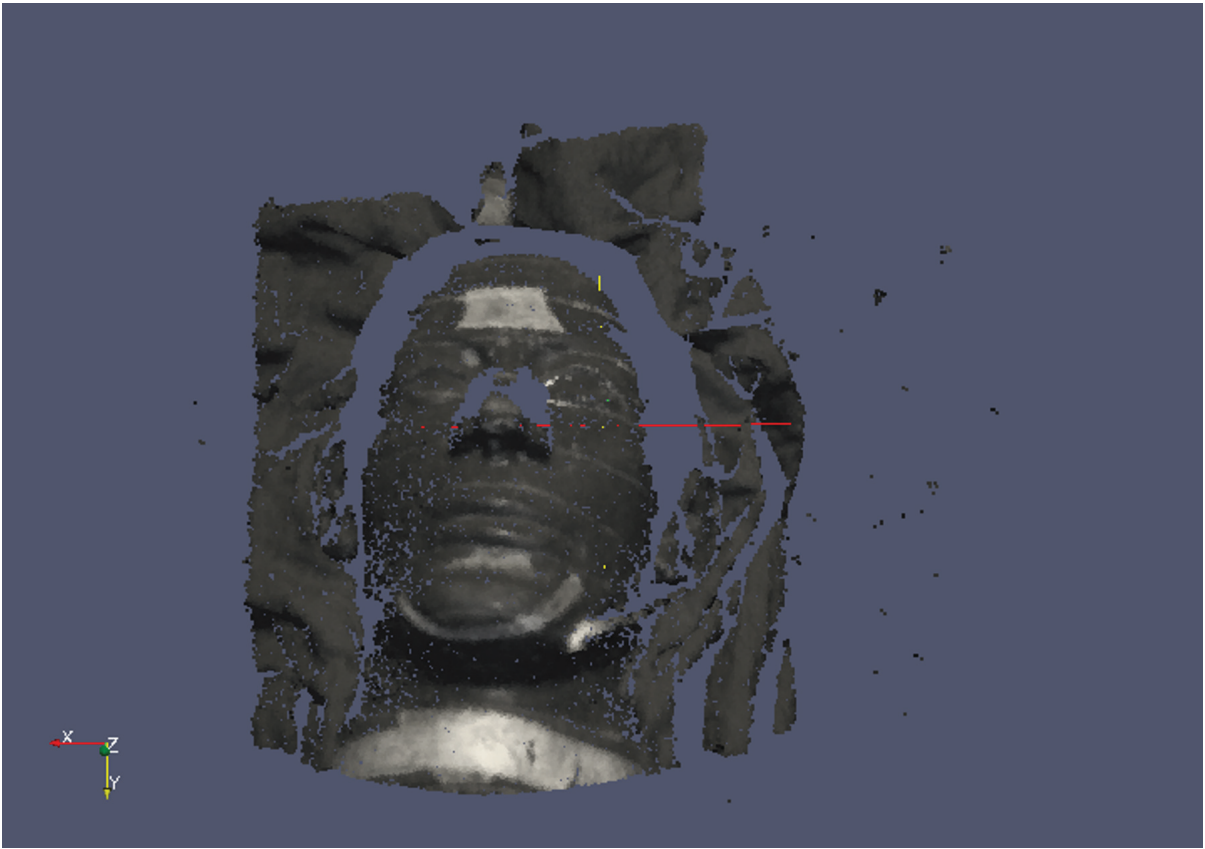
Figure 6.3: Optical topographical image of a Rando anthropomorphic phantom.
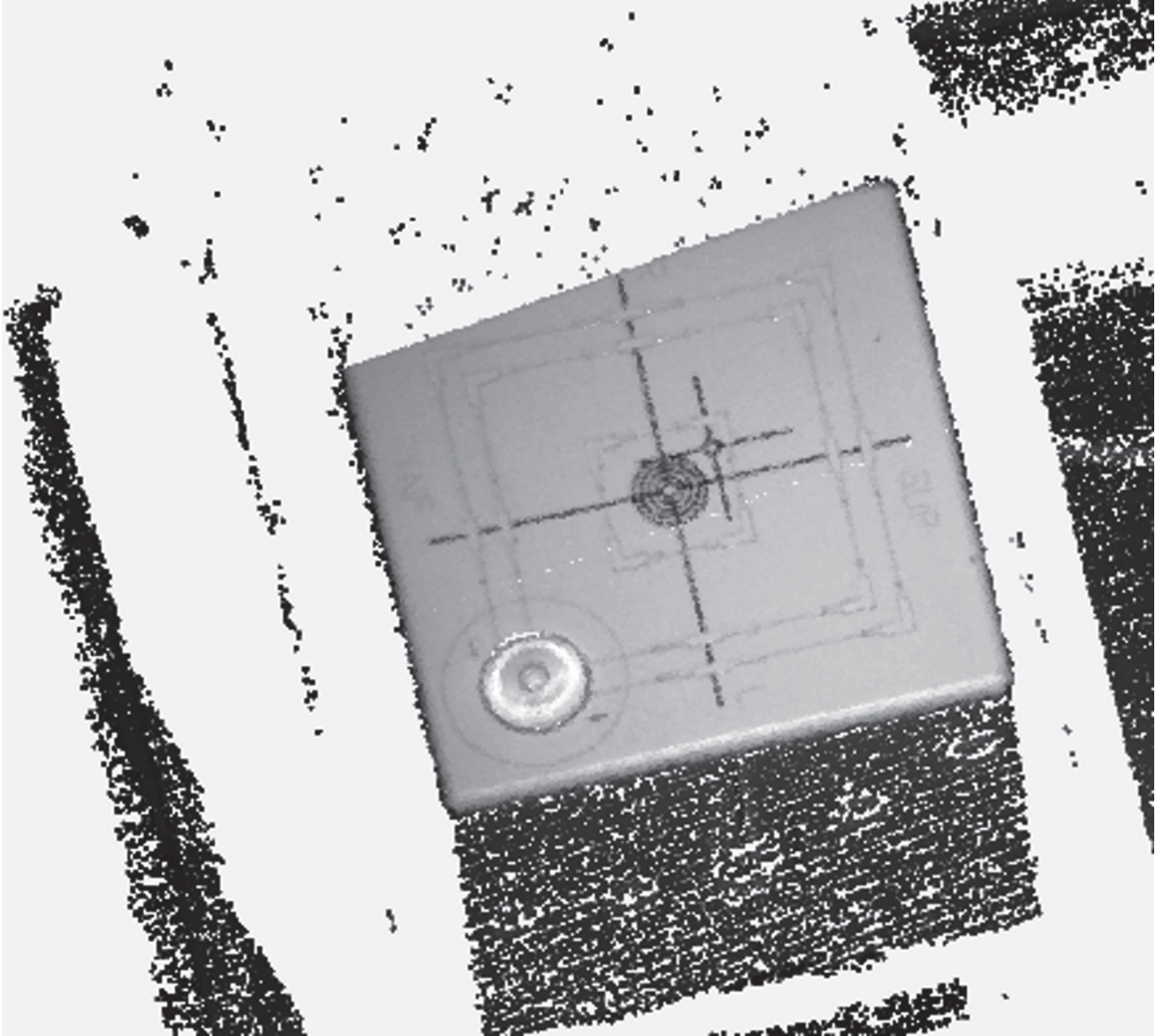
Figure 6.4: Optical topographical image of a calibration cube.
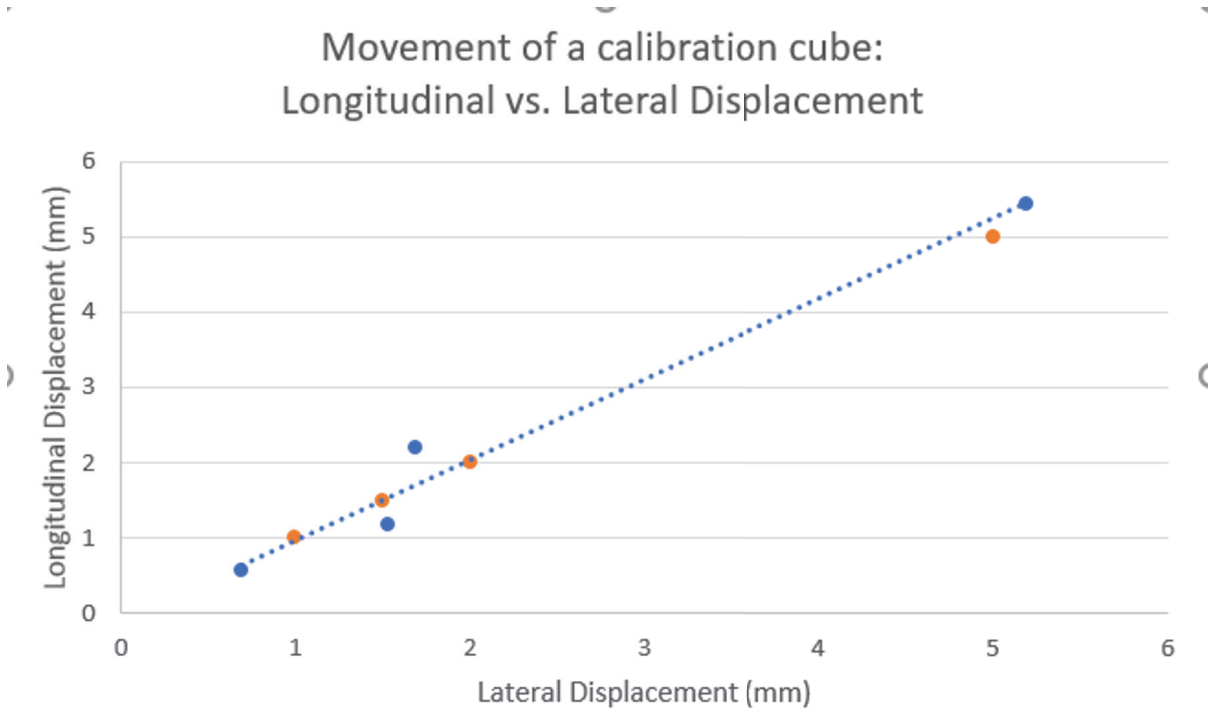
Figure 6.5: Displacement of a calibration cube: Longitudinal vs. Lateral (Detected Movement (Blue) and Actual Movement (Orange)

6.1.7 High Frequency Micro-Ultrasound (μUS) Imaging for Cranial Surgery

The introduction of high frequency micro-ultrasound (μUS) transducers with central frequencies up to 50 MHz is particularly attractive for cranial neurosurgery applications considering the potential for real-time microscopic visualization of the subsurface anatomy without exposing patients to radiation or disrupting surgical workflow. While most conventional ultrasound systems deliver image resolutions of 0.5 – 1 mm at penetration depths greater than 100 mm, μUS provides spatial resolution on the order of 15 –

100 μm with limited depth penetration up to 15 mm. Although improvement in spatial resolution must be considered in concert with reduced penetration depth, the trade-off is adequate in the context of an open surgical field where the bone is removed and the ultrasound probe can be placed directly adjacent to the region of interest. Integration of μUS into the operating room facilitates dynamic intraoperative feedback to surgeons, thus informing clinical decisions. We have obtained initial μUS images of a patient with a parietal lesion near the base of the skull showing well differentiated lobulated malignant epithelial cells, malignant tissues and grey matter/white matter with pathology grade resolution (Figure 6.6). Further integration of μUS can be adapted to brain tumour resection and fused with functional imaging to further impact surgical outcomes.
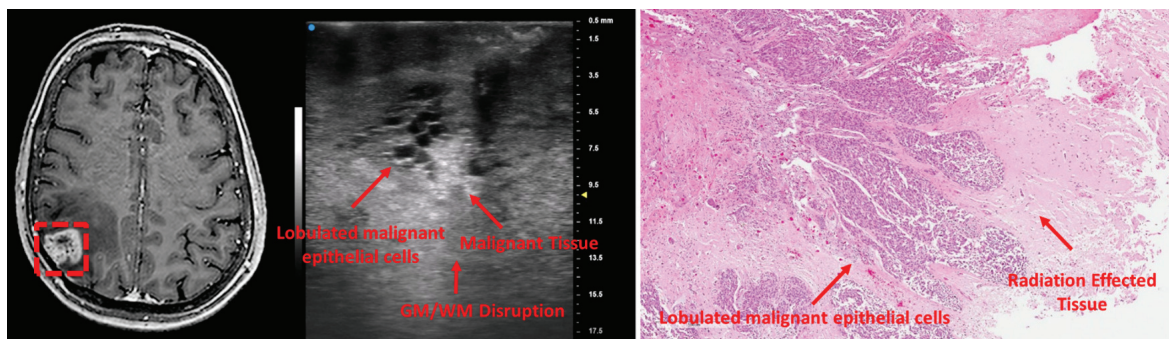
Figure 6.6: Cranial biopsy tumour resection: MRI, high frequency ultrasound, and pathology comparison shows clearly defined lobular structures characteristic of malignancy.

6.2 Conclusions

This dissertation represents a key step towards the integration of intraoperative, dosimetry guided spine separation. Although, the final endpoint of integrated ultrasound has not yet been achieved this work establishes feasibility and upon the incorporation of tracked ultrasound can be packaged into a complete radiation planning navigation system.

First, the dosimetric advantage of spine separation surgery was quantified retrospectively in Chapter 2. This forms the motivation for the subsequent application accuracy analyses and ensures that the surgeon can precisely pinpoint the tissues that require resection. Further, since treatment failure has been attributed to underdosing of the epidural space and aggressive resection has been shown to improve local control, it is logical to investigate the surgical need (i.e. how much epidural disease needs to be resected ensure adequate coverage). This chapter provides an understanding of the incremental nature of epidural disease resection and the potential impact of spine separation surgery on local control and tissue toxicity. This chapter also establishes the basis for the upcoming chapters establishing application accuracy and integrating μUS imaging into the operating theatre by determining the dosimetric advantage of each millimetre of epidural disease resected. Based on this chapter, the surgeon can utilize dose planning to determine the degree of epidural disease resection required to ensure adequate dose coverage.

However, while the retrospective review established a relationship between degree of resection and radiation dose, significant inter-patient variability exists. Therefore, the focus of future studies should seek to establish patient specific resection margins depending on the anatomical and geometrical limitations precluding adequate treatment with radiotherapy. This work would stratify patient eligibility for spine separation surgery based on dosimetric benefit (i.e. large epidural disease volumes in close proximity to the spinal cord) and would spare patients with little or no dosimetric advantage from unnecessary surgery.

With regards to surgical planning, the patient specific balance between the rigid dose tolerance of the spinal cord and the tumour objective dose must be established, such that dose planning essentially navigates the surgical plan. This objective can be achieved by simulating the dosimetric effect of the planned hardware insertion on pre-acquired data and performing the dose planning prior to surgical resection to identify regions of epidural disease that is at risk of being underdosed. This approach would shift the current paradigm whereby the extent of surgical resection is no longer determined by the surgeon and dependent on surgical skill, but is driven by the anatomical and physiological features of the patient. This work can transform the approach to treating spinal metastases, a hard to treat cancer where patients have limited life expectancy.

The remaining objectives of this dissertation were to quantify the absolute application accuracy associated with surgical navigation and to validate our revolutionary experimental optical topographical imaging system versus the commercially available navigation system in spine and brain. This work has the potential to be paradigm shifting as a significant improvement in workflow was noted without a resulting drop in application accuracy relative to the benchmark systems. Further, the implementation of an active calibration protocol during surgery resulted in a significant improvement in accuracy. Chapters 3 and 4 established the application accuracy of image-guided neurosurgery using the existing benchmarked technologies and our novel optical topographical neuronavigation system. This step was crucial as the surgeon's perspective during spine separation surgery is to remove as little tissue as possible and maintain the integrity of the spine. This can be achieved via minimally invasive surgery. However, the surgeon cannot evaluate whether he has met the dosimetric objective during surgery and therefore cannot gauge whether or the residual tumour can be treated effectively. If, however, fusion of patient images – specifically, the fusion of MRI, CT, optical topographical imaging, and ultrasound is achievable and can be processed in real-time, the surgeon will be able to gauge the precise amount of resection required in order to optimize radiotherapy and limit the extent of surgery.

Finally, the feasibility of image-guided high frequency micro-ultrasound during sur-

gical resection of spinal tumours was established as is evidenced in the 7 patient cohort that have undergone spinal cord decompression including 3 navigated surgeries. While this has not yet been achieved, this data combined with dosimetry will eventually guide the surgical procedure. This work will enable real-time feedback allowing for incremental tumour resection, thus positively impacting the efficacy of treatment, reducing dose to the spinal cord, and ultimately improving clinical outcomes. Chapters 5 lays the groundwork for tracked μUS ultrasound imaging by fusing surgical navigation with ultrasound during surgery, thus providing real-time surgical feedback which can be augmented by the dosimetric objectives and compared to the original anatomy. This would seamlessly integrate with the treatment plan and guide the surgeon as to what should be removed, and what can remain. Therefore, minimal surgical resection of the epidural disease could be achieved, simplifying the surgery, reducing risk of complication from blood-loss and infection, and allowing for optimized radiotherapy. This approach would lead to the development of a fully integrated navigated ultrasound/dose planning software package with the potential to shift the clinical paradigm by enabling dosimetry directed, surgical guidance within a real-time feedback loop.

References

[1] Harel R, Angelov L. (2010) Spine metastases: current treatments and future directions. European journal of cancer (Oxford, England: 1990). 46: 2696707. doi:10.1016/j.ejca.2010.04.025.

[2] Klimo J, Schmidt MH. (2004) Surgical Management of Spinal Metastases. Oncologist. 9: 18896. doi:10.1634/theoncologist.9-2-188.

[3] Perrin RG, Laxton AW. (2004) Metastatic spine disease: Epidemiology , pathophysiology , and evaluation of patients Article in Neurosurgery Clinics of North America November 2004 Metastatic spine disease: epidemiology , pathophysiology , and evaluation of patients. doi:10.1016/j.nec.2004.04.018.

[4] Batson OV (1940) The function of the vertebral veins and their role in the spread of metastases. Annals of surgery. 112: 13849. doi:10.1097/00000658-194007000-00016.

[5] Patchell RA, Tibbs PA, Regine WF, Payne R, Saris S, Kryscio RJ, et al. (2005) Direct decompressive surgical resection in the treatment of spinal cord compression caused by metastatic cancer: A randomised trial. Lancet. 366: 6438. doi:10.1016/S0140-6736(05)66954-1.

[6] Balagamwala EH, Cherian S, Angelov L, Suh JH, Djemil T, Lo SS, et al. (2012) Stereotactic body radiotherapy for the treatment of spinal metastases. Journal of Radiation Oncology. 1: 25565. doi:10.1007/s13566-012-0047-6.

[7] Heidecke V, Rainov NG, Burkert W, Goel A, Kulkarni A, Sonntong VKH. (2003) Results and outcome of neurosurgical treatment for extradural metastases in the cervical spine. Acta Neurochirurgica. 145: 87381. doi:10.1007/s00701-003-0107-1.

[8] van der Linden YM, Dijkstra SPDS, Vonk EJA, Marijnen CAM, Leer JWH, Dutch Bone Metastasis Study Group. (2005) Prediction of survival in patients with metastases in the spinal column: results based on a randomized trial of radiotherapy. Cancer. 103: 3208. doi:10.1002/cncr.20756.

[9] Cole JS, Patchell RA. (2008) Metastatic epidural spinal cord compression. The

Lancet Neurology. 7: 45966. doi:10.1016/S1474-4422(08)70089-9.

[10] Laufer I, Rubin DG, Lis E, Cox BW, Stubblefield MD, Yamada Y, et al. (2013). The NOMS Framework: Approach to the Treatment of Spinal Metastatic Tumors. The oncologist. 18: 74451. doi:10.1634/theoncologist.2012-0293.

[11] Bilsky MH, Laufer I, Fourney DR, Groff M, Schmidt MH, Varga PP, et al. (2010) Reliability analysis of the epidural spinal cord compression scale. Journal of neurosurgery. Spine. 13: 3248. doi:10.3171/2010.3.SPINE09459.

[12] Ryu S, Rock J, Jain R, Lu M, Anderson J, Jin JY, et al. (2010) Radiosurgical decompression of metastatic epidural compression. Cancer. 116: 22507. doi:10.1002/cncr.24993.

[13] Fisher CG, Versteeg AL, Schouten R, Boriani S, Varga PP, Rhines LD, et al. (2014) Reliability of the spinal instability neoplastic scale among radiologists: An assessment of instability secondary to spinal metastases. American Journal of Roentgenology. 203: 86974. doi:10.2214/AJR.13.12269.

[14] Wang XS, Rhines LD, Shiu AS, Yang JN, Selek U, Gning I, et al. (2012) Stereo-

tactic body radiation therapy for management of spinal metastases in patients without spinal cord compression: A phase 1-2 trial. The Lancet Oncology. 13: 395402. doi:10.1016/S1470-2045(11)70384-9.

[15] Al-Omair A, Masucci L, Masson-Cote L, Campbell M, Atenafu EG, Parent A, et al. (2013) Surgical resection of epidural disease improves local control following postoperative spine stereotactic body radiotherapy. Neuro-Oncology. 15: 1413-9. doi:10.1093/neuonc/not101.

[16] Ryu S, Yoon H, Stessin A, Gutman F, Rosiello A, Davis R. (2015) Contemporary treatment with radiosurgery for spine metastasis and spinal cord compression in 2015. Radiation Oncology Journal. 33: 1-11. doi:10.3857/roj.2015.33.1.1.

[17] Thibault I, Chang EL, Sheehan J, Ahluwalia MS, Guckenberger M, Sohn MJ, et al. (2015) Response assessment after stereotactic body radiotherapy for spinal metastasis: A report from the SPIne response assessment in Neuro-Oncology (SPINO) group. The Lancet Oncology. 16: e595-603. doi:10.1016/S1470-2045(15)00166-7.

[18] Redmond KJ, Lo SS, Fisher C, Sahgal A. (2016) Postoperative Stereotactic Body Radiation Therapy (SBRT) for Spine Metastases: A Critical Review to Guide Prac-

tice. International Journal of Radiation Oncology, Biology & Physics. 95: 1414-28. doi:10.1016/j.ijrobp.2016.03.027.

[19] Chow E, Harris K, Fan G, Tsao M, Sze WM. (2007) Palliative radiotherapy trials for bone metastases: A systematic review. Journal of Clinical Oncology. 25: 1423-36. doi:10.1200/JCO.2006.09.5281.

[20] Guckenberger M, Mantel F, Gerszten PC, Flickinger JC, Sahgal A, Ltourneau D, et al. (2014) Safety and efficacy of stereotactic body radiotherapy as primary treatment for vertebral metastases: a multi-institutional analysis. Radiation oncology (London, England). 9: 226. doi:10.1186/s13014-014-0226-2.

[21] Huo M, Sahgal A, Pryor D, Redmond K, Lo S, Foote M. (2017) Stereotactic spine radiosurgery: Review of safety and efficacy with respect to dose and fractionation. Surgical Neurology International. 8: 30. doi:10.4103/2152-7806.200581.

[22] Maitz AH, Wu A. (1998) Treatment planning of stereotactic convergent gamma-ray irradiation using Co-60 sources. Medical dosimetry: official journal of the American Association of Medical Dosimetrists. 23: 169-75.

[23] Lax I, Blomgren H. The clinical transition from intracranial to extracranial stereotactic radiation therapy. In: Kavanagh, B; Timmerman R, K, editors. Stereotact. Body Radiat. Ther., 2004, p. 1-7.

[24] Benedict SH, Yenice KM, Followill D, Galvin JM, Hinson W, Kavanagh B, et al. (2010) Stereotactic body radiation therapy: the report of AAPM Task Group 101. Medical physics. 37: 4078-101. doi:10.1118/1.3438081.

[25] Martin A, Gaya A. (2010) Stereotactic body radiotherapy: A Review. Clinical Oncology. 22: 157-72. doi:10.1016/j.clon.2009.12.003.

[26] Kim M, Kim W, Park IH, Kim HJ, Lee E, Jung J, et al. (2015) Radiobiological mechanisms of stereotactic body radiation therapy and stereotactic radiation surgery. 33: 265-75.

[27] Ho AK, Fu D, Cotrutz C, Hancock SL, Chang SD, Gibbs IC, et al. (2007) A study of the accuracy of cyberknife spinal radiosurgery using skeletal structure tracking. Neurosurgery. 60: 147-56. doi:10.1227/01.NEU.0000249248.55923.EC.

[28] Ryu S, Fang Yin F, Rock J, Zhu J, Chu A, Kagan E, et al. (2003) Image-guided

and intensity-modulated radiosurgery for patients with spinal metastasis. Cancer. 97: 2013-8. doi:10.1002/cncr.11296.

[29] Ma L, Sahgal A, Hossain S, Chuang C, Descovich M, Huang K, et al. (2009) Nonrandom Intrafraction Target Motions and General Strategy for Correction of Spine Stereotactic Body Radiotherapy. International Journal of Radiation Oncology Biology Physics. 75: 1261-5. doi:10.1016/j.ijrobp.2009.04.027.

[30] Rock JP, Ryu S, Shukairy MS, Yin FF, Sharif A, Schreiber F, et al. (2006) Postoperative radiosurgery for malignant spinal tumors. Neurosurgery. 58: 891-7. doi:10.1227/01.NEU.0000209913.72761.4F.

[31] Kumar R, Nater A, Hashmi A, Myrehaug S, Lee Y, Ma L, et al. (2015) The era of stereotactic body radiotherapy for spinal metastases and the multidisciplinary management of complex cases. Neuro-Oncology Practicenpv022. doi:10.1093/nop/npv022.

[32] Timmerman RD, Kavanagh BD. (2005) Stereotactic body radiation therapy. Current problems in cancer. 29: 120-57. doi:10.1016/j.currproblcancer.2005.05.001.

[33] Chang EL, Shiu AS, Mendel E, Mathews LA, Mahajan A, Allen PK, et al. (2007)

Phase I/II study of stereotactic body radiotherapy for spinal metastasis and its pattern of failure. Journal of Neurosurgery: Spine. 7: 151-60. doi:10.3171/SPI-07/08/151.

[34] Chan MW, Thibault I, Atenafu EG, Yu E, John Cho BC, Letourneau D, et al. (2016) Patterns of epidural progression following postoperative spine stereotactic body radiotherapy: implications for clinical target volume delineation. Journal of neurosurgery. Spine. 24: 652-9. doi:10.3171/2015.6.SPINE15294.

[35] Itshayek E, Yamada J, Bilsky M, Schmidt M, Shaffrey C, Gerszten P, et al. (2010) Timing of surgery and radiotherapy in the management of metastatic spine disease: a systematic review. International journal of oncology. 36: 533-44. doi:10.1016/j.jmir.2013.04.002.

[36] Sangha A, Korol R, Sahgal A. (2013) Stereotactic Body Radiotherapy for the Treatment of Spinal Metastases: An Overview of the University of Toronto, Sunnybrook Health Sciences Odette Cancer Centre, Technique. Journal of Medical Imaging and Radiation Sciences. 44: 126-33. doi:10.1016/j.jmir.2013.04.002.

[37] Sahgal A, Weinberg V, Ma L, Chang E, Chao S, Muacevic A, et al. (2013) Probabilities of radiation myelopathy specific to stereotactic body radiation therapy to guide

safe practice. International Journal of Radiation Oncology Biology Physics. 85: 341-7. doi:10.1016/j.ijrobp.2012.05.007.

[38] Liebross R, Tarkschall M, Ong P, Orton M, Okaslan Z, Omaki M. (2002) The effect of titanium stabilization rods on spinal cord radiation dose. 27: 21-4.

[39] Mesbahi A, Seyed F, Ade N. (2007) Monte Carlo study on the impact of spinal fixation rods on dose distribution in photon beams. Rep Pract Oncol Radiotherapy. 12: 261-6. doi:10.1016/S1507-1367(10)60064-8.

[40] Wang X, Yang JN, Li X, Tailor R, Vassilliev O, Brown P, et al. (2013) Effect of spine hardware on small spinal stereotactic radiosurgery dosimetry. Physics in medicine and biology. 58: 6733-47. doi:10.1088/0031-9155/58/19/6733.

[41] Al-omair A, Masucci L, Masson-cote L, Campbell M, Atenafu EG, Parent A, et al. (2013) Surgical resection of epidural disease improves stereotactic body radiotherapy. Neuro-Oncology 15: 1413-9.

[42] Sahgal A, Bilsky M, Chang EL, Ma L, Yamada Y, Rhines LD, et al. (2011) Stereotactic body radiotherapy for spinal metastases: current status, with a focus on its

application in the postoperative patient. Journal of Neurosurgery: Spine. 14: 151-66. doi:10.3171/2010.9.SPINE091005.

[43] Cox BW, Spratt DE, Lovelock M, Bilsky MH, Lis E, Ryu S, et al. (2012) International spine radiosurgery consortium consensus guidelines for target volume definition in spinal stereotactic radiosurgery. International Journal of Radiation Oncology Biology Physics. 83: e597-605. doi:10.1016/j.ijrobp.2012.03.009.

[44] Smith M, Davis MA, Stano M, Whedon JM. (2013) Aging baby boomers and the rising cost of chronic back pain: Secular trend analysis of longitudinal medical expenditures panel survey data for years 2000 to 2007. Journal of Manipulative and Physiological Therapeutics. 36: 2-11. doi:10.1016/j.jmpt.2012.12.001.

[45] Ma VY, Chan L, Carruthers KJ. (2014) Incidence, prevalence, costs, and impact on disability of common conditions requiring rehabilitation in the united states: Stroke, spinal cord injury, traumatic brain injury, multiple sclerosis, osteoarthritis, rheumatoid arthritis, limb loss, and back pa. Archives of Physical Medicine and Rehabilitation. 95: 986-995.e1. doi:10.1016/j.apmr.2013.10.032.

[46] Ortman BJM, Velkoff V a., Hogan H. (2014) An aging nation: The older popu-

lation in the United States. Economics and Statistics Administration, US Department of Commerce. 1964: 1-28.

[47] Manbachi A, Cobbold RSC, Ginsberg HJ. (2013) Guided pedicle screw insertion: techniques and training. The spine journal: official journal of the North American Spine Society. doi:10.1016/j.spinee.2013.03.029.

[48] Jain RK, di Tomaso E, Duda DG, Loeffler JS, Sorensen a G, Batchelor TT. (2007) Angiogenesis in brain tumours. Nature reviews. Neuroscience. 8: 610-22. doi:10.1038/nrn2175.

[49] Merloz P, Tonetti J, Pittet L. (1998) Pedicle screw placement using image guided techniques. Clinical orthopaedics and Related Research.

[50] Rampersaud YR, Simon DA, Foley KT. (2001) Accuracy requirements for image-guided spinal pedicle screw placement. Spine. 26: 352-9.

[51] Heary RF, Bono CM, Black M. (2004) Thoracic pedicle screws: postoperative computerized tomography scanning assessment. Journal of neurosurgery. 100: 325-31. doi:10.3171/spi.2004.100.4.0325.

[52] Ciol MA, Deyo RA, Howell E, Kreif S. (1996) An assessment of surgery for spinal stenosis: time trends, geographic variations, complications, and reoperations. Journal of the American Geriatrics Society. 44: 285-90.

[53] Wang Y, Xie J, Yang Z, Zhao Z, Zhang Y, Li T, et al. (2013) Computed tomography assessment of lateral pedicle wall perforation by free-hand subaxial cervical pedicle screw placement. Archives of orthopaedic and trauma surgery. 133: 901-9. doi:10.1007/s00402-013-1752-3.

[54] Hartl R, Theodore N, Dickman C a, Sonntag VK. (2004) Technique of thoracic pedicle screw fixation for trauma. Operative Techniques in Neurosurgery. 7: 22-30. doi:10.1053/j.otns.2004.04.005.

[55] Gelalis ID, Paschos NK, Pakos EE, Politis AN, Arnaoutoglou CM, Karageorgos AC, et al. (2012) Accuracy of pedicle screw placement: a systematic review of prospective in vivo studies comparing free hand, fluoroscopy guidance and navigation techniques. European spine journal: official publication of the European Spine Society, the European Spinal Deformity Society, and the European Section of the Cervical Spine Research Society. 21: 247-55. doi:10.1007/s00586-011-2011-3.

[56] Lund T, Laine T. (2012) Accuracy of computer assisted pedicle screw insertion: the evidence. Journal of Bone & Surgery. 2-3.

[57] Holly LT, Bloch O, Johnson JP. (2006) Evaluation of registration techniques for spinal image guidance. Journal of neurosurgery. Spine. 4: 323-8. doi:10.3171/spi.2006.4.4.323.

[58] West JB, Fitzpatrick JM, Toms SA, Maurer CR, Maciunas RJ. (2001) Fiducial point placement and the accuracy of point-based, rigid body registration. Neurosurgery. 48: 810-6-7.

[59] Shin BJ, James AR, Njoku IU, Hrtl R. (2012) Pedicle screw navigation: a systematic review and meta-analysis of perforation risk for computer-navigated versus freehand insertion. Journal of Neurosurgery: Spine. 17: 113-22. doi:10.3171/2012.5.SPINE11399.

[60] Hartl R, Lam KS, Wang J, Korge A, Kandziora F, Audig L. (2013) Worldwide survey on the use of navigation in spine surgery. World Neurosurgery. 79: 162-72. doi:10.1016/j.wneu.2012.03.011.

[61] Fitzpatrick JM, West JB, Maurer CR. (1998) Predicting error in rigid-body point-based registration. IEEE transactions on medical imaging. 17: 694-702. doi:10.1109/42.736021.

[62] Labadie RF, Davis BM, Fitzpatrick JM. (2005) Image-guided surgery: what is the accuracy? Current opinion in otolaryngology & head and neck surgery. 13: 27-31.

[63] Mathew JE, Mok K, Goulet B. (2013) Pedicle violation and Navigational errors in pedicle screw insertion using the intraoperative O-arm: A preliminary report. The International Journal of Spine Surgery. 7: e88-94. doi:10.1016/j.ijsp.2013.06.002.

[64] Starr P a, Christine CW, Theodosopoulos P V, Lindsey N, Byrd D, Mosley A, et al. (2002) Implantation of deep brain stimulators into the subthalamic nucleus: technical approach and magnetic resonance imaging-verified lead locations. Journal of neurosurgery. 97: 370-87. doi:10.3171/jns.2002.97.2.0370.

[65] Maciunas RJ, Galloway RL, Latimer JW. The application accuracy of stereotactic frames. Neurosurgery 1994;35:682-5. doi:10.1227/00006123-199410000-00015.

[66] Mascott CR, Sol JC, Bousquet P, Lagarrigue J, Lazorthes Y, Lauwers-Cances

V. (2006) Quantification of true in vivo (application) accuracy in cranial image-guided surgery: Influence of mode of patient registration. Neurosurgery. 59. doi:10.1227/01.NEU.0000220089.39533.4E.

[67] Willoughby T, Lehmann J, Bencomo J a., Jani SK, Santanam L, Sethi A, et al. (2012) Quality assurance for nonradiographic radiotherapy localization and positioning systems: Report of Task Group 147. Medical Physics. 39: 1728. doi:10.1118/1.3681967.

[68] Hidnert P, Krider HS. (1952) Thermal expansion of aluminum and some aluminum alloys. Journal of Research of the National Bureau of Standards. 48: 209. doi:10.6028/jres.048.030.

[69] Foster FS, Hossack J, Adamson SL. (2011) Micro-ultrasound for preclinical imaging. Interface focus. 1: 576-601. doi:10.1098/rsfs.2011.0037.

[70] Jaberi A, Muradali D, Marticorena RM, Dacouris N, Boutin A, Mulligan AM, et al. (2011) Arteriovenous fistulas for hemodialysis: application of high-frequency US to assess vein wall morphology for cannulation readiness. Radiology. 261: 616-24. doi:10.1148/radiol.11102439.

[71] Latham GJ, Veneracion ML, Joffe DC, Bosenberg AT, Flack SH, Low DK. (2013) High-frequency micro-ultrasound for vascular access in young children–a feasibility study by the High-frequency UltraSound in Kids studY (HUSKY) group. Paediatric anaesthesia. 23: 529-35. doi:10.1111/pan.12131.

[72] Kaufman CL, Ouseph R, Blair B. (2012) Graft Vasculopathy in Clinical Hand Transplantation.1004-16. doi:10.1111/j.1600-6143.2011.03915.x.

[73] Johansson M, Myredal A, Friberg P, Gan LM. (2010) High-resolution ultrasound showing increased intima and media thickness of the radial artery in patients with end-stage renal disease. Atherosclerosis. 211: 159-63. doi:10.1016/j.atherosclerosis.2010.01.031.

[74] Eklund C, Omerovic E, Haraldsson I, Friberg P, Gan L-M. (2014) Radial artery intima-media thickness predicts major cardiovascular events in patients with suspected coronary artery disease. European heart journal cardiovascular Imaging. 15: 769-75. doi:10.1093/ehjci/jet285.

[75] Osika W, Dangardt F, Grnros J, Lundstam U, Myredal A, Johansson M, et al. (2007) Increasing peripheral artery intima thickness from childhood to seniority. Arteriosclerosis, thrombosis, and vascular biology. 27: 671-6. doi:10.1161/

01.ATV.0000256468.95403.6f.

[76] Bohman H, Jonsson U, Von Knorring A, Von Knorring L, Olsson G, Pren A, et al. (2010) Thicker carotid intima layer, thinner media layer and higher intima/media ratio in women with recurrent depressive disorders: A pilot study using non-invasive high frequency ultrasound. The world journal of biological psychiatry: the official journal of the World Federation of Societies of Biological Psychiatry. 11: 71-5. doi:10.1080/ 15622970902789122.

[77] Sarkola T, Slorach C, Hui W, Bradley TJ, Redington AN, Jaeggi E. (2012) Transcutaneous very-high resolution ultrasound for the quantification of carotid arterial intima-media thickness in children - feasibility and comparison with conventional high resolution vascular ultrasound imaging. Atherosclerosis. 224: 102-7. doi:10.1016/ j.atherosclerosis.2012.06.054.

[78] Kolstad F, Rygh OM, Selbekk T, Unsgaard G, Nygaard OP. Three-dimensional ultrasonography navigation in spinal cord tumor surgery. Technical note. vol. 5. 2006. doi:10.3171/spi.2006.5.3.264.

[79] Rasmussen IA, Lindseth F, Rygh OM, Berntsen EM, Selbekk T, Xu J, et al.

(2007) Functional neuronavigation combined with intra-operative 3D ultrasound: Initial experiences during surgical resections close to eloquent brain areas and future directions in automatic brain shift compensation of preoperative data. Acta Neurochirurgica. 149: 365-78. doi:10.1007/s00701-006-1110-0.

[80] Zhou H, Miller D, Michael D, Benes L, Bozinov O, Sure U, et al. (2011) Intraoperative ultrasound assistance in treatment of intradural spinal tumours. Clinical Neurology and Neurosurgery. 113: 531-7. doi:10.1016/j.clineuro.2011.03.006.

[81] Prada F, Vetrano IG, Filippini A, Del Bene M, Perin A, Casali C, et al. (2014) Intraoperative ultrasound in spinal tumor surgery. Journal of Ultrasound. 17: 195-202. doi:10.1007/s40477-014-0102-9.

[82] Regelsberger J, Fritzsche E, Langer N, Westphal M. (2005) Intraoperative sonography of intra- and extramedullary tumors. Ultrasound in Medicine and Biology. 31: 593-8. doi:10.1016/j.ultrasmedbio.2005.01.016.

[83] Hulley SB, Cummings SR, Browner WS, Grady D, Newman TB. (2013) Designing clinical research : an epidemiologic approach. 4th ed. Philadelphia, PA: Lippincott Williams & Wilkins. Appendix 6C, page 79.

[84] Tseng C-L, Sussman MS, Atenafu EG, Letourneau D, Ma L, Soliman H, et al. (2015) Magnetic resonance imaging assessment of spinal cord and cauda equina motion in supine patients with spinal metastases planned for spine stereotactic body radiation therapy. International journal of radiation oncology, biology, physics. 91: 9951002. doi:10.1016/j.ijrobp.2014.12.037.

[85] Laufer I, Iorgulescu JB, Chapman T, Lis E, Shi W, Zhang Z, et al. (2013) Local disease control for spinal metastases following "separation surgery" and adjuvant hypofractionated or high-dose single-fraction stereotactic radiosurgery: outcome analysis in 186 patients. Journal of neurosurgery. Spine. 18: 20714. doi:10.3171/ 2012.11.SPINE12111.

[86] Bate BG, Khan NR, Kimball BY, Gabrick K, Weaver J. (2015) Stereotactic radiosurgery for spinal metastases with or without separation surgery. Journal of neurosurgery. Spine. 22: 40915. doi:10.3171/2014.10.SPINE14252.

[87] Hyde D, Ph D, Lochray F, Korol R, Ph D, Davidson M, et al. (2012) Spine Stereotactic Body Radiotherapy Utilizing Cone-Beam CT Image-Guidance With a Robotic Couch: Intrafraction Motion Analysis Accounting for all Six Degrees of Freedom. Radi-

ation Oncology Biology. 82: e55562. doi:10.1016/j.ijrobp.2011.06.1980.

[88] Sahgal A, Ma L, Weinberg V, Gibbs IC, Chao S, Chang U-K, et al. (2012) Reirradiation human spinal cord tolerance for stereotactic body radiotherapy. International journal of radiation oncology, biology, physics. 82: 10716. doi:10.1016/j.ijrobp.2010.08.021.

[89] Sahgal A, Ma L, Gibbs I, Gerszten PC, Ryu S, Soltys S, et al. (2010) Spinal cord tolerance for stereotactic body radiotherapy. International journal of radiation oncology, biology, physics. 77: 54853. doi:10.1016/j.ijrobp.2009.05.023.

[90] Chang EL, Shiu AS, Mendel E, Mathews L a, Mahajan A, Allen PK, et al. (2007) Phase I/II study of stereotactic body radiotherapy for spinal metastasis and its pattern of failure. Journal of neurosurgery. Spine. 7: 15160. doi:10.3171/SPI-07/08/151.

[91] Zindler JD, Thomas CR, Hahn SM, Hoffmann AL, Troost EGC, Lambin P. (2016) Increasing the Therapeutic Ratio of Stereotactic Ablative Radiotherapy by Individualized Isotoxic Dose Prescription. Journal of the National Cancer Institute. 108: 16. doi:10.1093/jnci/djv305.

[92] Garcia-barros AM, Paris F, Cordon-cardo C, Lyden D. (2010) Tumor Response to

Radiotherapy Regulated by Endothelial Cell Apoptosis Published by: American Association for the Advancement of Science Stable URL: http://www.jstor.org/stable/3834043. Advancement Of Science. 300: 11559.

[93] Kim MS, Kim W, Park IH, Kim HJ, Lee E, Jung JH, et al. (2015) Radiobiological mechanisms of stereotactic body radiation therapy and stereotactic radiation surgery. Radiation Oncology Journal. 33: 26575. doi:10.3857/roj.2015.33.4.265.

[94] Jakubovic R, Sahgal A, Ruschin M, Ana Pejović-Milić A, Milwid R, Aviv RI. (2015) Non Tumor Perfusion Changes Following Stereotactic Radiosurgery to Brain Metastases. Technology in cancer research & treatment. 14: 497503. doi:10.1177/1533034614600279.

[95] Lovelock DM, Zhang Z, Jackson A, Keam J, Bekelman J, Bilsky M, et al. (2010) Correlation of Local Failure With Measures of Dose Insufficiency in the High-Dose Single-Fraction Treatment of Bony Metastases. International Journal of Radiation Oncology Biology Physics. 77: 12827. doi:10.1016/j.ijrobp.2009.10.003.

[96] Kumar KA, Choi CYH, White EC, Qian Y, Gibbs IC, Adler JR, et al. (2015) Spinal Stereotactic Radiosurgery: Dosimetric Correlates of Tumor Control. International

Journal of Radiation Oncology*Biology*Physics. 93: E118.

doi:10.1016/ j.ijrobp.2015.07.848.

[97] Lee JY, Sharan A, Baron EM, Lim MR, Grossman E, Albert TJ, et al. (2006) Quantitative prediction of spinal cord drift after cervical laminectomy and arthrodesis. Spine. 31: 17958. doi:10.1097/01.brs.0000225992.26154.d0.

[98] Mesbahi A, Nejad FS. (2007) Monte Carlo study on the impact of spinal fixation rods on dose distribution in photon beams. Reports of Practical Oncology & Radiotherapy. 12: 2616. doi:10.1016/S1507-1367(10)60064-8.

[99] Liebross RH, Starkschall G, Wong PF, Horton J, Gokaslan ZL, Komaki R. (2002) The effect of titanium stabilization rods on spinal cord radiation dose. Medical Dosimetry. 27: 214. doi:10.1016/S0958-3947(02)00083-3.

[100] Kong Q, Zhang L, Liu L, Li T, Gong Q, Zeng J, et al. (2011) Effect of the decompressive extent on the magnitude of the spinal cord shift after expansive open-door laminoplasty. Spine. 36: 10306. doi:10.1097/BRS.0b013e3181e80507.

[101] Belmont PJ, Klemme WR, Dhawan A, Polly DW. (2001) In vivo accuracy of

thoracic pedicle screws. Spine. 26: 2340-6. doi:10.1097/00007632-200111010-00010.

[102] Kotani Y, Abumi K, Ito M, Takahata M. (2007) Accuracy Analysis of Pedicle Screw Placement in Posterior Scoliosis Surgery: Comparison Between Conventional Fluoroscopic and Computer-Assisted Techniques. Spine. 32: 1543-50. doi:10.1097/BRS.0b013e318068661e.

[103] Shrout PE., Fleiss JL. (1979) Intraclass correlations: uses in assessing rater reliability. Psychological Bulletin. 86: 420-8.

[104] Fisher, R. A. (1922) On the interpretation of Chi^2 from contingency tables, and the calculation of P. Journal of the Royal Statistical Society. 85 (1): 8794. JSTOR 2340521. doi:10.2307/2340521.

[105] Bowker, A. H. (1948). A test for symmetry in contingency tables. Journal of the american statistical association, 43(244), 572-574.

[106] Bandiera S, Ghermandi R, Gasbarrini A, Barbanti Brodano G, Colangeli S, Boriani S. (2013) Navigation-assisted surgery for tumors of the spine. European Spine Journal. 22: S919-24. doi:10.1007/s00586-013-3032-x.

[107] Sakai Y, Matsuyama Y, Nakamura H, Katayama Y, Imagama S, Ito Z, et al. (2008) Segmental pedicle screwing for idiopathic scoliosis using computer-assisted surgery. Journal of Spinal Disorders & Techniques. 21: 181-6. doi:10.1097/ BSD.0b013e318074d388.

[108] Bourgeois AC, Faulkner AR, Pasciak AS, Bradley YC. (2015) The evolution of image-guided lumbosacral spine surgery. Ann Transl Med. 3: 69. doi:10.3978/j.issn.2305-5839.2015.02.01.

[109] Rajasekaran S, Vidyadhara S, Ramesh P, Shetty AP. (2007) Randomized clinical study to compare the accuracy of navigated and non-navigated thoracic pedicle screws in deformity correction surgeries. Spine. 32: E56-64. doi:10.1097/ 01.brs.0000252094.64857.ab.

[110] Bydon M, Mathios D, Macki M, De la Garza-Ramos R, Aygun N, Sciubba DM, et al. (2014) Accuracy of C2 pedicle screw placement using the anatomic freehand technique. Clinical Neurology and Neurosurgery. 125: 24-7. doi:10.1016/j.clineuro.2014.07.017.

[111] Castro WH, Halm H, Jerosch J, Malms J, Steinbeck J, Blasius S. (1996) Accuracy of pedicle screw placement in lumbar vertebrae. Spine. 21: 1320-4.

[112] Nottmeier EW, Seemer W, Young PM. (2009) Placement of thoracolumbar pedicle screws using three-dimensional image guidance: experience in a large patient cohort. Journal of neurosurgery. Spine. 10: 33-9. doi:10.3171/2008.10.SPI08383.

[113] Amiot LP, Lang K, Putzier M, Zippel H, Labelle H. (2000) Comparative results between conventional and computer-assisted pedicle screw installation in the thoracic, lumbar, and sacral spine. Spine (Phila Pa 1976). 25: 606-14. doi:10.1097/00007632-200003010-00012.

[114] Bourgeois AC, Faulkner AR, Bradley YC, Pasciak AS, Barlow PB, Gash JR, et al. (2015) Improved Accuracy of Minimally Invasive Transpedicular Screw Placement in the Lumbar Spine With 3-Dimensional Stereotactic Image Guidance: A Comparative Meta-Analysis. Journal of spinal disorders & techniques. 28: 324-9. doi:10.1097/BSD.0000000000000152.

[115] Tian NF, Huang QS, Zhou P, Zhou Y, Wu RK, Lou Y, et al. (2011) Pedicle screw insertion accuracy with different assisted methods: a systematic review and meta-analysis of comparative studies. Eur Spine J. 20: 846-59. doi:10.1007/s00586-010-1577-5.

[116] Hecht N, Kamphuis M, Czabanka M, Hamm B, Knig S, Woitzik J, et al. (2008)

Clinical accuracy of 3D fluoroscopy-assisted cervical pedicle screw insertion. Journal of neurosurgery. Spine. 9: 450-3. doi:10.3171/SPI.2008.9.11.450.

[117] Barsa P, Frhlich R, ercl M, BuchvaldPvald P, Suchomel P. (2016) The intra-operative portable CT scanner-based spinal navigation: a viable option for instrumentation in the region of cervico-thoracic junction. European Spine Journal. 25: 1643-50. doi:10.1007/s00586-016-4476-6.

[118] Mason A, Paulsen R, Babuska JM, Rajpal S, Burneikiene S, Nelson EL, et al. (2014) The accuracy of pedicle screw placement using intraoperative image guidance systems. Journal of neurosurgery. Spine. 20: 196-203. doi:10.3171/2013.11.SPINE13413.

[119] Aoude AA, Fortin M, Figueiredo R, Jarzem P, Ouellet J, Weber MH. (2015) Methods to determine pedicle screw placement accuracy in spine surgery: a systematic review. European Spine Journal. 24: 990-1004. doi:10.1007/s00586-015-3853-x.

[120] Kleck CJ, Cullilmore I, LaFleur M, Lindley E, Rentschler ME, Burger EL, et al. (2016) A new 3-dimensional method for measuring precision in surgical navigation and methods to optimize navigation accuracy. European Spine Journal. 25: 1764-74. doi:10.1007/s00586-015-4235-0.

[121] Oertel MF, Hobart J, Stein M, Schreiber V, Scharbrodt W. (2011) Clinical and methodological precision of spinal navigation assisted by 3D intraoperative O-arm radiographic imaging. Journal of neurosurgery. Spine. 14: 532-6. doi:10.3171/ 2010.10.SPINE091032.

[122] Haberland N, Ebmeier K, Grunewald JP, Hliscs R, Kalff RL. (2000) Incorporation of intraoperative computerized tomography in a newly developed spinal navigation technique. Computer Aided Surgery. 5: 18-27. doi:10.1002/(SICI)1097-0150(2000)5:1<18 :AID-IGS3>3.0.CO;2-T.

[123] Scheufler K-M, Franke J, Eckardt A, Dohmen H. (2011) Accuracy of image-guided pedicle screw placement using intraoperative computed tomography-based navigation with automated referencing, part I: cervicothoracic spine. Neurosurgery. 69: 782-95; discussion 795. doi:10.1227/NEU.0b013e318222ae16.

[124] Scheufler K-M, Franke J, Eckardt A, Dohmen H. (2011) Accuracy of image-guided pedicle screw placement using intraoperative computed tomography-based navigation with automated referencing. Part II: thoracolumbar spine. Neurosurgery. 69: 1307-16. doi:10.1227/NEU.0b013e31822ba190.

[125] Cicchetti D V. (1994) Guidelines, criteria, and rules of thumb for evaluating normed and standardized assessment instruments in psychology. Psychological Assessment. 6: 284-90. doi:10.1037/1040-3590.6.4.284.

[126] Verma R, Krishan S, Haendlmayer K, Mohsen A. (2010) Functional outcome of computer-assisted spinal pedicle screw placement: a systematic review and meta-analysis of 23 studies including 5,992 pedicle screws. Eur Spine J. 19: 370-5. doi:10.1007/s00586-009-1258-4.

[127] Watkins RG, Gupta A et al. (2010) Cost-effectiveness of image-guided spine surgery. Open Orthop J. 4: 228-33. doi:10.2174/1874325001004010228.

[128] Dea N, Fisher CG, Batke J, Strelzow J, Mendelsohn D, Paquette SJ, et al. (2016) Economic evaluation comparing intraoperative cone beam CT-based navigation and conventional fluoroscopy for the placement of spinal pedicle screws: A patient-level data cost-effectiveness analysis. Spine Journal. 16: 23-31. doi:10.1016/j.spinee.2015.09.062.

[129] Gertzbein SD, Robbins SE. (1990) Accuracy of pedicular screw placement in vivo. Spine. 15: 11-4. doi:10.1097/00007632-199001000-00004.

[130] Guven O, Yalin S, Karahan M, Sevin TT. (1994) Postoperative evaluation of transpedicular screws with computed tomography. Orthopaedic Review. 23.

[131] O'Brien MF, Lenke LG, Mardjetko S, Lowe TG, Kong Y, Eck K, et al. (2000) Pedicle morphology in thoracic adolescent idiopathic scoliosis: is pedicle fixation an anatomically viable technique? Spine. 25: 2285-93. doi:10.1097/00007632-200009150-00005.

[132] Lavelle W, Ranade A, Samdani A, Gaughan J, D'Andrea L, Betz R. (2014) Inter- and Intra-Observer Reliability of Measurement of Pedicle Screw Breach Assessed by Post-operative CT Scans. International Journal of Spine Surgery. 8: 11-11. doi:10.14444/1011.

[133] Neo M, Sakamoto T, Fujibayashi S, Nakamura T. (2005) The clinical risk of vertebral artery injury from cervical pedicle screws inserted in degenerative vertebrae. Spine (Phila Pa 1976). 30: 2800-5. doi:10.1097/01.brs.0000192297.07709.5d.

[134] Abe Y, Ito M, Abumi K, Kotani Y, Sudo H, Minami A. (2011) A novel cost-effective computer-assisted imaging technology for accurate placement of thoracic pedicle screws. Journal of neurosurgery. Spine. 15: 479-85. doi:10.3171/2011.6.SPINE10721.

[135] Cui G, Wang Y, Kao T-H, Zhang Y, Liu Z, Liu B, et al. (2012) Application of Intraoperative Computed Tomography With or Without Navigation System in Surgical Correction of Spinal Deformity. Spine. 37: 891-900. doi:10.1097/BRS.0b013e31823aff81.

[136] Bledsoe JM, Fenton D, Fogelson JL, Nottmeier EW. (2009) Accuracy of upper thoracic pedicle screw placement using three-dimensional image guidance. The Spine Journal. 9: 817-21. doi:10.1016/j.spinee.2009.06.014.

[137] Schizas C, Thein E, Kwiatkowski B, Kulik G. (2012) Pedicle screw insertion: robotic assistance versus conventional C-arm fluoroscopy. Acta orthopaedica Belgica. 78: 240-5.

[138] Bai Y-S, Niu Y-F, Chen Z-Q, Zhu X-D, Gabriel LKP, Wong HK, et al. (2013) Comparison of the Pedicle Screws Placement Between Electronic Conductivity Device and Normal Pedicle Finder in Posterior Surgery of Scoliosis. Journal of Spinal Disorders and Techniques. 26: 316-20. doi:10.1097/BSD.0b013e318247f21d.

[139] Cho JY, Chan CK, Lee SH, Lee HY. (2012) The accuracy of 3D image navigation with a cutaneously fixed dynamic reference frame in minimally invasive trans-

foraminal lumbar interbody fusion. Computer Aided Surgery. 17: 300-9. doi:10.3109/10929088.2012.728625.

[140] Kim MC, Chung HT, Cho JL, Kim DJ, Chung NS. (2011) Factors affecting the accurate placement of percutaneous pedicle screws during minimally invasive transforaminal lumbar interbody fusion. European Spine Journal. 20: 1635-43. doi:10.1007/s00586-011-1892-5.

[141] Uneri A, Stayman JW, De Silva T, Wang AS, Kleinszig G, Vogt S, et al. (2015) Known-Component 3D-2D Registration for Image Guidance and Quality Assurance in Spine Surgery Pedicle Screw Placement. Proceedings of SPIE–the International Society for Optical Engineering. 9415: . doi:10.1117/12.2082210.

[142] Koivukangas T, Katisko JPA, Koivukangas JP. Technical accuracy of an O-arm registered surgical navigator. Proc. Annu. Int. Conf. IEEE Eng. Med. Biol. Soc. EMBS, IEEE; 2011, p. 2148-51. doi:10.1109/IEMBS.2011.6090402.

[143] Rajaee SS, Bae HW, Kanim LE, Delamarter RB. (2012) Spinal fusion in the United States: analysis of trends from 1998 to 2008. Spine (Phila Pa 1976). 37: 67-76. doi:10.1097/BRS.0b013e31820cccfb.

[144] Arand M, Schempf M, Fleiter T, Kinzl L, Gebhard F. (2006) Qualitative and quantitative accuracy of CAOS in a standardized in vitro spine model. Clinical orthopaedics and related research. 450: 118-28. doi:10.1097/01.blo.0000218731.36967.e8.

[145] Lee GYF, Massicotte EM, Raja Rampersaud Y. (2007) Clinical Accuracy of Cervicothoracic Pedicle Screw Placement. Journal of Spinal Disorders & Techniques. 20: 25-32. doi:10.1097/01.bsd.0000211239.21835.ad.

[146] Laine T, Lund T, Ylikoski M, Lohikoski J, Schlenzka D. (2000) Accuracy of pedicle screw insertion with and without computer assistance: a randomised controlled clinical study in 100 consecutive patients. Eur Spine J. 9: 235-40. doi:10.1007/s005860000146.

[147] Geng J. (2011) Structured-light 3D surface imaging: a tutorial. Advances in Optics and Photonics. 3: 128-60. doi:10.1364/AOP.3.000128.

[148] Wood MJ, McMillen J. (2014) The surgical learning curve and accuracy of minimally invasive lumbar pedicle screw placement using CT based computer-assisted navigation plus continuous electromyography monitoring - a retrospective review of 627 screws in 150 patients. International journal of spine surgery. 8: 27-27. doi:10.14444/1027.

[149] Assaker R, Reyns N, Vinchon M, Demondion X, Louis E. (2001) Transpedicular screw placement: image-guided versus lateral-view fluoroscopy: in vitro simulation. Spine. 26: 2160-4. doi:10.1097/00007632-200110010-00024.

[150] Mirza SK, Wiggins GC, Kuntz C, York JE, Bellabarba C, Knonodi MA, et al. (2003) Accuracy of thoracic vertebral body screw placement using standard fluoroscopy, fluoroscopic image guidance, and computed tomography image guidance. Spine. 28: 402-13. doi:10.1097/01.BRS.0000048461.51308.CD.

[151] Nelson EM, Monazzam SM, Kim KD, Seibert JA, Klineberg EO. (2014) Intraoperative fluoroscopy, portable X-ray, and CT: Patient and operating room personnel radiation exposure in spinal surgery. Spine Journal. 14: 2985-91. doi:10.1016/j.spinee.2014.06.003.

[152] Pereira VM, Smit-Ockeloen I, Brina O, Babic D, Breeuwer M, Schaller K, et al. (2015) Volumetric Measurements of Brain Shift Using Intraoperative Cone-Beam Computed Tomography. Neurosurgery1. doi:10.1227/NEU.0000000000000999.

[153] Okamoto T, Onda S, Yanaga K, Suzuki N, Hattori A. (2015) Clinical application

of navigation surgery using augmented reality in the abdominal field. Surgery Today. 45: 397-406. doi:10.1007/s00595-014-0946-9.

[154] Qureshi AI, Suri MFK, Nasar A, Kirmani JF, Ezzeddine MA, Divani AA, et al. (2007) Changes in cost and outcome among US patients with stroke hospitalized in 1990 to 1991 and those hospitalized in 2000 to 2001. Stroke. 38: 2180-4. doi:10.1161/ STROKEAHA.106.467506.

[155] Wang W, Steward CE, Desmond PM. (2009) Diffusion tensor imaging in glioblastoma multiforme and brain metastases: the role of p, q, L, and fractional anisotropy. AJNR. American journal of neuroradiology. 30: 203-8. doi:10.3174/ajnr.A1303.

[156] Guha D, Jakubovic R, Gupta S, Alotaibi NM, Cadotte D, da Costa LB, et al. (2016) Spinal intra-operative three-dimensional navigation: correlation between clinical and absolute engineering accuracy. The Spine Journal. doi:10.1016/j.spinee.2016.10.020.

[157] Yu CC, Yuh RT, Bajwa NS, Toy JO, Ahn UM, Ahn NU. (2015) Lower thoracic pedicle morphometry: male, taller, and heavier specimens have bigger pedicles. Spine. 40: E323-31. doi:10.1097/BRS.0000000000000760.

[158] Acharya S, Dorje T, Srivastava A. (2010) Lower dorsal and lumbar pedicle mor-
phometry in Indian population: a study of four hundred fifty vertebrae. Spine. 35:
E378-84. doi:10.1097/BRS.0b013e3181cb7f2b.

[159] Bourgeois G, Magnin M, Morel A, Sartoretti S, Huisman T, Tuncdogan E, et
al. (1999) Accuracy of MRI-guided stereotactic thalamic functional neurosurgery. Neu-
roradiology. 41: 636-45. doi:10.1007/s002340050816.

[160] Jakubovic R, Farooq H, Alarcon J, Yang VXD. Accuracy of image-guided sur-
gical navigation using near infrared (NIR) optical tracking BT - Optical Techniques
in Neurosurgery, Neurophotonics, and Optogenetics II, February 7, 2015 - February
10, 2015. In: Hirschberg H, Madsen SJ, Jansen ED, Luo Q, Mohanty SK, Thakor N
V., editors. vol. 9305, 2015, p. Plexon Inc.; The Society of Photo-Optical Instrume.
doi:10.1117/12.2079722.

[161] Bucholz RD, Smith KR, Laycock KA, McDurmont LL. (2001) Three-dimensional
localization: from image-guided surgery to information-guided therapy. Methods (San
Diego, Calif.). 25: 186-200. doi:10.1006/meth.2001.1234.

[162] Sahgal A, Larson DA, Chang EL. (2008) Stereotactic body radiosurgery for

spinal metastases: a critical review. International journal of radiation oncology, biology, physics. 71: 65265. doi:10.1016/j.ijrobp.2008.02.060.

[163] Burch S, Bisland SK, Bogaards a, Yee a JM, Whyne CM, Finkelstein J a, et al. (2005) Photodynamic therapy for the treatment of vertebral metastases in a rat model of human breast carcinoma. Journal of orthopaedic research: official publication of the Orthopaedic Research Society. 23: 995-1003. doi:10.1016/j.orthres.2004.12.014.

[164] Yee A, Burch S, Akens M, Won E, Lo V, Wise-Milestone L, et al. (2013) Photo-dynamic therapy as a local therapeutic adjunct for the treatment of vertebral metastases. 8565: 85656O-85656O-6. doi:10.1117/12.2019796.

[165] Starr PA, Christine CW, Theodosopoulos P V., Lindsey N, Byrd D, Mosley A, et al. (2002) Implantation of deep brain stimulators into subthalmic nucleus: technical approach and magnetic imagingverified electrode locations. Journal of Neurosurgery. 97: 370-87. doi:10.3171/jns.2002.97.2.0370.

[166] Ruschin M, Nayebi N, Carlsson P, Brown K, Tamerou M, Li W, et al. (2010) Performance of a novel repositioning head frame for gamma knife perfexion and image-guided linac-based intracranial stereotactic radiotherapy. International journal of radia-

tion oncology, biology, physics. 78: 306-13. doi:10.1016/j.ijrobp.2009.11.001.

[167] Minniti G, Clarke E, Lanzetta G, Osti MF, Trasimeni G, Bozzao A, et al. (2011) Stereotactic radiosurgery for brain metastases: analysis of outcome and risk of brain radionecrosis. Radiation oncology (London, England). 6: 48. doi:10.1186/1748-717X-6-48.

[168] Li W, Bootsma G, Von Schultz O, Carlsson P, Laperriere N, Millar B-A, et al. (2016) Preliminary Evaluation of a Novel Thermoplastic Mask System with Intrafraction Motion Monitoring for Future Use with Image-Guided Gamma Knife. Cureus. 8: . doi:10.7759/cureus.531.

[169] Wen N, Snyder KC, Scheib SG, Schmelzer P, Qin Y, Li H, et al. (2016) Technical Note: Evaluation of the systematic accuracy of a frameless, multiple image modality guided, linear accelerator based stereotactic radiosurgery system. Medical Physics. 43: 252737. doi:10.1118/1.4947199.

[170] Schell M, Bova F, Larson D, Leavitt D. (1995) AAPM Report no. 54. Report of Task Group.

[171] Yeung D, Palta J, Fontanesi J, Kun L. (1994) Systematic analysis of errors in

target localization and treatment delivery in stereotactic radiosurgery (SRS). International Journal of Radiation Oncology*Biology*Physics. 28: 493-8. doi:10.1016/0360-3016(94)90076-0.

[172] Podgorsak, EB; Podgorsak M. Stereotactic Irradiation. In: Van Dyk J, editor. Mod. Technol. Radiat. Oncol. Vol. 1; A Compedium Med. Phys. Radiat. Oncol., Madison, Wisconsin: Medical Physics Publishing; 1999, p. 589-639.

[173] Jaffray D, Kupelian P, Djemil T, Macklis RM. (2007) Review of image-guided radiation therapy. Expert review of anticancer therapy. 7: 89-103. doi:10.1586/14737140.7.1.89.

[174] Rosenfelder N a., Corsini L, McNair H, Pennert K, Burke K, Lamb CM, et al. (2013) Achieving the Relocation Accuracy of Stereotactic Frame-based Cranial Radiotherapy in a Three-point Thermoplastic Shell. Clinical Oncology. 25: 66-73. doi:10.1016/j.clon.2012.06.007.